AD-A229 486

DTIC FILE COPY

(2)

REPORT DOCUMENTATION PAGE

Form Approved
OMB No 0704-0188

1 AGENCY USE ONLY (Leave blank)	2. REPORT DATE	3 REPORT TYPE AND DATES COVERED
		Final Report/1 Sep 87-31 Aug 90

4. TITLE AND SUBTITLE
Theoretical Investigations of Negative Ions in a Hydrogen Source

5 FUNDING NUMBERS
61102F/2301/A7

6. AUTHOR(S)
Jogindra Wadehra

7 PERFORMING ORGANIZATION NAME(S) AND ADDRESS(ES)
Wayne State University
Department of Physics and Astronomy
Detroit, MI 48202

8. PERFORMING ORGANIZATION REPORT NUMBER
AFOSR-TR- 90 1138

9. SPONSORING / MONITORING AGENCY NAME(S) AND ADDRESS(ES)
AFOSR/NP
Bolling AFB DC 20332-6448

10. SPONSORING / MONITORING AGENCY REPORT NUMBER
AFOSR-87-0342

11. SUPPLEMENTARY NOTES

12a. DISTRIBUTION / AVAILABILITY STATEMENT
Approved for public release; distribution is unlimited.

12b. DISTRIBUTION CODE

13. ABSTRACT *(Maximum 200 words)*

The principal results of the research are two-fold. First, the time-dependent behavior of electron swarms in various atomic and molecular gases were obtained using a novel numerical procedure. The electrons injected in the gaseous source excite and ionize the atoms as well as molecules and, more importantly, cause dissociation and vibrational excitation of the molecular species. Second, the cross sections and the rates of negative ion production via the process of dissociatve electron attachment to various light molecules were calculated The role played by initial rovibrational excitation of the molecule in enhancing the rates of production of negative ion beams were investigated in detail. Since the processes of dissociative attachment and of vibrational excitation are complementary in nature (both proceed via the excitation of molecular hydrogen and its five isotopes were also examined. Very useful scaling law for these excitation cross sections were discovered. Using this scaling property it is possible to obtain the cross sections for vibrational excitation or deexcitation, by electron impact, of heavier isotopes of H_2 from the corresponding sections for molecular hydrogen.

14. SUBJECT TERMS	15. NUMBER OF PAGES
atomic, molecular, gases, electron, isotopes, [illegible]	101
	16. PRICE CODE

17 SECURITY CLASSIFICATION OF REPORT	18 SECURITY CLASSIFICATION OF THIS PAGE	19 SECURITY CLASSIFICATION OF ABSTRACT	20. LIMITATION OF ABSTRACT
UNCLASSIFIED	UNCLASSIFIED	UNCLASSIFIED	SAR

GENERAL INSTRUCTIONS FOR COMPLETING SF 298

The Report Documentation Page (RDP) is used in announcing and cataloging reports. It is important that this information be consistent with the rest of the report, particularly the cover and title page. Instructions for filling in each block of the form follow It is important to *stay within the lines* to meet *optical scanning requirements*.

Block 1 Agency Use Only *(Leave blank)*

Block 2. Report Date Full publication date including day, month, and year, if available (e g 1 Jan 88). Must cite at least the year

Block 3. Type of Report and Dates Covered State whether report is interim, final, etc If applicable, enter inclusive report dates (e g. 10 Jun 87 - 30 Jun 88).

Block 4. Title and Subtitle. A title is taken from the part of the report that provides the most meaningful and complete information When a report is prepared in more than one volume, repeat the primary title, add volume number, and include subtitle for the specific volume O i classified documents enter the title classification in parentheses.

Block 5. Funding Numbers To include contract and grant numbers; may include program element number(s), project number(s), task number(s), and work unit number(s). Use the following labels:

C	- Contract	PR	- Project
G	- Grant	TA	- Task
PE	- Program Element	WU	- Work Unit Accession No

Block 6. Author(s) Name(s) of person(s) responsible for writing the report, performing the research, or credited with the content of the report. If editor or compiler, this should follow the name(s).

Block 7. Performing Organization Name(s) and Address(es). Self-explanatory.

Block 8. Performing Organization Report Number. Enter the unique alphanumeric report number(s) assigned by the organization performing the report.

Block 9. Sponsoring/Monitoring Agency Name(s) and Address(es) Self-explanatory

Block 10. Sponsoring/Monitoring Agency Report Number. *(If known)*

Block 11. Supplementary Notes. Enter information not included elsewhere such as: Prepared in cooperation with...; Trans. of. ; To be published in.... When a report is revised, include a statement whether the new report supersedes or supplements the older report.

Block 12a. Distribution/Availability Statement. Denotes public availability or limitations Cite any availability to the public. Enter additional limitations or special markings in all capitals (e.g NOFORN, REL, ITAR).

DOD	- See DoDD 5230 24, "Distribution Statements on Technical Documents "
DOE	- See authorities
NASA	- See Handbook NHB 2200.2
NTIS	- Leave blank

Block 12b. Distribution Code

DOD	- Leave blank.
DOE	- Enter DOE distribution categories from the Standard Distribution for Unclassified Scientific and Technical Reports.
NASA	- Leave blank
NTIS	- Leave blank

Block 13. Abstract Include a brief *(Maximum 200 words)* factual summary of the most significant information contained in the report

Block 14. Subject Terms Keywords or phrases identifying major subjects in the report.

Block 15. Number of Pages. Enter the total number of pages

Block 16. Price Code. Enter appropriate price code *(NTIS only)*

Blocks 17. - 19. Security Classifications. Self-explanatory. Enter U S Security Classification in accordance with U S Security Regulations (i e , UNCLASSIFIED) If form contains classified information, stamp classification on the top and bottom of the page

Block 20. Limitation of Abstract This block must be completed to assign a limitation to the abstract. Enter either UL (unlimited) or SAR (same as report). An entry in this block is necessary if the abstract is to be limited. If blank, the abstract is assumed to be unlimited

PROJECT TITLE:	Theoretical Investigations of Negative Ions in a Hydrogen Source.
GRANT NUMBER:	AFOSR - 87 - 0342
PRINCIPAL INVESTIGATOR:	Professor J. M. Wadehra
	Department of Physics and Astronomy
	Wayne State University, Detroit, Michigan 48202
PERIOD OF EFFORT:	September 1, 1987 - August 31, 1990.

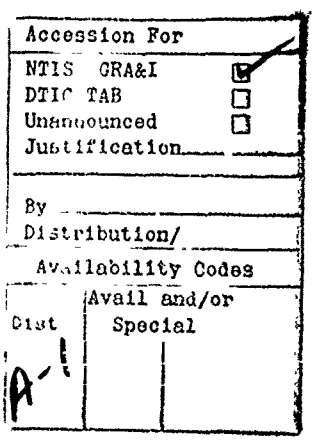

The principal objectives of our research work (Grant Number AFOSR-87-0342) have been two-fold. First, we have obtained the *time - dependent* behavior of electron swarms in various atomic and molecular gases using a novel numerical procedure that we recently developed. The electrons injected in the gaseous source excite and ionize the atoms as well as molecules and, more importantly, cause dissociation and vibrational excitation of the molecular species. Second, we have calculated the cross sections and the rates of negative ion production via the process of dissociative electron attachment to various light molecules. We have also investigated, in detail, the role played by initial rovibrational excitation of the molecule in enhancing the rates of production of negative ion beams. Since the processes of dissociative attachment and of vibrational excitation are complementary in nature (both proceed via the formation of an intermediate resonant anion state), we have also investigated the isotope effect for the vibrational excitation of molecular hydrogen and its five isotopes. As part of this project we have discovered a very useful scaling law for these excitation cross sections. Using this scaling property it is possible to obtain the cross sections for vibrational excitation or deexcitation, by electron impact, of heavier isotopes of H_2 from the corresponding cross sections for molecular hydrogen.

During three years of our investigations we made the following specific advances:

(a) Time Dependent behavior of Electron Swarms in Various Gases.

With the ultimate aim of investigating the temporal evolution of the electron velocity distribution as it attains its equilibrium in a hydrogen source, we have been devising stable numerical algorithms and developing corresponding computer codes for obtaining the electron velocity distribution in a general gaseous source. It should be remarked that the procedure which we have developed[1,2] is general enough in that it can be easily adapted for obtaining velocity distribution of positron swarms or ion swarms in a gas as long as the relevant collision cross sections are available. In order to obtain the electron velocity distribution majority of previous investigators have attempted to solve the Boltzmann equation either analytically or numerically. Analytical solutions of the Boltzmann equation have made use of simple model collision cross sections which, though reasonable, are not necessarily very accurate. The use of actual cross

sections, either experimentally observed or theoretically calculated, in the Boltzmann equation forces one to apply numerical techniques for its solution. The procedure used most frequently in the past is to expand the angular dependence of the distribution function as a power series in the Legendre polynomials, truncate the series after a few (typically two) terms and solve the resulting set of equation numerically. This expansion procedure has some inherent problems. For example, for high values of E/N (the ratio of the applied electric field to the gas number density) a large number of terms in the Legendre expansion may contribute to the distribution function. A large number of terms in the Legendre expansion may also be necessary at low values of E/N for a gas with relatively high inelastic cross sections. Inclusion of a large number of terms in the expansion can make this procedure computationally expensive and sometimes numerically unstable. Furthermore, no systematic study of the convergence behavior of the expansion techniques for an arbitrary gas is available. We felt that it is desirable to have alternative procedures, especially the ones which do not involve any expansion of the distribution function, for obtaining the electron velocity distribution function in a gas mixture.

The starting point of our procedure is to realize that in the absence of collisions with the ambient gas particles the electron swarm is accelerated constantly by the applied electric field **E** in such a manner that in a time interval Δt the velocity of each electron is changed by an amount $\Delta \mathbf{v} = -e\mathbf{E}/m$. Thus the difference between $f(\mathbf{v},t)$, the distribution function at time t, and $f(\mathbf{v} + \Delta\mathbf{v}, t + \Delta t)$, the distribution function at the later time $t + \Delta t$, must be due to collisions of electrons with gas particles. (The frequency of electron-electron collisions is relatively small.) Thus one can write

$$f(\mathbf{v} + \Delta\mathbf{v},\, t + \Delta t) = f(\mathbf{v},t) + R(\mathbf{v},t)\,\Delta t, \tag{1}$$

where $R(\mathbf{v},t)$ is the collision term containing all the relevant cross sections. The standard Boltzmann equation is obtained by simply expanding the left hand-side of Eq. (1) to first order in Δt and then taking the limit $\Delta t \to 0$. Thus, for the purposes of obtaining the electron velocity distribution function Eq. (1) is more fundamental than the standard Boltzmann equation and is certainly computationally more convenient than the Boltzmann equation.

Now choosing the z axis to be along the applied electric field **E**, the electrons have a

constant acceleration along the z direction and zero acceleration in the transverse direction. Thus, in Cartesian coordinates Eq. (1) is rewritten as

$$f[v_x, v_y, v_z - (eE/m)\Delta t, t + \Delta t] = f(v_x, v_y, v_z, t) + R(\mathbf{v},t)\Delta t \qquad (2)$$

Because of the axial symmetry along v_z, f is stored in a two-dimensional array only as a function of v_z and v_x with the step size Δv given by $\Delta v = (eE/m)\Delta t$. The temporal evolution of the distribution function then involves, in part, a shifting of the array containing f along v_z at each time interval Δt. This shifting of the array essentially achieves the same effect as the acceleration of the electrons due to the applied electric field without accumulating any round-off error. This shifting procedure in itself greatly improves the numerical stability in obtaining the electron distribution function as compared to the alternative approach of evaluating derivatives numerically in the traditional solution of the Boltzmann equation. A criterion for numerical stability is that, for each value of |v|, the time step Δt should be chosen small enough such that the distribution function is larger than the corresponding collision term $R(\mathbf{v},t)\Delta t$, that is,

$$f(\mathbf{v},t) > R(\mathbf{v},t)\Delta t \qquad \text{for all v.} \qquad (3)$$

By meeting this criterion one can avoid generating physically-meaningless negative values of the electron velocity distribution function. Interestingly, the standard Courant-Lewy-Friedrichs condition, namely, that the step sizes Δv and Δt must satisfy the inequality:

$$(eE/m)\Delta t \leq \Delta v, \qquad (4)$$

which is a necessary condition for the numerical stability of a *partial* differential equation is not necessary in our case.

A step-by-step procedure for attaining the equilibrium velocity distribution on the computer is, then, as follows:

Step 1. Start with a given distribution function at time t which is stored in a two-dimensional array $f(v_x,v_z)$. It could either be an analytical function (for example, a Maxwellian or a Druyvesteyan or a delta function) representing the distribution function at the starting time $t = 0$ or be a numerically generated function at some earlier time t_0.

Step 2. Compute the collision terms $R(v_x,v_z)$ for each value of v_x and v_z. Multiply the collision terms by Δt and add to the distribution function from which they were obtained [see Eq. (2)].

Step 3. Shift the resulting array along the v_z index [$f(v_x,v_z) \rightarrow f(v_x, v_z + \Delta v)$] to obtain the new distribution function at the later time $t + \Delta t$.

Step 4. Calculate various swarm parameters corresponding to the later time $t + \Delta t$ using the new distribution function. Repeat from step 1 unless the swarm parameters stop changing in time which indicates that the equilibrium has been reached.

We have used this procedure for obtaining the average energy, drift velocity and ionization rate for electron-neon[1] and electron-argon[2] systems for various values of E/N. The equilibrium values of various swarm parameters for electrons in gaseous neon for a few different values of E/N are given in Table I below.

TABLE I

E/N (in Td)	Ionization rate (in 10^7 s^{-1})	Drift velocity (in 10^7 cm s^{-1})	Average energy (in eV)
141	3.0074	3.1110	15.298
190	4.7470	3.8049	17.176
237	6.7463	4.4547	19.012
283	9.1608	5.0139	20.962
353	12.979	5.8074	23.787
424	17.113	6.5471	26.657
495	21.437	7.2327	29.573
566	26.013	7.8715	32.610

This unique procedure, that we have described above for obtaining the electron energy distribution in a gas, is computationally stable and analytically exact. In particular, this procedure provides a detailed time evolution of various swarm parameters, such as the average electron energy or the rate of ionization of ambient gas particles by electron impact etc., whose final equilibrium values can be experimentally determined. These final equilibrium values depend only on the ratio of the applied electric field to the gas number density, E/N, and are independent of the

initial electron energy distribution function. Recently, we also used our innovative procedure for obtaining the *positron* velocity distribution function in various rare gases[3].

The ultimate aim of our investigations is to calculate, in the future, the electron energy distribution in a realistic mixture of atomic and molecular hydrogen using all the theoretical tools that we have been developing and numerically testing for noble gases. For this purpose we will be requiring a critical compilation[4] of data pertaining to cross section for elementary processes in atomic and molecular hydrogen. In the case of noble gases, however, we have discovered that the transient behavior of any swarm parameter as it evolves to its final equilibrium value depends on the initial conditions even though the final equilibrium value that the parameter attains is independent of the initial conditions. We have further discovered that this transient behavior of any swarm parameter, A(t), can be accurately fitted by a sum of two exponentially decaying factors as follows:

$$A(t) = c_1 \exp (- \alpha_1 t) + c_2 \exp (- \alpha_2 t) . \qquad (5)$$

The decay constants α_1 and α_2 are determined by the applied electric field. We have noted that a single exponential function does *not* provide a good fit. This observation indicates that perhaps the initial electron swarm could be regarded as consisting of two components with each component having its own decay time to reach equilibrium independently. Figure 1 shows the temporal evolution of various swarm parameters for electrons in gaseous neon, for E/N = 566 Td., for two different initial conditions. In this figure, 'diamonds' represent the actually calculated points while the solid lines are the two-exponential fits based on the above relation. The fitting is indeed superb. Note that the decay constants α_1 and α_2 are the same for <u>all</u> swarm parameters for a given set of initial conditions.

At the present moment we are attempting to generalize our computer code to include (i) anisotropic scattering of electrons by target gas atoms via differential cross sections, (ii) a mixture of gases since a realistic calculation of electron swarm parameters in a hydrogen source must include a mixture of atomic and molecular hydrogen, and (iii) electron swarms subjected to *time - dependent* electric fields.

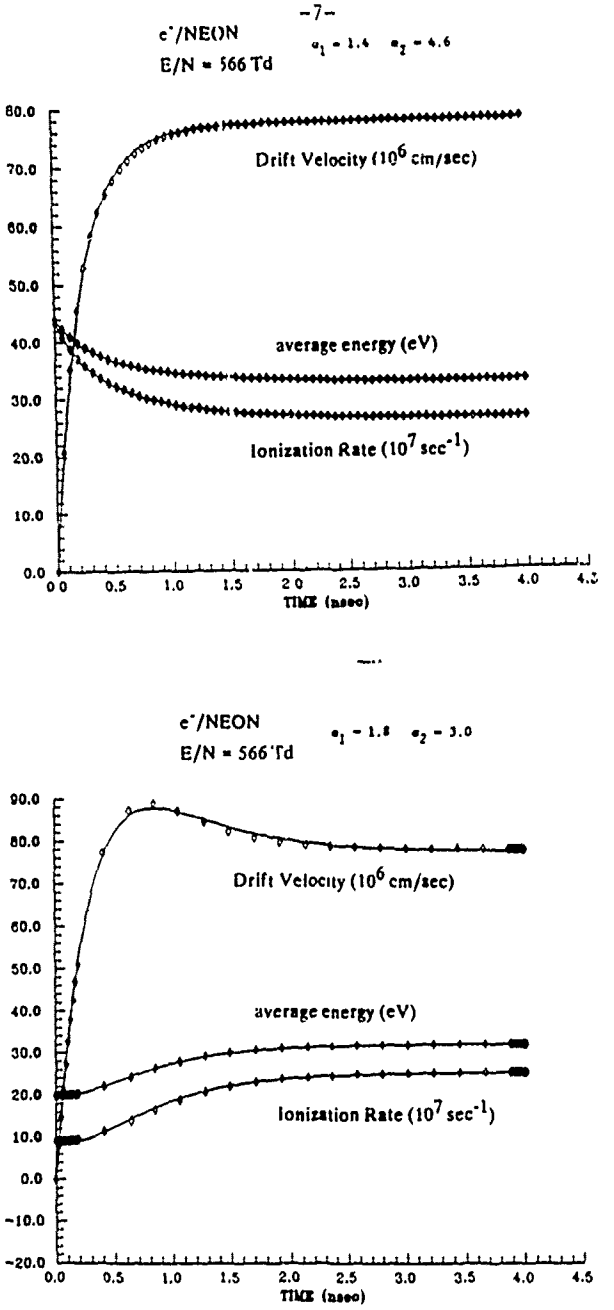

Figure 1. Analytic fit to the transient behavior of electron swarm parameters in neon using two exponentially decaying factors (E/N = 566 Td).

(b) Nonlocal effects in dissociative electron attachment to H_2 and its isotopes.

The production of negative ions via the process of dissociative electron attachment to molecular hydrogen (and its isotopes), $e^- + H_2 \rightarrow H + H^-$, is known to occur when the incoming electron and the neutral target molecule form an intermediate resonant anion state, which has the ability of decaying by autodetaching the electron. The motion of the nuclei in this resonant state is governed by a wave function $\xi(R)$ which satisfies an integrodifferential equation involving a complex, nonlocal potential. In solving this equation one can make use of a local approximation in which one assumes that the set of vibrational levels which are accessible for a given incident electron energy can be regarded as complete. While this approximation may yield acceptable values for the cross sections well above threshold, it is expected to be less accurate near threshold where there are fewer energetically open vibrational channels. During the present investigations we solved the full nonlocal integrodifferential equation for the nuclear wave function $\xi(R)$ near threshold using a newly developed technique which involves matrix inversion. This investigation has allowed us to compare the resulting nonlocal attachment cross sections with those that utilize the nuclear wave function $\xi(R)$ which is obtained using the local approximation to the full integrodifferential equation. Besides providing an assessment of the effect of the local approximation on the electron attachment cross sections, the present calculations will also provide cross sections for H^- production which are more accurate than previously calculated[5]. The nuclear wave function $\xi(R)$ satisfies the following integrodifferential equation:

$$[\, T_N(R) + V^-(R) - E \,]\, \xi(R) = -V(E - E_{v_i J_i}, R)\, \chi_{v_i J_i}(R) - \int dR'\, K(R, R')\, \xi(R') \,, \tag{6}$$

with the kernel $K(R, R')$ given by

$$K(R, R') = \sum_{v,J} \chi^*_{vJ}(R')\, \chi_{vJ}(R)\, \lim_{\eta \to +0} \int_0^\infty d\varepsilon \, \frac{V^*(\varepsilon, R')\, V(\varepsilon, R)}{E - E_{vJ} - \varepsilon + i\eta} \,, \tag{7}$$

where T_N is the kinetic energy of the nuclei, V^- is the effective potential energy in which they move in the resonant state and E is the total energy of the interacting system. The quantity $V(\varepsilon, R)$ is referred to as the interaction matrix element, it represents the coupling between the discrete and

continuum states. This coupling leads to an energy shift of the resonance (the principal part integral on the right hand side of (7)) and provides a width to the resonance (the imaginary part on the right hand side of (7)) which determines the lifetime of the resonance.

In Figure 2 the nonlocal cross section for attachment to H_2 in the J = 0, v = 0 level is compared to its local counterpart. It can be seen that the difference between the two cross sections at a given energy is small, on the order of 10 percent near threshold where the difference is largest. That the nonlocal cross section is larger than the local one reflects the fact that in the local calculation, all vibrational channels are considered to be open, whether or not they are actually energetically accessible. The two cross section curves evidently do not merge into each other even at higher energies because, in the present calculations, excitation of the continuum levels (corresponding to H + H + e) was not taken into account.

The most significant difference between the local and nonlocal cross sections is the conspicuous step structure in the nonlocal cross section in the energy range below about 4.5 eV. This step structure could not be clearly seen in the available experimental data[6] since the energy resolution of the apparatus used was of the order of 0.1 eV. These steps occur at energies for which a new vibrational channel opens up. Thus, for example, the first step in the cross section for attachment to H_2 in v = 0, J = 0 level at about 3.83 eV corresponds to the opening of the v = 10 channel, while the last is at 4.39 eV, where the v = 13 level becomes energetically accessible. It might be tempting to attribute the loss of attachment flux at these steps merely to diversion into the newly opened vibrational channel, but Figure 3 shows that this is an oversimplification. The opening of a new vibrational level is accompanied by upward jumps in the cross sections for the vibrational excitation of previously open channels. The magnitude of the upward jumps becomes smaller as we consider levels farther removed in energy from the newly opened level. The jumps are such that the sum of all discontinuities, including both in the dissociative attachment and in the vibrational excitation cross sections, is indeed zero. The disappearance of the step structure in the local treatment is not very surprising since the local approximation entails replacing the quantity $E - E_{vJ}$ in the denominator on the right hand side of Eq. (7) by the incident electron energy and

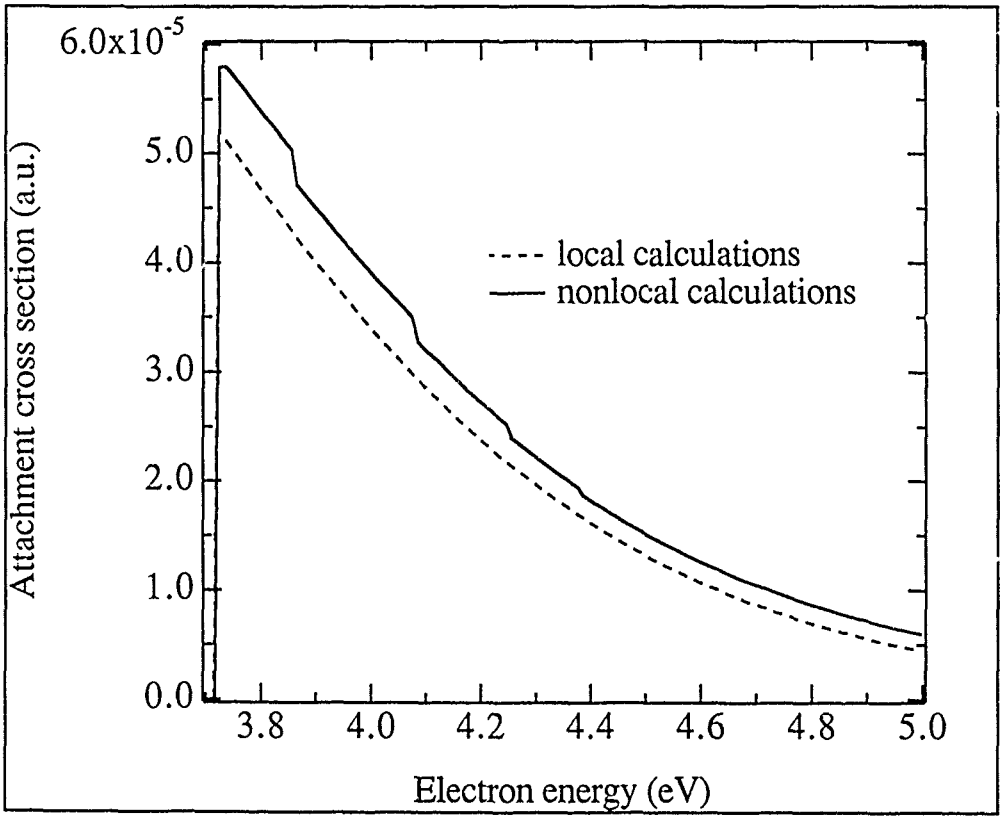

Figure 2. Local and nonlocal cross sections for attachment to H_2 in the lowest rovibrational level.

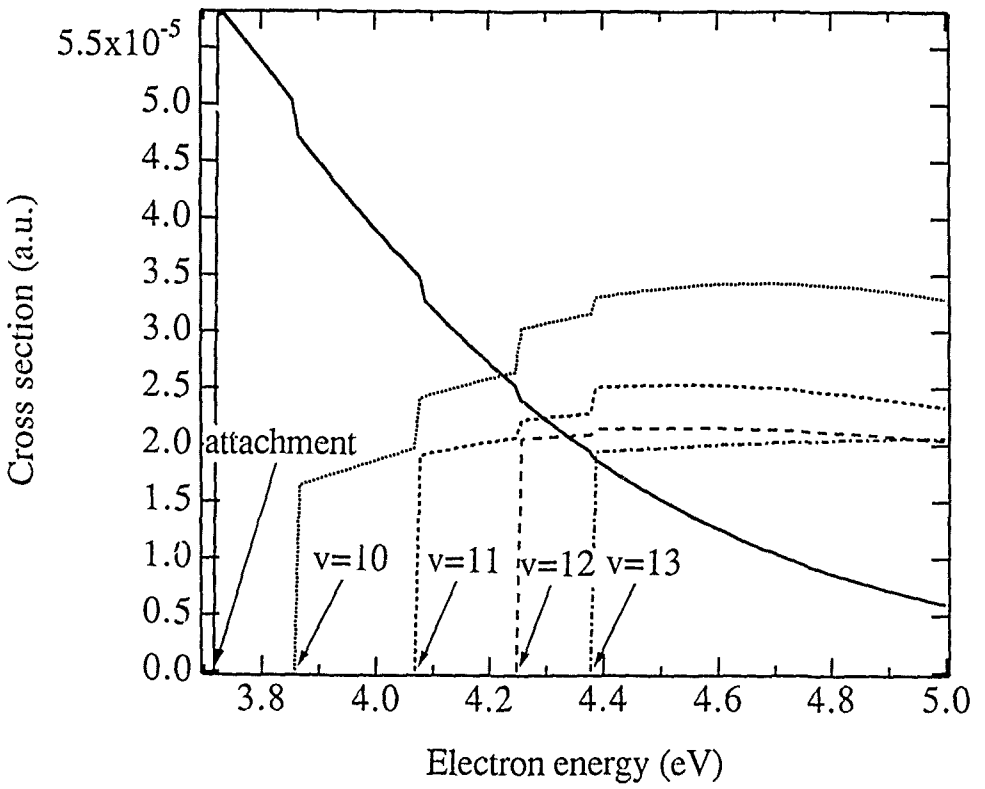

Figure 3. Various nonlocal cross sections for scattering from the lowest rovibrational level of H_2, including that for dissociative attachment and those for excitation of the v = 10 to v = 13 levels. The cross sections for vibrational excitation of v = 10, 11, 12 and 13 levels are multiplied by factors of 15, 25, 50 and 100, respectively.

assuming that the set of vibrational levels over which one sums can be regarded as complete; naturally, in such an approximation all sensitivity to the number of open channels is washed out.

Finally, Figure 4 shows the peak total attachment cross sections for various rotationless levels of H_2 and HD against electron energy on a logarithmic plot. We have discovered a tight upper bound on the attachment cross sections in terms of the incident electron energy $\varepsilon = \hbar^2k^2/2m_e$. The dot-dashed curve on the top represents $1/k^2$, which is seen to provide an upper bound to the attachment cross sections for all six isotopes of H_2 for all values of the incident electron energies considered. This is consistent with an observation of Gauyacq[7] that the dissociative attachment cross section is of the form

$$\sigma_{DA}(k) = \frac{\pi}{k^2} P_{det}(k) ,$$

where $P_{det}(k)$, representing the probability that the electron does not autodetach in the resonant state, is less than unity. In fact, $1/k^2$ provides a tighter upper bound than π/k^2. Details of these investigations will soon be appearing[8] in Physical Review A.

(c) Isotope effect in vibrational excitation of molecular hydrogen.

The process of vibrational excitation is closely related to the process of dissociative attachment in that it, too, proceeds via an intermediate resonant anion state. Using the nonlocal equation described above, we have also obtained cross sections for vibrational excitation of molecular hydrogen via the $^2\Sigma_u^+$ resonance for electron energies up to 5 eV. Our objective in studying vibrational excitation has been twofold: to compare, as with dissociative attachment, the nonlocal cross sections with those obtained using the local approximation and also to examine the dependence of the cross sections on the nuclear mass (that is, the isotope effect).

Figure 5 shows, as a typical example, cross sections for excitation from the ground level ($v_i = 0$) to the $v_f = 4$ level using both the local and the nonlocal formulations of the theory. The nonlocal effects are seen to be small here, although differences of up to a factor of two are seen for excitation of the highest vibrational levels. The prominent feature here, however, is the well-defined structure in the cross sections which, we emphasize, is by no means a nonlocal effect,

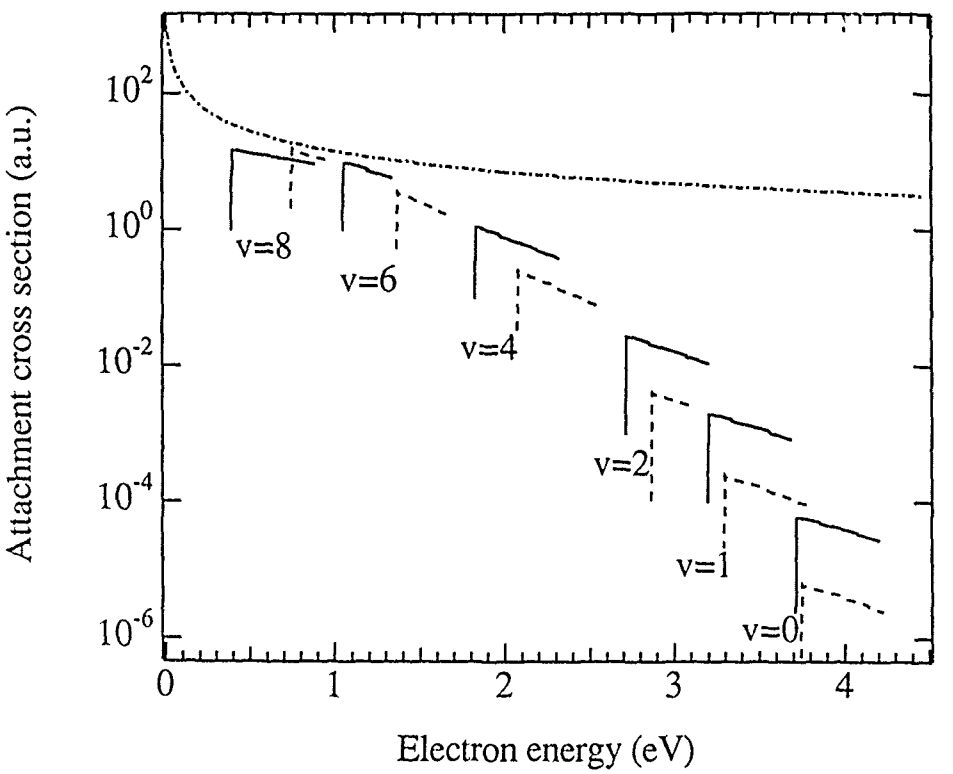

Figure 4. Total cross sections for attachment to H_2 (solid curve) and HD (dashed curves) in various rotationless vibrational levels. The dot-dashed curve on the top represents an upper bound provided by $1/k^2$ where $\hbar^2k^2/2m_e$ is the energy of the incident electron.

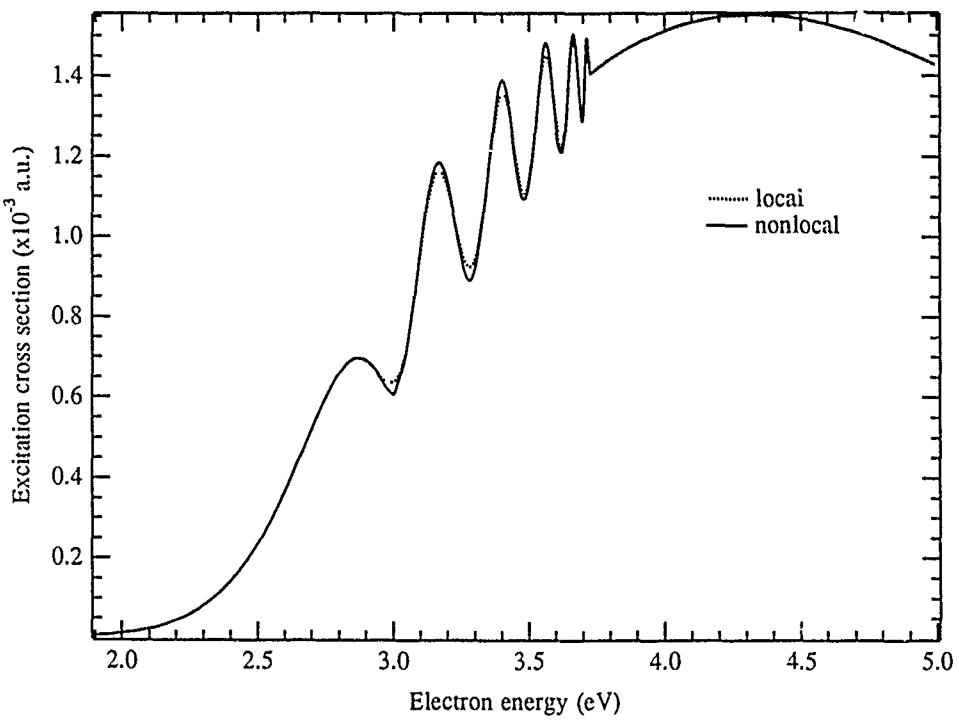

Figure 5. Cross sections for vibrational excitation ($v = 0 \rightarrow 4$) of H_2 using both nonlocal and local formalisms of the theory.

being present in the local cross section as well. This structure is seen only for electron energies below the threshold for dissociative attachment and, for excitation from the ground level, is entirely absent for $v_f < 3$, becoming more pronounced with increasing v_f. This behavior is in qualitative agreement with experimental observations[9], as well as in quantitative agreement with theoretical results reported by other authors[10]. We attribute the peaks in the cross sections to the existence of singularities in the scattering amplitude in the complex energy plane. These singularities are associated with the bound vibrational levels of the resonant anion potential energy, and coincide with them (in energy) in the limit as the level width tends to zero. We have confirmed that as the width is made smaller, the peaks in the cross section become sharper and occur at values of the electron energy which approach those at which an anion bound state could be excited. The same structure is also seen in excitation from higher vibrational levels, and it occurs there for lower values of v_f, appearing in the superelastic cross sections by $v_i = 2$. The exact reason for the behavior of the structure as a function of v_f is, at present, under investigation.

We have also obtained cross sections for excitation from various initial levels to higher vibrational levels for all heavier isotopes of hydrogen, namely, for HD, D_2, HT, DT, and T_2. As part of our research endeavors we have discovered a very useful scaling law for these excitation cross sections. Using this scaling property it is possible to obtain the cross sections for vibrational excitation or deexcitation, by electron impact, of heavier isotopes of H_2 from the corresponding cross sections for molecular hydrogen. Now, using separately the potential curves of linear harmonic oscillators as well as of Morse oscillators to mimic the actual potential curves of the neutral molecule H_2 and its resonant state H_2^-, we have derived analytically that, in the impulse limit of a resonance, an arbitrary vibrational excitation cross section $\sigma(v_i \rightarrow v_f)$ is proportional to $M^{-|v_i - v_f|/2}$ where M is the reduced nuclear mass. [The relative masses of the isotopes H_2, HD, D_2, HT, DT, or T_2 are 1.00, 1.33, 1.50, 2.00, 2.40 and 3.00, respectively.] That this scaling law is obeyed quite well by vibrational excitation cross sections (calculated using the *actual* potential curves of H_2 and H_2^-) can be seen in Figure 6 where the quantity

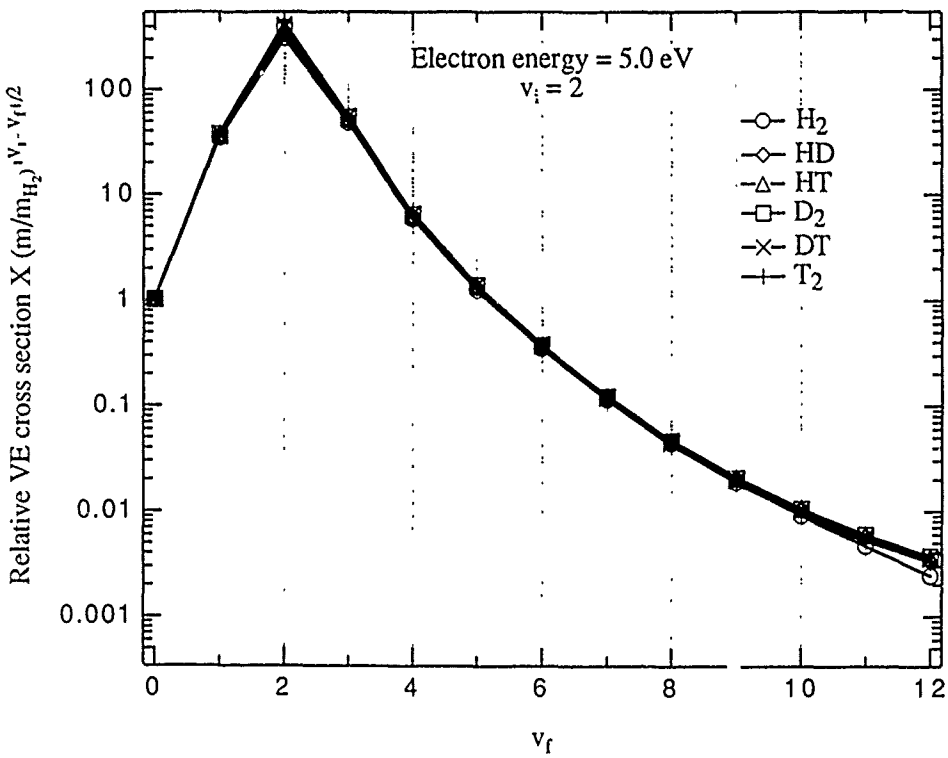

Figure 6. Relative cross sections for vibrational excitation of various isotopes of H_2.

$$\frac{\sigma_X(v_i \rightarrow v_f)}{\sigma_{H_2}(v_i \rightarrow 0)}\left[\frac{M_X}{M_{H_2}}\right]^{|v_i - v_f|/2} \qquad (8)$$

(with X = H_2, HD, D_2, HT, DT, and T_2) is shown, for $v_i = 2$ and incident electron energy $\varepsilon = 5$ eV, as a function of v_f. Our calculated excitation cross sections are in quite good agreement with this scaling behavior for all values of v_i and v_f up to and including 5. This is because the resonant state under present consideration, namely the $^2\Sigma_u^+$ state of H_2^-, has a relatively large width (or small lifetime) and, therefore, can be construed as the impulse limit of the resonance. It is rather remarkable, as seen in Figure 6, that the above isotope scaling law for vibrational excitation cross sections of molecular hydrogen is applicable for cross section values varying over several orders of magnitude! We intend to write the details of these investigations soon in the form of a paper for publication in a refereed journal.

Finally, an updated list of all the publications and presentations carried out under the tenure of the present Grant is provided in the appendices A and B.

A personal note of thanks

The kind support of the Air Force Office of Scientific Research for our research efforts, *for which we are extremely grateful*, has allowed us to investigate the behavior of electrons in atomic and molecular gases. Specifically, we have obtained accurate cross sections for dissociative electron attachment to and vibrational excitation of molecular hydrogen and its isotopes. During these studies we numerically discovered very compact upper bounds on attachment cross sections, and analytically discovered (and numerically verified) a very useful isotope scaling law among vibrational excitation cross sections. The support of AFOSR also permitted us to develop an innovative procedure for obtaining the time - dependent behavior of electron swarms in gaseous sources. We would like to continue, under the future sponsorship of AFOSR, our investigations of the effects of external time - dependent electric fields and of the temperature of the background gas on the temporal behavior of experimentally measurable electron swarm parameters.

References

1. P.J. Drallos and J.M. Wadehra, J. Appl. Phys. 63, 5601 (1988).

2. P. J. Drallos and J. M. Wadehra, Phys. Rev. A40, 1967 (1989).

3. J. M. Wadehra and P. J. Drallos in Proceedings of the Third International Workshop on Positron and Positronium Chemistry, D. M. Schrader and Y. C. Jean, eds. pp. XXXX (World Scientific, 1990).

4. R. K. Janev, W. D. Langer, K. Evans, Jr. and D. E. Post, Jr., "Elementary Processes in Hydrogen-Helium Plasmas" (Springer-Verlag, Berlin, 1987).

5. J. N. Bardsley and J. M. Wadehra, Phys. Rev. A20, 1398 (1979).

6. G. J. Schulz and R. K. Asundi, Phys. Rev. 158, 25 (1967).

7. J. P. Gauyacq, "Dynamics of Negative Ions" (World Scientific, Singapore, 1987).

8. D. E. Atems and J. M. Wadehra, Phys. Rev. A42, XXXX (Nov. 1, 1990).

9. M. Allan, J. Phys. B18, L451 (1985).

10. C. Mundel, M. Berman, and W. Domcke, Phys Rev A32, 181 (1985).

Appendix A : Publications

During the tenure of the present Grant, AFOSR - 87 - 0342, the following papers were published in various refereed journals. Reprints of some of these papers are attached to the present Report.

A. Refereed Journals

1. "A novel algorithm for calculating the time evolution of the electron energy distribution in gaseous discharges", *P.J. Drallos and J.M. Wadehra*, J. Appl. Phys. 63, 5601(1988).

2. "Formation of ground and excited states of antihydrogen", *Sultana N. Nahar and J.M. Wadehra*, Phys. Rev. A37, 4118 (1988).

3. "Approximate Green's functions in electron (positron) - atom collisions", *S.P. Khare and J.M. Wadehra*, Comments in At. Molec. Phys. 23, 55 (1989).

4. "Exact time-dependent evolution of electron velocity distribution functions in a gas using the Boltzmann equation", *P.J. Drallos and J.M. Wadehra*, Phys. Rev. A40, 1967 (1989).

5. "Analytical expressions and recursion relations of two-center harmonic oscillator matrix elements of arbitrary functions", *P.J. Drallos and J.M. Wadehra*, Int. J. Quantum Chem. 37, 797 (1990).

6. "Rovibrationally enhanced dissociative electron attachment to molecular lithium", *J. M. Wadehra*, Phys. Rev. A41, 3607 (1990).

7. "Nonlocal effects in dissociative electron attachment to H_2", *D. E. Atems and J. M. Wadehra*, Phys. Rev. A42, XXXX (1990).

8. "Relativistic approach for e^- scattering from argon", *S. N. Nahar and J. M. Wadehra*, Phys. Rev. A42, XXXX (1990).

9. "Structure and stability of Li_xH_y molecules and anions", *H. H. Michels and J. M. Wadehra*, Int. J. Quantum Chem. (submitted, 1990).

B. Conference Proceedings

10. "Particle beam production via dissociative electron attachment to molecules", *J.M. Wadehra*, Proceedings of SPIE - The International Society for Optical Engineering, vol. 1061, pp. 522-527 (1989).

11. "Dissociative electron attachment to light molecules: A comparative study of H_2, LiH and Li_2", *H. H. Michels and J.M. Wadehra*, Proceedings of the Fifth International Symposium on the Production and Neutralization of Negative Ions and Beams, A. Hershcovitch, ed. pp. 114-120. (American Institute of Physics, 1990).

12. "Isotope effect in vibrational excitation of H_2 by low energy electron impact", *D. E. Atems and J.M. Wadehra*, Proceedings of the Fifth International Symposium on the Production and Neutralization of Negative Ions and Beams, A. Hershcovitch, ed. pp. 121-128. (American Institute of Physics, 1990).

13. "Gas phase alkali-hydrogen interactions in negative ion sources", *H. H. Michels and J.M. Wadehra*, Proceedings of the Fifth International Symposium on the Production and Neutralization of Negative Ions and Beams, A. Hershcovitch, ed. pp. 142-151. (American Institute of Physics, 1990).

14. "Time - dependent behavior of positrons in noble gases", *J. M. Wadehra and P. J. Drallos*, Proceedings of the Third International Workshop on Positron and Positronium Chemistry, D. M. Schrader and Y. C. Jean, eds. pp. XXXX (World Scientific Publishing Co., 1990)

Appendix B: Presentations

During the tenure of the Grant, AFOSR - 87 - 0342, the following presentations were made at various national and international meetings. Abstracts of some of these presentations are attached to the present Report.

1. "Formation of ground and excited states of antihydrogen", Bull. Am. Phys. Soc. 33, 991 (1988) (with Sultana N. Nahar); presented at the 1988 annual meeting of the Division of Atomic, Molecular and Optical Physics, Baltimore, Maryland, April 18-20, 1988.

2. "Relativistic approach for e scattering from argon", Bull. Am. Phys. Soc. 33, 935 (1988) (with Sultana N. Nahar); presented at the 1988 annual meeting of the Division of Atomic, Molecular and Optical Physics, Baltimore, Maryland, April 18-20, 1988.

3. "An exact numerical solution of the time dependent Boltzmann equation", Bull. Am. Phys. Soc. 34, 295 (1989) (with P.J. Drallos); presented at the 41st Annual Gaseous Electronics Conference, Minneapolis, Minnesota, October 18-21, 1988.

4. "Particle beam production via dissociative electron attachment to molecules", presented at the SPIE's OE/LASE'89, Los Angeles, California, January 15-20, 1989.

5. "High-field time-dependent positron velocity distribution functions", Bull. Am. Phys. Soc. 34, 1409 (1989) (with P.J. Drallos); presented at the 1989 annual meeting of the Division of Atomic, Molecular and Optical Physics, Windsor, Ontario, May 17-19, 1989.

6. "Energetics of negative ion formation via dissociative attachment of e + LiH", Bull. Am. Phys. Soc. 34, 1401 (1989) (with H.H. Michels); presented at the 1989 annual meeting of the Division of Atomic, Molecular and Optical Physics, Windsor, Ontario, May 17-19, 1989.

7. "Nonlocal effects in dissociative electron attachment to H_2", (with D.E. Atems); presented at the Sixteenth International Conference on the Physics of Electronic and Atomic Collisions, New York, July 26- August 1, 1989.

8. "Temporal evolution of electron swarms in argon and neon" (with P.J. Drallos); presented at the Sixteenth International Conference on the Physics of Electronic and Atomic Collisions, New York, July 26- August 1, 1989.

9. "An exact theory for the transient behavior of electron swarm parameters" (with P.J. Drallos); presented at the Sixth International Swarm Seminar, Glen Cove, New York, August 3-5, 1989.

10. "Energetics of negative ion formation via dissociative attachment of e + LiH", (with H. H. Michels); presented at the 42st Annual Gaseous Electronics Conference, Menlo Park, California, October 17-20, 1989.

11. "Dissociative electron attachment to light molecules: A comparative study of H_2, LiH and Li_2", (with H. H. Michels); presented at the Fifth International Symposium on the Production and Neutralization of Negative Ions and Beams, Upton, New York, October 30 - November 3, 1989.

12. "Isotope effect in vibrational excitation of H_2 by low energy electron impact", (with D. E. Atems); presented at the Fifth International Symposium on the Production and Neutralization of Negative Ions and Beams, Upton, New York, October 30 - November 3, 1989.

13. "Gas phase alkali-hydrogen interactions in negative ion sources", (with H. H. Michels); presented at the Fifth International Symposium on the Production and Neutralization of Negative Ions and Beams, Upton, New York, October 30 - November 3, 1989.

14. "Energetics of neutral and negative ions of Li_mH_n clusters", Bull. Am. Phys. Soc. 35, 1177 (1990) (with H. H. Michels); presented at the 1990 annual meeting of the Division of Atomic, Molecular and Optical Physics, Monterey, California, May 21-23, 1990.

15. "Time - dependent behavior of positrons in noble gases", (with P. J. Drallos); presented at the Third International Workshop on Positron and Positronium Chemistry, Milwaukee, Wisconsin, July 16 - 18, 1990.

A novel algorithm for calculating the time evolution of the electron energy distribution function in gaseous discharges

P. J. Drallos and J. M. Wadehra
Department of Physics and Astronomy, Wayne State University, Detroit, Michigan 48202

(Received 12 November 1987; accepted for publication 22 January 1988)

We are presenting a novel numerical technique for obtaining the time evolution of the electron velocity and electron energy distribution functions in the presence of a uniform electric field. Using this technique, the various swarm parameters can be evolved for sufficiently long times so that equilibrium can be reached without incurring any numerical instabilities. Results are presented for electron swarms in gaseous neon for various values of E/N.

In nearly all aspects of gaseous electronics, the electron energy distribution is of fundamental importance. Knowledge of the electron energy distribution function (EEDF) is usually gained through its relation with the electron velocity distribution function (EVDF) which is a solution of the Boltzmann equation for a given set of collision cross sections. The Boltzmann equation can be solved analytically for an EEDF for only a few simple cases.[1] In practice, however, numerical methods have to be used for its solution. In traditional techniques for solving the Boltzmann equation, the distribution function is expanded in the Legendre polynomials—either a two-term expansion or a multiterm expansion—and the resulting set of equations are solved numerically for the equilibrium EEDF after making some simplifying approximations for the collision cross sections.

However, these expansion techniques do have some inherent drawbacks.[2] For example, the two-term expansion method breaks down for high values of E/N but works well for low E/N values. The EEDF under high E/N situations can, in principle, be obtained by taking more terms in the Legendre expansion of the Boltzmann equation. It is not always clear when the multiterm expansion is to be preferred over the two term, nor just how many terms in the expansion of the EEDF are to be included. The convergence behavior of a multiterm expansion, especially for high values of E/N, is also not completely understood. Furthermore, the cross sections, which are adjusted to reproduce the experimental swarm parameters in a two-term expansion, do not yield the same EEDF or the corresponding swarm parameters when used with a multiterm expansion and vice versa. It would be desirable, then, to have a procedure for obtaining the equilibrium EEDF and equilibrium EVDF that does not involve Legendre expansion of the distribution function. Here we have utilized a finite-difference scheme, previously used by Tagashira and co-workers,[3,4] in which no expansion of the EVDF in spherical harmonics is needed and the time evolution of the EVDF to its equilibrium value is obtained explicitly. Thus, the question of how many terms should be taken in the expansion of the EVDF, which is the solution of the Boltzmann equation, is completely avoided.

In this communication we present a novel algorithm for obtaining the time evolution of the EVDF numerically. This is accomplished by beginning with the Boltzmann equation which can be written as

$$\frac{\partial f(\mathbf{v},t)}{\partial t} + \mathbf{a}\cdot\nabla_{\mathbf{v}} f(\mathbf{v},t) = R(\mathbf{v},t), \tag{1}$$

where $\mathbf{a} = -(e\mathbf{E}/m)$ is the acceleration of the electrons of mass m due to the electric field $\mathbf{E}$, and $R(\mathbf{v},t)$ is the collision term containing all of the relevant cross sections. Now we multiply both sides of Eq. (1) by a finite time interval Δt and then add $f(\mathbf{v},t)$ to each side which yields,

$$f(\mathbf{v},t) + \left(\Delta t\frac{\partial}{\partial t} + \Delta\mathbf{v}\cdot\nabla_{\mathbf{v}}\right) f(\mathbf{v},t) = f(\mathbf{v},t) + R(\mathbf{v},t)\Delta t, \tag{2}$$

with $\Delta\mathbf{v} = \mathbf{a}\Delta t$ The terms on the left-hand side of Eq. (2) can be combined to yield the final result,

$$f(\mathbf{v}+\Delta\mathbf{v},t+\Delta t) = f(\mathbf{v},t) + R(\mathbf{v},t)\Delta t. \tag{3}$$

Equation (3) describes the time evolution of the EVDF and can thus be used to obtain the time evolution of the EEDF and the various electron swarm parameters. Note that Eq. (3) is entirely equivalent to Eq. (1) and is perhaps even more fundamental than Eq. (1), as Eq. (3) is a necessary step that one must go through in a textbook derivation of the Boltzmann equation.[5] In such a derivation, one would normally expand the left-hand side of Eq. (3) to first order in Δt, then take the limit $\Delta t \to 0$ to obtain the Boltzmann equation [Eq. (1)]. In the velocity space, the collision term $R(\mathbf{v},t)$ in Eq. (3) is difficult to evaluate in Cartesian coordinates, but straightforward in spherical coordinates since the collision cross sections depend only on the electron impact speed v. Thus, it might seem that spherical coordinates would be the natural choice for evaluation of Eq. (3). In their calculations, Kitamori, Tagashira, and Sakai[4] used spherical coordinates to evaluate the term $\mathbf{a}\cdot\nabla_{\mathbf{v}} f(\mathbf{v},t)$ of Eq. (1). This involves derivatives of f with respect to v and θ (polar coordinates in velocity space) which must be evaluated numerically. This procedure leads to strong numerical instabilities in the EVDF and is computationally expensive.

On the other hand, as we will now show, $f(\mathbf{v}+\Delta\mathbf{v},t+\Delta t)$ of Eq. (3) is extremely easy to evaluate in Cartesian coordinates. The acceleration of electrons along $\mathbf{E}$ (which we choose to be along the z direction) is constant, and is zero in the transverse directions. Thus, in Cartesian coordinates, Eq. (3) is written as

$$f[v_x, v_y, v_z - (eE/m)\Delta t, t+\Delta t] = f(v_x, v_y, v_z, t) + R(\mathbf{v},t)\Delta t. \tag{4}$$

Equation (4) is very well suited for evaluation on a computer. Since there is axial symmetry along v_z, f need only be stored as a function of v_z and v_x (or v_y) in such a way that the velocity increments Δv satisfy $\Delta v = (eE/m)\Delta t$. Evaluation

 0021-8979/88/115601-03$02.40

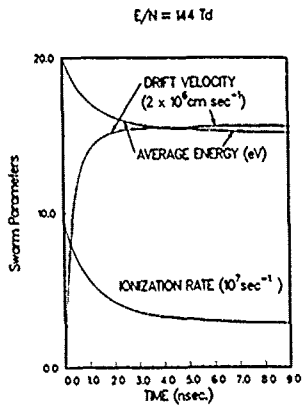

FIG 1 The time evolution of various electron swarm parameters in gaseous neon for $E/N = 144$ Td.

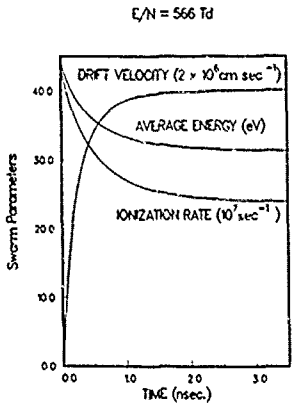

FIG. 3. The time evolution for various electron swarm parameters in gaseous neon for $E/N = 566$ Td.

of f in Eq. (4) then merely involves, in part, a shifting of the array $f(v_x,v_z)$ along v_z at each time interval Δt. This shifting procedure accomplishes all the acceleration effects of the electrons due to the electric field without incurring the related problems of numerical instabilities which arise mainly from the evaluation of derivatives. The evaluation of the collision term[4] in Eq. (4) involves an integral over the polar angle θ (in the velocity space) and requires a knowledge of the distribution function at various values of v and θ, that is, at various v-θ grid points in the velocity space. This integration can be carried out, even though f is known only as a function of v_x and v_z, by simply interpolating $f(v_x,v_z)$ to get $f(v,\theta)$.

Thus, the novel algorithm for evaluating the time evolution of the EVDF is as follows: Starting from a distribution function at some time t (a Maxwellian at $t = 0$, for example) which is stored in a two-dimensional array $f(v_x,v_z)$ such that $\Delta v = (eE/m)\Delta t$, the collision terms $R(v_x,v_z)$ for each v_x and v_z are calculated. These collision terms are then multiplied by Δt and added to the distribution function from which they were obtained in accordance with Eq. (4). The resulting array is then shifted along the v_z index $[f(v_x,v_z) \rightarrow f(v_x,v_z + \Delta v)]$ and it becomes the new distribution function at the later time $t + \Delta t$. This procedure is repeated while various swarm parameters are calculated from each new distribution function corresponding to a new time $t + \Delta t$. Equilibrium is obtained when the swarm parameters cease to change in time.

We have used this method to obtain the time evolution of various electron swarm parameters for the electron-neon system for various values of E/N. In all of our calculations we assumed an initial Maxwellian velocity distribution at $t = 0$ and a gas density N of $3.54 \times 10^{+16}$ cm^{-3} or 1.32×10^{-3} amagat (1 Torr at 273 K). The velocity steps Δv ranged from 2.2×10^7 to 3.4×10^7 cm/s and the time steps Δt ranged from 0.064 to 0.032 ns as E/N was varied from 144 to 566 Td. We point out that, in practice, Δt may be chosen to

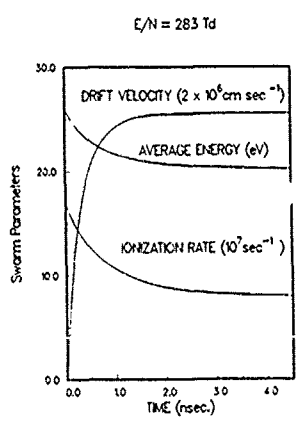

FIG 2 The time evolution for various electron swarm parameters in gaseous neon for $E/N = 283$ Td.

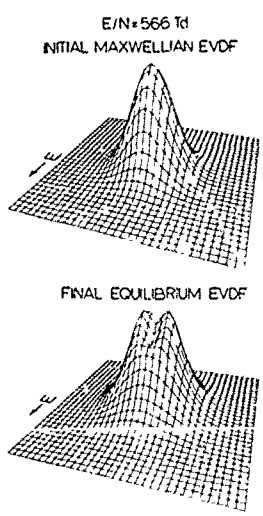

FIG. 4 The initial Maxwellian and final equilibrium electron velocity distribution function in neon for $E/N = 566$ Td.

be a proper fraction of $m\Delta v/eE$ and only this fraction of each element of the EVDF is shifted per time step. Such a procedure is observed to enhance the numerical stability. Another criterion for choosing Δt is that the term $R(v,t)\Delta t$ of Eq. (4) be smaller than $f(v,t)$ for all values of v. Figures 1–3 display the calculated time-dependent behavior of various electron swarm parameters in gaseous neon for three different values of E/N. The relevant collision cross sections were taken from Ref. 4. The equilibrium values of these swarm parameters are in very good agreement with those calculated by Kitamori, Tagashira, and Sakai.[4] We have also noted that the final equilibrium values of the swarm parameters are unaffected by the average energy value of the *initial* velocity distribution, although the transient behavior may be somewhat different. For example, an overshoot in the drift velocity is observed if the initial average energy of the distribution function is less than the final equilibrium value of the energy. Figure 4 shows the initial and final EVDF for the case $E/N = 566$ Td.

The FORTRAN 77 code which we used was less than 400 lines in length and required about 500 CPU seconds to reach equilibrium for $E/N = 566$ Td on an Amdahl 470/V6 mainframe computer.

The support of the U.S. Air Force Office of Scientific Research through Grant No. AFOSR-87-0342 is gratefully acknowledged.

[1] L. C. Pitchford, Technical Report No. AFWAL-TR-85-2016 (1985).
[2] L. C. Pitchford, S. V. O'Neil, and J. R. Rumble, Jr., Phys. Rev. A 23, 294 (1981).
[3] H. Tagashira, Y. Sakai, and S. Sakamoto, J. Phys. D 10, 1051 (1977).
[4] K. Kitamori, H. Tagashira, and Y. Sakai, J. Phys. D 11, 283 (1978).
[5] K. Huang, *Statistical Mechanics* (Wiley, New York, 1963), p. 57.

Formation of ground and excited states of antihydrogen

Sultana N. Nahar and J. M. Wadehra
Department of Physics and Astronomy, Wayne State University, Detroit, Michigan 48202
(Received 20 November 1987)

Differential and integrated cross sections for the formation of antihydrogen by the impact of intermediate-energy (20–500 keV) antiprotons on positronium are calculated using the first Born approximation. The calculations are carried out for the formation of antihydrogen in ground and various excited electronic states ($n=1-3$) when positronium, the target atom, is in the ground state, and for the formation of antihydrogen in the ground state when the positronium is in various excited electronic states ($n=1-2$). The $1/n^3$ behavior for the capture cross sections is used to calculate the total (that is, all states added together) integrated cross sections. The cross sections for the formation of antihydrogen presented here are obtained from those for the formation of positronium by the impact of positrons on hydrogen atoms by using charge invariance and the principle of detailed balance.

I. INTRODUCTION

Because of the recent availability of an antiproton beam at the Low-Energy Antiproton Ring (LEAR) facility at Organisation Européenne pour la Recherche Nucléaire (CERN), experiments for the formation of one of the simplest atoms of antimatter, namely, antihydrogen ($\bar{\mathrm{H}}$), are being proposed and planned.[1-4] One reason for the strong interest in the formation of antihydrogen is its relative stability compared to other exotic atoms such as muonium, protonium, positronium, etc., which makes it more suitable for carrying out experiments with antihydrogen for various diagnostic purposes. In the present work the cross sections are calculated for the formation of $\bar{\mathrm{H}}$ by positron (e^+) capture during the collisions of intermediate-energy (20–500 keV) antiprotons ($\bar{p}$) with positronium (Ps) using the first Born approximation (FBA). Schematically the processes are

$$\bar{p}+\mathrm{Ps}(1s)\rightarrow\bar{\mathrm{H}}(nlm)+e^- , \tag{1}$$

where $nlm=1s_0$, $2s_0$, $2p_0$, $2p_{\pm1}$, $3s_0$, $3p_0$, $3p_{\pm1}$, $3d_0$, $3d_{\pm1}$, and $3d_{\pm2}$, and

$$\bar{p}+\mathrm{Ps}(nlm)\rightarrow\bar{\mathrm{H}}(1s)+e^- , \tag{2}$$

where $nlm=1s_0$, $2s_0$, $2p_0$, and $2p_{\pm1}$. The $1/n^3$ behavior for the capture cross sections in the Born approximation is used to estimate the differential and integrated cross section for the formation of higher excited states of antihydrogen starting from the ground state of Ps as well as for the formation of ground state of $\bar{\mathrm{H}}$ starting from the higher excited states of Ps.

II. THEORY

Following earlier works,[2,3] the cross sections ($\sigma_{\bar{\mathrm{H}}}$) for the formation of $\bar{\mathrm{H}}$ by the impact of $\bar{p}$ on Ps of Eqs. (1) and (2) are, by charge invariance, the same as those for the formation of hydrogen (H) by the impact of protons (p) on positronium, that is,

$$\sigma_{\bar{\mathrm{H}}}=\sigma(\bar{p}+\mathrm{Ps}\rightarrow\bar{\mathrm{H}}+e^-)=\sigma(p+\mathrm{Ps}\rightarrow\mathrm{H}+e^+) . \tag{3}$$

Furthermore, the cross sections for the formation of H by the impact of protons on Ps are related, by the principle of detailed balance, to the cross sections for the formation of Ps by the impact of positrons on hydrogen. Hence one can write

$$\sigma_{\bar{\mathrm{H}}}=\sigma(p+\mathrm{Ps}\rightarrow\mathrm{H}+e^+)=\frac{k_i^2}{k_f^2}\sigma_{\mathrm{Ps}} . \tag{4}$$

σ_{Ps} is the cross section for the process

$$e^++\mathrm{H}(nlm)\rightarrow\mathrm{Ps}(1s)+p , \tag{5a}$$

or for the process

$$e^++\mathrm{H}(1s)\rightarrow\mathrm{Ps}(nlm)+p . \tag{5b}$$

$\hbar\mathbf{k}_i$ and $\hbar\mathbf{k}_f$ are the relative momenta of the positron (in the initial channel) and the positronium (in the final channel) of Eqs. (5). In the present work, the values of σ_{Ps} for the processes of Eqs. (5) for various sets of nlm are calculated first, and then Eq. (4) is used to obtain the values of the cross sections ($\sigma_{\bar{\mathrm{H}}}$) for the formation of antihydrogen which are now labeled σ_{nlm}.

The coordinate system used for calculating σ_{Ps} of Eqs. (5) is shown in Fig. 1. It is clear from Fig. 1 that $\mathbf{r}_i$ ($\mathbf{r}_f$) and $\mathbf{R}_i$ ($\mathbf{R}_f$) are the internal coordinate and the coordinate of the center of mass of the bound system in the in-

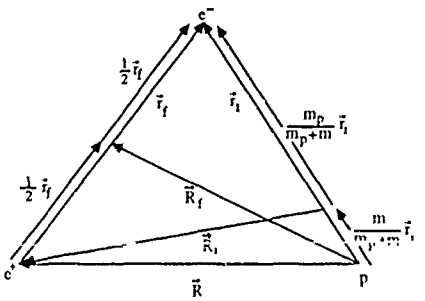

FIG. 1. The coordinate system for the processes of Eqs. (5).

tial (final) channel, respectively. R locates the incoming positron with respect to the proton. Atomic units are used throughout this paper unless specified otherwise. To obtain the impact energy of the positron for the processes of Eqs. (5) corresponding to an impact energy of the antiproton for the processes of Eqs. (1) and (2), conservation of momentum is used. Let $E=k_{\bar{p}}^2/2m_p$ be the laboratory impact energy of the antiproton of mass m_p with respect to the positronium at rest. Then the wave number k_f of the positronium with respect to the stationary antiproton is

$$k_f=m_{\mathrm{Ps}}k_{\bar{p}}/m_p\ , \tag{6}$$

where m_{Ps} is the mass of the positronium. Hence, in the frame of a stationary antiproton, the energy of the positronium is $k_f^2/(2m_{\mathrm{Ps}})$. The wave number k of the positron, of Eqs. (5), is obtained from the conservation of energy, namely,

$$k_i^2/(2\nu_i)=k_f^2/(2\nu_f)-\varepsilon_f+\varepsilon_i\ , \tag{7}$$

where ε_i and ε_f are the (positive) binding energies of H and Ps, respectively. If m is the mass of an electron (or a positron), then $\nu_i=m(m+m_p)/(2m+m_p)$ is the reduced mass of the system $(e^++\mathrm{H})$ in the initial channel and $\nu_f=2m_pm/(2m+m_p)$ is the reduced mass of the system $(\mathrm{Ps}+p)$ in the final channel of Eqs. (5). In the first Born approximation, the differential cross section for the processes (5) is related to the T-matrix element as

$$\frac{d\sigma}{d\Omega}=\frac{\nu_i\nu_f}{(2\pi)^2}\frac{k_f}{k_i}|T|^2\ , \tag{8}$$

where

$$T=\begin{cases}\langle\psi_f|V_i|\psi_i\rangle & \text{in the prior form}\ , \quad (9a)\\ \langle\psi_f|V_f|\psi_i\rangle & \text{in the post form}\ . \quad (9b)\end{cases}$$

ψ_i and ψ_f are the wave functions for the system (e^+,H) in the initial channel and the system (Ps,p) in the final channel, respectively; that is,

$$\psi_i=\exp(i\mathbf{k}_i\cdot\mathbf{R}_i)\phi_i(\mathbf{r}_i)$$

and (10)

$$\psi_f=\exp(i\mathbf{k}_f\cdot\mathbf{R}_f)\phi_f(\mathbf{r}_f)\ ,$$

where $\phi_i(\mathbf{r}_i)$ and $\phi_f(\mathbf{r}_f)$ are the bound-state wave functions of H and Ps, respectively. The initial and the final interaction potentials V_i and V_f are

$$V_i=V(R)-V(r_f)\ , \tag{11a}$$

$$V_f=V(R)-V(r_i)\ , \tag{11b}$$

where $V(x)=1/x$. The integrated cross section is given by

$$\sigma=2\pi\int_0^\pi\left|\frac{d\sigma}{d\Omega}\right|\sin\theta\,d\theta\ . \tag{12}$$

Substituting V_i and V_f from Eqs. (11) in the T-matrix elements, we get

$$T=\begin{cases}\langle\psi_f|V(R)|\psi_i\rangle-\langle\psi_f|V(r_f)|\psi_i\rangle & \\ \qquad=N_1+N_2\ \text{(prior form)}\ , & (13a)\\ \langle\psi_f|V(R)|\psi_i\rangle-\langle\psi_f|V(r_i)|\psi_i\rangle & \\ \qquad=N_1+N_3\ \text{(post form)}\ . & (13b)\end{cases}$$

These T-matrix terms, N_1, N_2, and N_3, can be evaluated[5] easily for the cases when only the spherically symmetric states are involved. Such cases, for example, are the formation of Ps(1s) from different s states of H of Eq. (5a) or the formation of different s states of Ps from H(1s) of Eq. (5b). Complexity arises when the initial or the final bound-state wave functions in Eqs. (5) are not spherically symmetric as in the case of formation of Ps in the p or d state or when the target H is in an excited p state. The complexity due to the nonspherical wave functions can be reduced by expressing the angular dependence of the wave functions in terms of derivatives of an exponential factor $\exp(i\,\mathbf{A}\cdot\mathbf{r})$, where the value of the parameter A is eventually set to zero. In particular, for the processes (5a) we introduce a function $X_i(\mathbf{r})$ as follows:

$$X_i(nlm,\mathbf{r})=\rho(nlm,r)\exp(i\,\mathbf{A}\cdot\mathbf{r})\ , \tag{14}$$

where $\rho(nlm,r)$ represents R_{nl}, the radial part of the wave function of hydrogen, multiplied by the constants of Y_{lm}, the angular part of the wave function. Then the complete bound-state wave functions $\phi_i(\mathbf{r})$, of Eq. (10), can be obtained by merely taking the appropriate derivatives of $X_i(\mathbf{r})$ with respect to either A_x or A_y or A_z and then setting $\mathbf{A}=0$. As an example, for the $3d_0$ state of hydrogen, the wave function is

$$\begin{aligned}\phi_i(3d_0,\mathbf{r})&=R_{32}(r)\left[\frac{5}{16\pi}\right]^{1/2}(3\cos^2\theta-1)\\ &=\rho(3d_0,r)\left[\frac{z^2}{r^2}-\frac{1}{3}\right]\\ &=\left[-\frac{d^2}{dA_z^2}[\exp(i\,\mathbf{A}\cdot\mathbf{r})\rho(3d_0,r)/r^2]-\exp(i\,\mathbf{A}\cdot\mathbf{r})\rho(3d_0,r)/3\right]_{\mathbf{A}=0}\\ &=\left[-\frac{d^2}{dA_z^2}[X_i(3d_0,\mathbf{r})/r^2]-X_i(3d_0,\mathbf{r})/3\right]_{\mathbf{A}=0}\ ,\end{aligned} \tag{15}$$

where, using the explicit form of R_{32},

$$\rho(3d_0,r)=\frac{1}{27\sqrt{6\pi}}r^2\exp(-r/3)\ . \quad (16)$$

This kind of trick has been used earlier by Sil *et al.*[6] in calculations of charge-transfer cross sections.

Let Q_i and Q_f be the momentum-transfer vectors in the initial and final channel, respectively, i.e.,

$$Q_i=[m_p/(m+m_p)]k_i-k_f,\quad Q_f=k_f/2-k_i \quad (17)$$

and let μ be the reduced mass of the final atom positronium of the processes (5). Then the parts of the T-matrix elements for the processes (5a), upon replacing $\phi_i(r)$ by $\chi_i(nlm,r)$ of Eq. (14), can be written as

$$N_1=(2\pi)^{3/2}\int\tilde{\phi}_f^*(Q_f-t)\tilde{v}(t)\tilde{\rho}(-t-Q_i-A)d^3t\ , \quad (18a)$$

$$N_2=-(2\pi)^3\left[\left(\frac{Q_f^2}{2\mu}+\varepsilon_f\right)\tilde{\phi}_f^*(Q_f)\tilde{\rho}(-Q_i-A)\right]\ , \quad (18b)$$

$$N_3=-(2\pi)^{3/2}\tilde{\phi}_f^*(Q_f)\int\tilde{v}(t)\tilde{\rho}(-t-Q_i-A)d^3t\ , \quad (18c)$$

where the overtilde represents the Fourier transform of the respective function. For example, the Fourier transform $\tilde{f}(t)$ of a function $f(r)$ is defined as

$$\tilde{f}(t)=(2\pi)^{-3/2}\int d^3r\exp(-it\cdot r)f(r)\ .$$

Substituting the explicit forms for the potential V_i and the wave functions ϕ_i and ϕ_f, the term N_1 incurs an integral of the form

$$I_1=\int d^3t\frac{1}{(t-P)^2+p^2}\frac{1}{(t-B)^2+b^2}\frac{1}{t^2+z^2}\ , \quad (19)$$

which, upon using the Feynman identity, can be reduced to a one-dimensional integral as[5]

$$I_1=\pi^2\int_0^1\frac{dx}{E[F^2+(E+z)^2]}\ , \quad (20)$$

where $E^2=x(1-x)(P-B)^2+xp^2+(1-x)b^2$ and $F=(P-B)x+B$. N_2 can be written in a pure analytic fashion. The term N_3 involves integral of the form

$$I_3=\int d^3t\frac{1}{[(t-P)^2+p^2]^2}\frac{1}{t^2+z^2} \quad (21)$$

which can be done analytically to obtain

$$I_3=\pi^2\frac{1}{p[P^2+(p+z)^2]}\ . \quad (22)$$

Integral I_3 of Eq. (21) easily follows from integral I_1 of Eq. (19) by setting $P=B$ and $p=b$. P, B, p, b, and z of Eqs. (19) and (21) are, of course, related to Q_i, Q_f and the parameter A of Eqs. (18a) and (18c). In the case of p- and d-state wave functions, N_1, N_2, and N_3 will involve derivatives with respect to the Cartesian components of A. Note that since ϕ_{nlm} is a complex conjugate of ϕ_{nl-m}, and $|T|^2$ is used to calculate the cross section, the cross sections with both the wave functions ($\phi_{nl\pm m}$) are the same. This technique of using the derivatives of the factor $\exp(i\,A\cdot r)$ for representing the angular dependence of the wave functions can also be used for the formation of various excited states of Ps from H(1s) of Eq. (5b). In this case the factor $\exp(i\,A\cdot r)$ is introduced in the final bound-state wave function $\phi_f(r)$ rather than in the initial bound-state wave function $\phi_i(r)$. Thus after calculating the cross sections for the processes of Eqs. (5), the corresponding cross sections for the formation of antihydrogen are obtained using Eq. (4).

It was predicted by Oppenheimer[7] that the cross section for capture into any ns excited hydrogenic state at high incident energies falls as $1/n^3$. Later, Omidvar[8] showed that the cross section for the capture into s, p, and d states as well as the sum of the cross sections over lm states falls as $1/n^3$ in the first Born approximation. There is also an experimental evidence of the cross section for electron capture into excited states falling as $1/n^3$ in collisions of high-energy fluorine ions with argon.[9] Hence using the $1/n^3$ dependence of the capture cross sections of Eq. (1) for the formation of H in excited states ($n\geq 4$), the total cross section could be written as

$$\sigma_T=\sigma_1+\sigma_2+\sigma_3\left[1+\left(\frac{n}{n+1}\right)^3+\left(\frac{n}{n+2}\right)^3+\left(\frac{n}{n+3}\right)^3+\cdots\right], \quad (23)$$

where

$$\begin{aligned}\sigma_1&=\sigma_{1s_0}\ ,\\ \sigma_2&=\sigma_{2s_0}+\sigma_{2p_0}+2\sigma_{2p_1}\ ,\\ \sigma_3&=\sigma_{3s_0}+\sigma_{3p_0}+2\sigma_{3p_1}+\sigma_{3d_0}+2\sigma_{3d_1}+2\sigma_{3d_2}\ ,\end{aligned} \quad (24)$$

and $n=3$. The value of the series within the large square brackets of Eq. (23) is 2.0805 for $n=3$. In the case of H(1s) formation from various states of Ps, of Eq. (2), the $1/n^3$ rule is used for positronium states $n\geq 3$. Hence using $n=2$ the value of the series within the large square brackets of Eq. (23) is 1.616.

III. RESULTS AND DISCUSSIONS

The present work on charge-transfer processes has been carried out using both the prior and the post forms of the interaction. The difference in the values of the cross sections using these two forms of the interaction (that is, the post-prior discrepancy) is quite small (a few parts in a thousand). Hence only the prior form of the results is presented. The n^{-3} behavior for the capture cross sections is used for antihydrogen formation in states $n\geq 4$ from Ps(1s) [see Eq. (1)] and for $\bar{H}$(1s) formation from Ps in states $n\geq 3$ [see Eq. (2)]. The differential cross sections (DCS's) for the formation of antihydrogen in all states (ground and all possible excited states added together) by the impact of antiprotons on positronium in ground state are shown in Fig. 2 and those for the formation of antihydrogen in the ground state from all possible states of positronium are shown in Fig. 3. From Figs. 2 and 3 we see that the nature of the DCS curves in these two cases are very similar. DCS curves in Fig. 2 show

that following the forward peak there is a very shallow minimum at lower energies that deepens with increasing antiproton impact energies while its position stays at roughly the same angle (~24°). At larger scattering angles, the values of DCS's fall smoothly at all energies. Similar is the case with the curves of Fig. 3, except that the minima in the DCS values at lower impact energies are more pronounced than those of Fig. 2. The minima in the DCS curves arise from the opposite nature (attractive versus repulsive) of antiproton-positron and antiproton-electron interactions; essentially the N_1 and the N_2 parts of the T-matrix element [Eq. (13)] cancel one another. The integrated cross sections for the formation of antihydrogen in individual states $1s_0$, $2s_0$, $2p_0$, $2p_1$, $3s_0$, $3p_0$, $3p_1$, $3d_0$, $3d_1$, $3d_2$, as well as in all possible states, using the n^{-3} behavior, from Ps($1s$), are numerically presented in Table I and are shown in Fig. 4. The integrated cross sections for the formation of $\bar{H}(1s)$ from Ps in individual states $1s_0$, $2s_0$, $2p_0$, $2p_1$, as well as in all possible states, using the n^{-3} behavior, are numerically presented in Table II and are shown in Fig. 5. All the curves for integrated cross sections in Figs. 4 and 5 decay very smoothly with increasing $\bar{p}$ impact energies. From Table I and Fig. 4 we see that formation of the p and d states of antihydrogen dominates over the formation of any other state at lower antiproton impact energy (<50 keV). However, at higher impact energies the formation of $\bar{H}(1s)$ dominates over the formation of all other states. In case of formation of $\bar{H}(1s)$ from various states of Ps, as seen in Table II and Fig. 5, the formation from Ps($1s$) dominates significantly over formation from any other state of positronium almost at all energies considered.

The use of $1/n^3$ behavior of the capture cross sections for the entire range of antiproton impact energies to calculate the cross sections for states $n \gtrsim 4$ for processes of Eq. (1) and for states $n \gtrsim 3$ for processes of Eq. (2) is

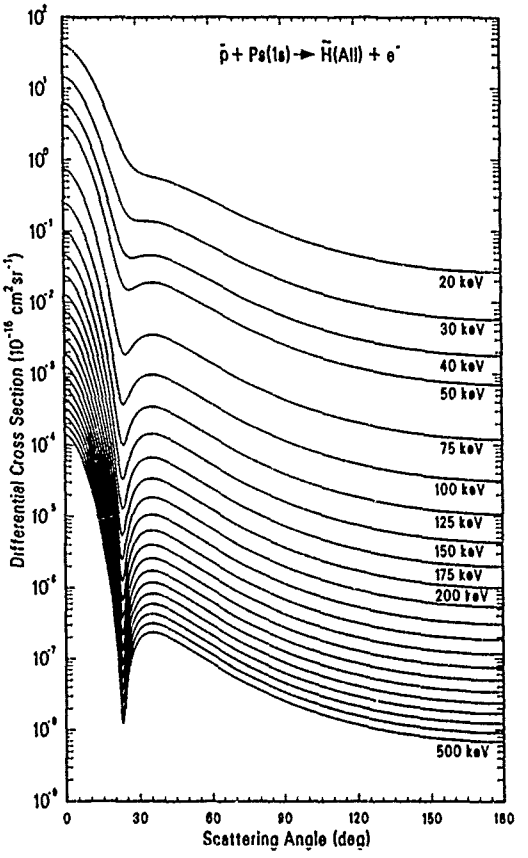

FIG 2. The differential cross sections for the formation of antihydrogen in all possible states by the impact of antiprotons on Ps($1s$), Eq. (1). The DCS curves between 200 and 500 keV correspond to sequential increase of impact energy at an interval of 25 keV.

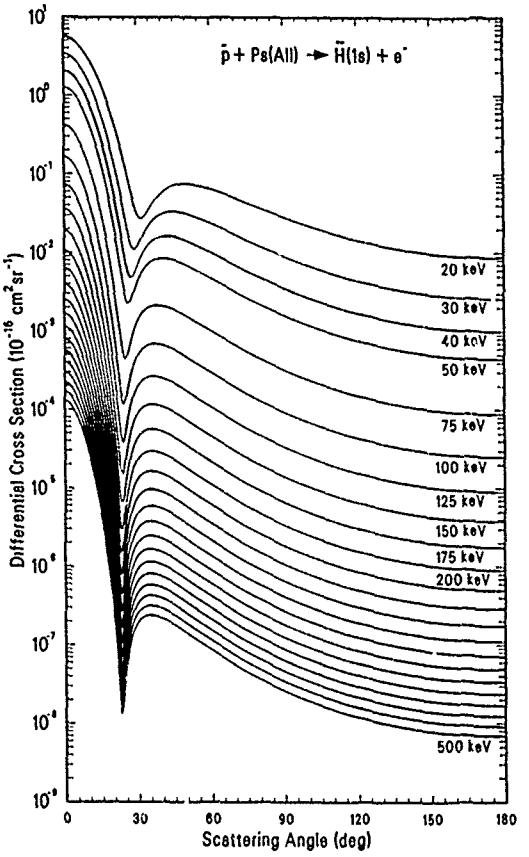

FIG. 3. The differential cross sections for the formation of antihydrogen in the ground state by the impact of antiprotons on all possible states of positronium, Eq. (2) The DCS curves between 200 and 500 keV correspond to sequential increase of impact energy at an interval of 25 keV.

found to be quite reasonable. For example, the value of the ratio $(n+1)^3\sigma_{n+1}/n^3\sigma_n$, which ideally should be 1 if the $1/n^3$ behavior is valid, is 1.54 at 20 keV and 1.07 at 500 keV for the process of Eq. (1) when $n=2$. The same ratio for the process of Eq. (2) is 1.26 at 20 keV and 1.02 at 500 keV for $n=1$. These numbers suggest that the use of $1/n^3$ rule holds relatively more accurately at higher impact energies than at lower impact energies.

In the earlier works, Neuman *et al.*[1] have carried out a laser-enhanced electron-ion–capture calculation to evaluate the rate of total recombination for antihydrogen formation. Humberston *et al.*[2] presented the values of cross sections for the formation of $\overline{\mathrm{H}}(1s)$ from Ps(1*s*) at lower impact energies using the *s*-, *p*-, and *d*-wave positronium-formation phase shifts obtained by elaborate variational calculations. Later, Darewych[3] calculated the cross sections for the formation of $\overline{\mathrm{H}}$ in states $1s_0$, $2s_0$, $2p$ (all m), and $3s_0$ from Ps(1*s*) at low antiproton impact energies using the first Born approximation (FBA). Since the FBA is not a good approximation for scattering calculations at low projectile energies, the present work is carried out in an intermediate range of impact energies. However, for computational checking purposes, cross sections at a few low impact energies were calculated and it was observed that both Ref. 3 and the present work agree very well for the formation of $\overline{\mathrm{H}}$ in *s* states, while the values of the cross sections for $2p$- (all m) state formation in the present work are much larger than those of Ref. 3. As a

TABLE I The values of the integrated cross sections ($\sigma_{\overline{\mathrm{H}}}$) for the formation of $\overline{\mathrm{H}}$ in ground and various excited states as well as in all possible states by the impact of $\bar{p}$ on Ps(1*s*) in the incident-energy range of $E=20$–500 keV. The notation a[b] for the values of the cross sections means $a\times10^b$.

	$\sigma_{\overline{\mathrm{H}}}$ (10^{-16} cm^2) at various $\bar{p}$ energies, E (keV)							
States	$E=20$	30	40	50	75	100	125	150
$1s_0$	0.1048[1]	0.4640	0.2302	0.1242	0.3425[−1]	0.1208[−1]	0.5025[−2]	0.2352[−2]
$2s_0$	0.2780	0.1109	0.5372[−1]	0.2837[−1]	0.7344[−2]	0.2438[−2]	0.9624[−3]	0.4315[−3]
$2p_0$	0.9554	0.2794	0.9847[−1]	0.3994[−1]	0.6384[−2]	0.1516[−2]	0.4643[−3]	0.1697[−3]
$2p_1$	0.4057	0.1001	0.3150[−1]	0.1176[−1]	0.1643[−2]	0.3593[−3]	0.1040[−3]	0.3646[−4]
$3s_0$	0.1149	0.4015[−1]	0.1862[−1]	0.9648[−2]	0.2439[−2]	0.7973[−3]	0.3112[−3]	0.1383[−3]
$3p_0$	0.3173	0.1009	0.3674[−1]	0.1511[−1]	0.2429[−2]	0.5741[−3]	0.1747[−3]	0.6345[−4]
$3p_1$	0.1264	0.3439[−1]	0.1124[−1]	0.4270[−2]	0.6042[−3]	0.1321[−3]	0.3813[−4]	0.1333[−4]
$3d_0$	0.9331[−1]	0.2305[−1]	0.6651[−2]	0.2241[−2]	0.2451[−3]	0.4359[−4]	0.1061[−4]	0.3211[−5]
$3d_1$	0.5982[−1]	0.1323[−1]	0.3564[−2]	0.1144[−2]	0.1157[−3]	0.1961[−4]	0.4613[−5]	0.1360[−5]
$3d_2$	0.1886[−1]	0.3340[−2]	0.7996[−3]	0.2379[−3]	0.2149[−4]	0.3417[−5]	0.7709[−6]	0.2206[−6]
All	0.5039[1]	0.1608[1]	0.6393	0.2957	0.6499[−1]	0.2035[−1]	0.7873[−2]	0.3514[−2]
	$E=175$	200	225	250	275	300	325	350
$1s_0$	0.1204[−2]	0.6611[−3]	0.3843[−3]	0.2340[−3]	0.1483[−3]	0.9710[−4]	0.6546[−4]	0.4525[−4]
$2s_0$	0.2131[−3]	0.1136[−3]	0.6438[−4]	0.3837[−4]	0.2385[−4]	0.1537[−4]	0.1021[−4]	0.6969[−5]
$2p_0$	0.7069[−4]	0.3256[−4]	0.1624[−4]	0.8637[−5]	0.4848[−5]	0.2847[−5]	0.1737[−5]	0.1096[−5]
$2p_1$	0.1471[−4]	0.6604[−5]	0.3225[−5]	0.1686[−5]	0.9324[−6]	0.5405[−6]	0.3262[−6]	0.2038[−6]
$3s_0$	0.6786[−4]	0.3598[−4]	0.2030[−4]	0.1206[−4]	0.7478[−5]	0.4808[−5]	0.3189[−5]	0.2173[−5]
$3p_0$	0.2629[−4]	0.1205[−4]	0.5984[−5]	0.3172[−5]	0.1775[−5]	0.1039[−5]	0.6325[−6]	0.3981[−6]
$3p_1$	0.5360[−5]	0.2399[−5]	0.1169[−5]	0.6096[−6]	0.3364[−6]	0.1946[−6]	0.1173[−6]	0.7315[−7]
$3d_0$	0.1141[−5]	0.4583[−6]	0.2030[−6]	0.9738[−7]	0.4990[−7]	0.2704[−7]	0.1537[−7]	0.9112[−8]
$3d_1$	0.4729[−6]	0.1864[−6]	0.8111[−7]	0.3822[−7]	0.1923[−7]	0.1023[−7]	0.5702[−8]	0.3309[−8]
$3d_2$	0.7495[−7]	0.2901[−7]	0.1244[−7]	0.5791[−8]	0.2884[−8]	0.1520[−8]	0.8408[−9]	0.4846[−9]
All	0.1740[−2]	0.9323[−3]	0.5317[−3]	0.3190[−3]	0.1997[−3]	0.1295[−3]	0.8656[−4]	0.5941[−4]
	$E=375$	400	425	450	475	500		
$1s_0$	0.3198[−4]	0.2304[−4]	0.1690[−4]	0.1259[−4]	0.9512[−5]	0.7280[−5]		
$2s_0$	0.4869[−5]	0.3473[−5]	0.2524[−5]	0.1864[−5]	0.1398[−5]	0.1062[−5]		
$2p_0$	0.7121[−6]	0.4746[−6]	0.3236[−6]	0.2251[−6]	0.1595[−6]	0.1149[−6]		
$2p_1$	0.1312[−6]	0.8677[−7]	0.5874[−7]	0.4060[−7]	0.2860[−7]	0.2049[−7]		
$3s_0$	0.1517[−5]	0.1081[−5]	0.7844[−6]	0.5790[−6]	0.4338[−6]	0.3294[−6]		
$3p_0$	0.2581[−6]	0.1716[−6]	0.1168[−6]	0.8112[−7]	0.5738[−7]	0.4127[−7]		
$3p_1$	0.4703[−7]	0.3106[−7]	0.2100[−7]	0.1450[−7]	0.1020[−7]	0.7301[−8]		
$3d_0$	0.5604[−8]	0.3560[−8]	0.2328[−8]	0.1562[−8]	0.1074[−8]	0.7534[−9]		
$3d_1$	0.1989[−8]	0.1233[−8]	0.7860[−9]	0.5133[−9]	0.3426[−9]	0.2332[−9]		
$3d_2$	0.2896[−9]	0.1786[−9]	0.1132[−9]	0.7361[−10]	0.4893[−10]	0.3319[−10]		
All	0.4173[−4]	0.2991[−4]	0.2184[−4]	0.1620[−4]	0.1219[−4]	0.9303[−5]		

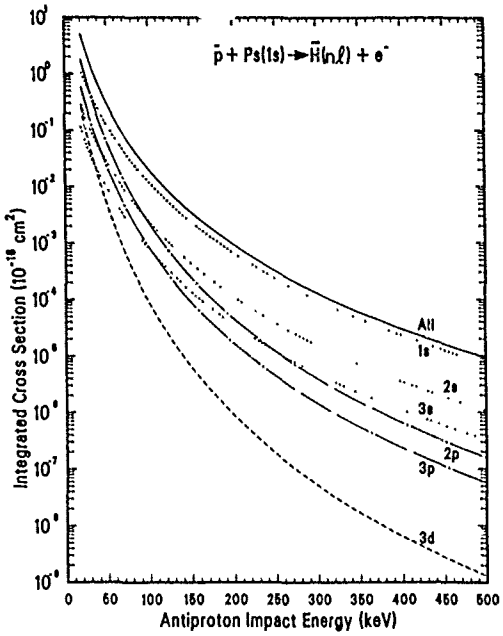

FIG. 4 The integrated cross sections for the formation of antihydrogen in various s, p, and d states (summed over m quantum numbers) by the impact of antiprotons on Ps(1s), Eq. (1). The solid curve corresponds to the total integrated (i.e., sum of all possible nl states of antihydrogen) cross sections.

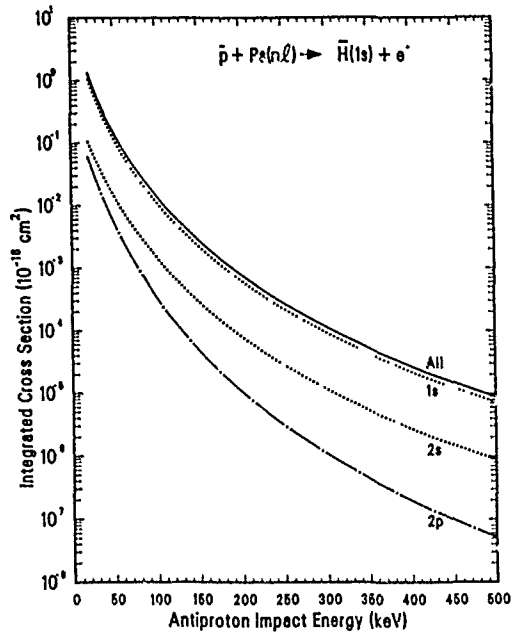

FIG. 5. The integrated cross sections for the formation of antihydrogen in the ground state by the impact of antiprotons on positronium in various s and p states (summed over m quantum numbers), Eq. (2). The solid curve corresponds to the total integrated (i.e., sum of all possible nl states of positronium) cross sections.

TABLE II. The values of the integrated cross sections ($\sigma_{\bar{H}}$) for the formation of $\bar{H}(1s)$ by the impact of $\bar{p}$ on ground and various excited states as well as on all possible states of Ps in the incident-energy range of $E = 20$–500 keV. The notation a[b] for the values of the cross sections means $a \times 10^b$.

	Ps state $\sigma_{\bar{H}}$ (10^{-16} cm^2)				
E (keV)	$1s_0$	$2s_0$	$2p_0$	$2p_1$	All
20	0.1048[1]	0.1054	0.3934[−1]	0.1020[−1]	0.1315[1]
30	0.4640	0.5235[−1]	0.1659[−1]	0.4220[−2]	0.5890
40	0.2302	0.2757[−1]	0.7753[−2]	0.1877[−2]	0.2933
50	0.1242	0.1539[−1]	0.3896[−2]	0.8978[−3]	0.1583
75	0.3425[−1]	0.4408[−2]	0.8889[−3]	0.1854[−3]	0.4341[−1]
100	0.1208[−1]	0.1572[−2]	0.2622[−3]	0.5093[−4]	0.1521[−1]
125	0.5025[−2]	0.6545[−3]	0.9291[−4]	0.1711[−4]	0.6288[−2]
150	0.2352[−2]	0.3054[−3]	0.3773[−4]	0.6665[−5]	0.2928[−2]
175	0.1204[−2]	0.1555[−3]	0.1702[−4]	0.2907[−5]	0.1492[−2]
200	0.6611[−3]	0.8490[−4]	0.8342[−5]	0.1387[−5]	0.8163[−3]
225	0.3843[−3]	0.4903[−4]	0.4375[−5]	0.7106[−6]	0.4729[−3]
250	0.2340[−3]	0.2967[−4]	0.2427[−5]	0.3864[−6]	0.2872[−3]
275	0.1483[−3]	0.1867[−4]	0.1411[−5]	0.2208[−6]	0.1814[−3]
300	0.9710[−4]	0.1216[−4]	0.8544[−6]	0.1316[−6]	0.1186[−3]
325	0.6546[−4]	0.8146[−5]	0.5355[−6]	0.8132[−7]	0.7975[−4]
350	0.4525[−4]	0.5599[−5]	0.3459[−6]	0.5187[−7]	0.5503[−4]
375	0.3198[−4]	0.3936[−5]	0.2295[−6]	0.3401[−7]	0.3882[−4]
400	0.2304[−4]	0.2823[−5]	0.1558[−6]	0.2285[−7]	0.2793[−4]
425	0.1690[−4]	0.2060[−5]	0.1081[−6]	0.1569[−7]	0.2046[−4]
450	0.1259[−4]	0.1528[−5]	0.7639[−7]	0.1099[−7]	0.1522[−4]
475	0.9512[−5]	0.1150[−5]	0.5492[−7]	0.7829[−8]	0.1149[−4]
500	0.7280[−5]	0.8768[−6]	0.4010[−7]	0.5668[−8]	0.8781[−5]

check on the present computer code, the cross sections[10] for the formation of H, by the process of electron capture during proton-hydrogen collisions, in states $1s$ and $2p$ were reproduced.

In conclusion, we have presented a simple first Born calculation of cross sections for the formation of antihydrogen, by the impact of intermediate-energy (20–500 keV) antiprotons on positronium, in ground and in various excited states.

ACKNOWLEDGMENT

We gratefully acknowledge the support of the U.S. Air Force Office of Scientific Research through Grant No. AFOSR-87-0342.

[1]J. Berger *et al.*, CERN Report No. PSCC 1985, p. 86 (unpublished), (quoted in Ref. 2); R. Neuman, H. Poth, A. Winnacker, and A Wolf, Z. Phys. A **313**, 253 (1983).

[2]J. W. Humberston, M. Charlton, F. M. Jacobsen, and B. I. Deutch, J. Phys. B **20**, L25 (1987).

[3]J. W. Darewych, in Abstracts of the NATO Advanced Reserach Workshop on Atomic Physics with Positrons, University College London, 1987 [J. Phys. B **20**, 5917 (1987)].

[4]B. I. Deutch, F. M. Jacobsen, L. H. Andersen, P. Hvelplund, H. Knudsen, M. Holzscheiter, M. Charlton, and G. Laricchia (private communication).

[5]R. Shakeshaft and J. M. Wadehra, Phys. Rev. A **22**, 968 (1980); Sultana N. Nahar and J. M. Wadehra, *ibid.* **35**, 4533 (1987).

[6]N. C. Sil, B. C. Saha, H. P. Saha, and P. Mandal, Phys. Rev. A **19**, 655 (1979)

[7]J. R. Oppenheimer, Phys. Rev. **31**, 349 (1928).

[8]K. Omidvar, Phys. Rev. A **12**, 911 (1975).

[9]J. R. Macdonald, P. Richard, C. L Cocke, M. Brown, and I. A. Sellin, Phys. Rev. Lett. **31**, 684 (1973).

[10]D. R. Bates and A. Dalgarno, Proc. Phys. Soc. London, Sect. A **66**, 972 (1953)

Approximate Green's Functions in Electron (Positron)–Atom Collisions

The role of approximate Green's functions in electron (positron)–atom collisions is discussed. It is explicitly demonstrated that the scattering amplitude in various approximation methods, like the Massey–Mohr, simplified second Born, plane wave (adiabatic as well as nonadiabatic), Glauber (with and without the Wallace correction), eikonal Born series (including unitarization) and Schwinger variational principle, is obtained by mere approximations of the relevant Green's function. Some of the shortcomings of different methods are pointed out. It is shown that the Schwinger variational method with suitable choice of trial wave function yields practically the same values of the differential and integrated cross sections for the elastic scattering as well as the total collisional scattering for the $e^{\pm}$-H system as obtained by the use of the unitarized eikonal Born series method.

Key Words: *electron–atom scattering, positron–atom scattering, Green's functions, approximate methods*

It is well known that an exact evaluation of the electron (positron)–atom scattering amplitude is not possible at present. A number of approximate methods starting from the Lippmann–Schwinger integral equation have been developed for an evaluation of the direct scattering amplitude.[1] In this paper we will explicitly demonstrate that most of these approximate methods for evaluating the scattering amplitude employ different approximate forms of the Green's function. We will also compare somewhat in detail the numerical results of the elastic and total scattering of electrons and positrons by a hydrogen atom obtained recently by Byron et al.[2] using the unitarized eikonal Born series (UEBS) method and by Khare and co-workers[3,4] using the Schwinger variational (SV) principle.

Comments At. Mol. Phys.
1989, Vol. 23, Nos. 1 & 2, pp. 55–68
Reprints available directly from the publisher
Photocopying permitted by license only

The exact direct scattering amplitude for the $e^{\mp}$-atom scattering from the initial target state i to the final state f is given by[1]

$$f^{fi}(\mathbf{k}_f,\mathbf{k}_i) = -2\pi^2 \langle \mathbf{k}_f, f | U \sum_{n=1}^{\infty} (G_0^+ U)^{n-1} | \mathbf{k}_i, i \rangle \equiv \sum_{n=1}^{\infty} \bar{f}_{Bn} \qquad (1)$$

with

$$f_{Bp} = \sum_{n=1}^{p} \bar{f}_{Bn}.$$

Here $\mathbf{k}_i$ and $\mathbf{k}_f$ are initial and final momenta of the projectile and U is the reduced interaction energy, that is, $U = (2m/\hbar^2)\, V$ where V is the actual total Coulomb interaction between the projectile (electron or positron) and the target atom. G_0^+ is the free Green's function of the noninteracting projectile and target. The Green's function G_0^+ is given by

$$G_0^+ = \mathrm{S} \int \frac{|\mathbf{q},m\rangle \langle \mathbf{q},m|}{k_m^2 - q^2 + i\epsilon}\, d\mathbf{q} \qquad (2)$$

where $|\mathbf{q}\rangle$ and $|m\rangle$ are the intermediate states of the projectile and target, respectively, and $k_m^2 = k_i^2 - 2(E_m - E_i)$, E_m and E_i being the intermediate and initial target state energies. (We will use atomic units, that is, $\hbar = 1$, $m = 1$ and $e = 1$ unless stated explicitly otherwise). The nth term of series (1), $\bar{f}_{Bn}$, is referred to as the nth Born term and f_{Bp} is the pth Born approximation for the scattering amplitude. The nonconvergence of the Born series for rearrangement collisions, including the exchange effects, was explicitly demonstrated by Aaron et al.[5] We may remark that the investigations of Rosenberg[6] strongly suggest that the Born series for the direct scattering amplitude for the $e^{\mp}$-atom system may also not converge. Furthermore, the evaluation of $\bar{f}_{Bn}$, for $n > 1$, is extremely difficult due to the presence of the operator $(G_0 + U)^{n-1}$. The first Born term, $\bar{f}_{B1}$, which does not contain G_0^+, is easy to evaluate. However, it completely neglects the effects due to distortions of the wave functions of the projectile and the target. The Green's function contains these effects through the intermediate states $|\mathbf{q}\rangle$ and $|m\rangle$. Different approximations, which have been developed to obtain $f^{fi}(\mathbf{k}_f,\mathbf{k}_i)$ using an integral equation approach, treat the Green's function in different approximate ways.

For fast projectiles the most important correction to $\bar{f}_{B1}$ is the

second Born term $\bar{f}_{B2}$ given by

$$\bar{f}_{B2}(\mathbf{k}_f,\mathbf{k}_i) = -2\pi^2 \langle \mathbf{k}_f,f|UG_0^+U|\mathbf{k}_i,i\rangle. \tag{3}$$

An exact evaluation, either analytical or numerical, of $\bar{f}_{B2}$ is an involved problem. So far only Ermolaeve and Walters[7] have succeeded in this task. Their numerical method has been discussed briefly by Walters.[8]

The first attempt for an approximate analytical evaluation of $\bar{f}_{B2}$ was made by Massey and Mohr.[9] They replaced k_m^2 by k_i^2 in (2) for all values of m. Then using the closure relation one obtains the Green's function $G_0^+(\mathbf{R},\mathbf{R}';\ \mathbf{x},\mathbf{x}') = \langle \mathbf{R},\mathbf{x}|G_0^+|\mathbf{R}',\mathbf{x}'\rangle$ in the Massey–Mohr approximation given by

$$G_{0M}^+(\mathbf{R},\mathbf{R}';\ \mathbf{x},\mathbf{x}') = G_{0p}^+(\mathbf{R},\mathbf{R}')\ \delta(\mathbf{x} - \mathbf{x}'), \tag{4}$$

where $\mathbf{R}$ and $\mathbf{x}$ are the coordinates of the projectile (electron or positron) and the bound state electrons of the target, respectively. G_{0p}^+ is the free particle Green's function of the projectile only and is given, in operator form, by

$$G_{0p}^+ = \int \frac{|\mathbf{q}\rangle\langle\mathbf{q}|}{k_i^2 - q^2 + i\epsilon}\, d\mathbf{q} \tag{5}$$

Use of (4) and (5) in (3) yields an integral expression for $\bar{f}_{B2}$ which does not contain intermediate target states $|m\rangle$ and the integration over $\mathbf{x}'$ becomes trivial due to the presence of the delta function $\delta(\mathbf{x} - \mathbf{x}')$. Thus, in the Massey–Mohr approximation we have

$$\bar{f}_{B2M}(\mathbf{k}_f,\mathbf{k}_i) = \langle f|\bar{f}_{B2}(\mathbf{x})|i\rangle \tag{6}$$

where $\bar{f}_{B2}(\mathbf{x})$ is the second Born scattering term for the scattering of the projectile by a target, in which the bound electrons are frozen at the position $\mathbf{x}$, and is given by

$$\bar{f}_{B2}(\mathbf{x}) = -2\pi^2 \langle \mathbf{k}_f|UG_{0p}^+U|\mathbf{k}_i\rangle. \tag{7}$$

It is evident from (6) and (7) that the *Massey–Mohr approximation completely neglects the effects due to the distortion of the target wave function*. Since this approximation assumes the excitation energies to be zero, it turns out[1] that for the elastic scattering

the imaginary part of the second Born term, Im $\bar{f}_{B2M}$, diverges in the forward direction and, for e^--atom elastic scattering, the real part in the forward direction, Re $\bar{f}_{B2M}(0)$, asymptotically goes as k_i^{-2} instead of k_i^{-1}, the correct dependence.[10] A similar divergence in the forward direction is also observed for *s-s* excitation, for the e^--atom system, which arises due to the absence of the intermediate *p* states in the evaluation of the second Born term. To a certain extent these discrepancies are removed by taking $k_m^2 = k_i^2 - 2\Delta$ with Δ as the mean excitation energy. In an average sense the signature of the intermediate target states are carried to $\bar{f}_{B2}$ through Δ. The choice of Δ is not unique. Ermolaeve and Walters[7,8] have discussed the various options. To obtain better values of the differential cross sections, particularly for the case with momentum transfer $|\mathbf{K}|$ large in which the higher Born terms play an important role, a few low lying excited states should be explicitly included in the summation of Eq. (2). Based on these ideas Holt and Moiseiwitsch[10] proposed to include in Eq. (2) a finite number of low lying target states exactly and the rest by summing up through closure. The simplified second Born approximation (SSBA) of Holt and Moiseiwitsch, thus obtained, has been one of the most popular ways for evaluating the second Born term.

An approximation just opposite to that of Massey and Mohr was attempted by Khare and Shobha[11] when they evaluated $\bar{f}_{B2}$ in the plane wave approximation. They took $q^2 = k_i^2$ in (2). Thus $G_0^+(\mathbf{R},\mathbf{R}';\ \mathbf{x},\mathbf{x}')$ reduced to $G_{0t}^+(\mathbf{x},\mathbf{x}')\cdot\delta(\mathbf{R} - \mathbf{R}')$, where G_{0t}^+, the target Green's function, is given, in operator form, by

$$G_{0t}^+ = \mathrm{S}' \frac{|m\rangle\langle m|}{k_m^2 - k_i^2}. \tag{8}$$

The prime excludes the final and initial states from the summation; hence, these states do not contribute to the polarization of the target wave functions. Use of (8) in (3) yields as the second Born term in the plane wave approximation.

$$\bar{f}_{B2p}(\mathbf{k}_f,\mathbf{k}_i) = -2\pi^2 \langle \mathbf{k}_f | U_{\mathrm{ap}} | \mathbf{k}_i \rangle \tag{9}$$

where

$$U_{\mathrm{ap}} = \mathrm{S}' \frac{\langle f|U|m\rangle\langle m|U|i\rangle}{k_m^2 - k_i^2}. \tag{10}$$

It is evident that (9) *completely neglects the effects due to the distortion of the projectile wave function but includes those due to the distortion of the target wave function*. Since the projectile is being represented by a plane wave in (9), this approximation is referred to as the plane wave approximation. U_{ap} serves as the interaction potential between the projectile and the distorted (polarized) target. Note that since (10) does not depend upon the velocity of the projectile the polarization potential U_{ap} is adiabatic. The approximate Green's function, including nonadiabatic effects up to the first order in the interaction, can be obtained by taking $q^2 = -\nabla_R^2$ and using

$$\frac{1}{k_m^2 + \nabla_R^2} = \frac{1}{k_m^2 - k_i^2 + (\nabla_R^2 + k_i^2)} \cong \frac{1}{k_m^2 - k_i^2} - \frac{\nabla_R^2 + k_i^2}{(k_m^2 - k_i^2)^2} \tag{11}$$

in (2). We note that $(\nabla_R^2 + k_i^2)$ when operating on a plane wave yields zero. On using this approximate Green's function in Eq. (3) we obtain

$$\bar{f}_{i32p}(\mathbf{k}_f, \mathbf{k}_i) = -2\pi^2 \langle \mathbf{k}_f | U_{ap} + U_{nap} | \mathbf{k}_i \rangle \tag{12}$$

where the nonadiabatic potential U_{nap} in its Hermitian form is given by[12]

$$U_{nap}(\mathbf{R}) = \mathrm{S}' \frac{\nabla_R \langle f|U|m\rangle \cdot \nabla_R \langle m|U|i\rangle}{(k_m^2 - k_i^2)^2}. \tag{13}$$

It is easy to show[12] that for elastic scattering the asymptotic form of the dynamic interaction potential is given by

$$U_{ap}(\mathbf{R}) + U_{nap}(\mathbf{R}) = -\frac{\alpha_d}{R^4} - \frac{(\alpha_q - 6\beta_1)}{R^6}, \tag{14}$$

where α_d and α_q are dipole and quadrupole polarizabilities and β_1 is the dipole nonadiabatic coefficient of the target, a result obtained earlier by Kleinman *et al.*[13] using a different approach. Although the plane wave approximation has been successful in explaining the differential cross sections for the elastic scattering of fast electrons by light targets like hydrogen[12] and helium[14] atoms as well

as hydrogen molecules,[15] it suffers from the defect that $\bar{f}_{B2p}$ is purely real. Thus, although this approximation can be used to obtain the total elastic scattering cross section by integrating $(\bar{f}_{B1} + \bar{f}_{B2p})^2$ over all solid angles, it cannot be used to obtain the total collisional cross section (elastic plus inelastic) which is related to the imaginary part of the forward scattering amplitude via the optical theorem. Furthermore, even at very high energies $\bar{f}_{B1} + \bar{f}_{B2p}$ does not approach $\bar{f}_{B1}$ for any value of the momentum transfer $|\mathbf{K}|$. In 1959 Glauber[16] employed the eikonal approximation[17] of potential scattering theory to discuss the many-particle scattering process. To obtain the eikonal wave function for the projectile one introduces a new variable $\mathbf{p}$ defined by $\mathbf{p} = \mathbf{k}_i - \mathbf{q}$ in (5) and approximately writes

$$\frac{1}{k_i^2 - q^2 + i\epsilon} \approx \frac{1}{2\mathbf{k}_i\cdot\mathbf{p} + i\epsilon} + \frac{p^2}{(2\mathbf{k}_i\cdot\mathbf{p} + i\epsilon)^2}. \tag{15}$$

If we put only the first term of (15) in (5) we get the linearized Green's function of the projectile leading to the eikonal wave function. However, the inclusion of the second term gives the leading Wallace phase correction.[18] Use of the linearized Green's function in (1) yields the scattering amplitude in the Glauber approximation, given by

$$f_G(\mathbf{k}_f,\mathbf{k}_i) = \langle f|f_E(\mathbf{x})|i\rangle \tag{16}$$

where $f_E(\mathbf{x})$ is the scattering amplitude in the eikonal approximation for the scattering of a particle by a target atom in which the bound electrons are frozen at $\mathbf{x}$. Similarities between (11) and (15) as well as between (6) and (16) are to be noted. If we include the leading Wallace phase correction, $f_E(\mathbf{x})$ changes to $f_{EW}(\mathbf{x})$ given by[19]

$$f_{EW}(\mathbf{x}) =$$

$$\frac{k_i}{2\pi i}\int d^2b\, \exp(i\mathbf{K}\cdot\mathbf{b})\, \{\exp[i(k_i^{-1}\chi_0(\mathbf{b},\mathbf{x}) + k_i^{-3}\chi_1(\mathbf{b},\mathbf{x}))] - 1\}. \tag{17}$$

$\mathbf{K}$ is, as above, the momentum transfer. The eikonal phase $\chi_0(\mathbf{b},\mathbf{x})$ is of first order and the leading Wallace phase correction $\chi_1(\mathbf{b},\mathbf{x})$ is[19] of second order in the interaction potential U. Of course, one

gets $f_E(\mathbf{x})$ on dropping the term containing χ_1. We note that the *Glauber approximation with or without the Wallace correction completely neglects the effect due to the distortion of the target wave function*. f_G as well as f_W, defined by

$$f_W(\mathbf{k}_f,\mathbf{k}_i) = \langle f|f_{EW}(\mathbf{x})|i\rangle, \tag{18}$$

suffer from the same discrepancies as noticed earlier for $\bar{f}_{B2,M}$. The scattering amplitudes f_G and f_W can each be expanded, in a manner analogous to the Born series, in powers of U to yield the Glauber series and the Wallace series, respectively. $\bar{f}_{Gn}$ and $\bar{f}_{Wn}$ will refer to terms of order n in the Glauber and in the Wallace series, respectively. However, whereas the Glauber series terms are alternately real and imaginary, the terms of the Wallace series are complex (for $n > 1$). Furthermore, at large momentum transfers, the terms of the Wallace series are nearly equal to the corresponding terms of the Born series. Byron *et al.*[19] took advantage of the above property and proposed a unitarized eikonal Born amplitude given by

$$f_{\text{UEBS}} = f_W - \bar{f}_{W2} + \bar{f}_{B2} \tag{19}$$

where $\bar{f}_{W2}$ is the second term of the Wallace series. However, difficulties arise in the evaluation of the Wallace terms $\bar{f}_{Wn}$ (with $n \geq 4$) of the $e^{\pm}$-atom scattering amplitude. This led Byron *et al.*[2] to redefine the unitarized eikonal Born series in the following manner:

$$f_{\text{UEBS}} = \bar{f}_W - \bar{f}_{W2} + \bar{f}_{B2}, \tag{20}$$

where $\bar{f}_W$ is again obtained from (18) except for the difference that in the evaluation of $f_{EW}(\mathbf{x})$ the phase term $\exp[ik_i^{-3}\chi_1(\mathbf{b},\mathbf{x})]$ is replaced by $1 + ik_i^{-3}\chi_1(\mathbf{b},\mathbf{x})$. We note that the eikonal Born series as well as the unitarized eikonal Born series include the effect due to the distortion of the target wave function only up to the second order in the interaction potential through $\bar{f}_{B2}$, which is usually evaluated following the procedure of Holt and Moiseiwitsch.[10]

Recently Byron *et al.*[2] utilized the UEBS method to obtain the cross sections for the elastic and inelastic scattering of electrons and positrons by atomic hydrogen at intermediate and high ener-

gies. At about the same time Khare and Prakash[3] utilized the Schwinger variational method to investigate the e^--H scattering. We now explicitly demonstrate that the scattering amplitude in the Schwinger variational approach follows by approximating the Green's function in Eq. (1). On splitting the infinite sum in Eq. (1) at $n = p$, the scattering amplitude can be written in the following alternate form:

$$f^{fi}(\mathbf{k}_f,\mathbf{k}_i) = f_{Bp} - 2\pi^2 \langle \mathbf{k}_f, f|U(G_0^+ U)^p \sum_{n=1}^{\infty} (G_0^+ U)^{n-1}|\mathbf{k}_i, i\rangle, \quad (21)$$

in which f_{Bp} is the pth Born approximation for the scattering amplitude. The Green's function appears explicitly in the infinite sums of Eqs. (1) and (21). Now we make the approximation of truncating these two infinite sums to finite sums of m terms each and replacing the Green's function G_0^+ in the surviving m terms by a multiple CG_0^+ of the Green's function, with the complex multiplying factor C to be determined later. On using this approximation for the Green's function in Eqs. (1) and (21), we get two approximate expressions for the scattering amplitude which we label as f_1 and f_2, respectively. These are

$$f_1 = C f_{Bm}$$

and

$$f_2 = f_{Bp} + C\{f_{B\overline{p+m}} - f_{Bp}\}.$$

The multiplying factor C is now determined by simply equating f_1 and f_2, as they would have been the same if the Green's function was not approximated. This procedure yields

$$C = \frac{f_{Bp}}{f_{Bm} + f_{Bp} - f_{B\overline{p+m}}}. \quad (22)$$

On substituting this expression for C in either f_1 or in f_2 above, we obtain for the scattering amplitude

$$[f_{pm}] = \frac{f_{Bm} f_{Bp}}{f_{Bm} + f_{Bp} - f_{B\overline{p+m}}}. \quad (23)$$

The same expression for the scattering amplitude is obtained[3] if one takes incoming and outgoing scattered waves correct to $(p-1)$th and $(n-1)$th order in the interaction potential in the Schwinger variational principle. Khare and Prakash[3] took $m = p = 2$, replaced $\bar{f}_{B4}$ by $\bar{f}_{G4}$, and noting that $\bar{f}_{B3}(0)$ is zero in the closure approximation for $e^{\mp}$-H scattering,[20] found

$$[f_{22}] = \frac{(\bar{f}_{B1} + \bar{f}_{B2})^2}{f_{B1} + \bar{f}_{B2} - \bar{f}_{G4}} \tag{24}$$

for the scattering amplitude in the forward direction. The use of (24) along with the optical theorem gave slightly different values of the total cross sections Q_T for electron and positron scattering at lower impact energies even when exchange was excluded. On the other hand the UEBS method of Byron *et al.*[2] gave different values of $Q_T(e^{\mp})$ only when exchange was included. In Table I we show the two sets of values which are in good agreement with each other, particularly for positron scattering where exchange does not play any role. For the electron case the difference between the two sets of values seems to arise mainly due to the exchange contribution. Such an agreement is not surprising because $[f_{22}(0)]$ and $f_{\text{UEBS}}(0)$ agree with one another asymptotically up to the order of k_i^{-3}. A comparison of the theoretical values of the cross sections for the electrons with the adopted cross sections of de Heer *et*

TABLE I

Total collisional cross sections (in a_0^2) for the scattering of electrons and positrons by a hydrogen atom

E(eV)	SV[a]		UEBS[b]		H[c]
	e^-	e^+	e^-	e^+	e^-
100	6.77	6.82	7.04	6.84	6.85
200	4.18	4.18	4.23	4.18	4.18
300	2.93	2.93	3.10	3.07	3.06
400	2.43	2.43	2.45	2.44	2.43
500	2.03	2.03	–	–	–

[a]SV are the results of Khare and Prakash (Ref. 3) who employed the Schwinger variational method, Eq. (23), with $m = p = 2$.

[b]UEBS are the results of Byron *et al.* (Refs. 2 and 19) who employed the unitarized eikonal Born series method.

[c]H are the adopted cross sections of de Heer *et al.* (Ref. 21).

al.,[21] presented in Table I, shows that the agreement between them is quite satisfactory. It may be noted that de Heer *et al.* used theoretical as well as experimental cross sections for elastic and inelastic processes from various different sources to obtain the total collisional cross sections.

For a better comparison of the two methods—the Schwinger variational and the UEBS—one should compare the values of the differential cross sections rather than the total collisional cross sections. However, at nonzero scattering angles $\tilde{f}_{B3}(\theta)$ is not zero and no tractable method is so far available for obtaining Im $\tilde{f}_{B3}(\theta)$, which falls as k_i^{-3}. Hence Khare and Lata[4] took $m = 2$ and $p = 1$ in (23), replaced Re$\tilde{f}_{B3}(\theta)$ by $\tilde{f}_{G3}(\theta)$ and neglected Im $\tilde{f}_{B3}(\theta)$. Thus they obtained $[f_{21}(\theta)]$ which agrees with $f_{\text{UEBS}}(\theta)$ asymptotically only up to the order of k_i^{-2}. Furthermore, Khare and Lata obtained the exchange contribution through the Ochkur approximation whereas Byron *et al.* obtained the exchange contribution through a more sophisticated method. Tables II and III compare the two sets of cross sections for the elastic scattering of e^- by hydrogen atoms in the energy region of 100 to 400 eV. At the highest impact energy, that is, 400 eV, the agreement between the two sets is very good. The maximum difference is only 3.6%. However, with the decrease of the impact energy the difference between the two sets of cross sections increases. At 100 eV the maximum difference is about 25%. Such behavior is expected because the scattering amplitudes obtained by the two methods agree with one another only up through terms of order k_i^{-2}. In general the differences between the two sets of values are relatively larger at higher scattering angles and both sets of values are smaller than the experimental values of Williams[22] and van Wingerden *et al.*[23] At larger angles though, $I_{\text{UEBS}}(\theta)$ yields closer agreement with the experimental data of Williams.[22] However, we note that Byron *et al.* have commented that so far no theoretical method has given excellent agreement with the experimental data of Williams at large scattering angles. According to Kingston and Walters,[24] the data of Williams are consistently larger at larger angles. Perhaps the same could be said for the data of van Wingerden *et al.*

In summary, various approximate forms of the Green's functions have been shown to give rise to practically all the theoretical methods used for investigations of scattering of fast projectiles. In their

TABLE II

Differential and integrated cross sections (in a_0^2) for the elastic scattering of electrons by a hydrogen atom

θ(deg)\E(eV)	100				200				300		400		
	SV[a]	UEBS[b]	W[c]	V[d]	SV	UEBS	W	V	SV	UEBS	SV	UEBS	W
0	8 29	8.2	–	–	5 50	5 6	–	–	4 42	4 50	3.82	3.88	–
10	2 28	2.4	–	–	1.15	1 1	–	–	7 71-1	7 84-1	6.23-1	6 27-1	
20	8.4-1[e]	8.5-1	1.10	1.17	3.90-1	3.8-1	4.19-1	5 77-1	2 45-1	2 39-1	1 70-1	1 67-1	1 96-1
30	3.86-1	3 6-1	5.09-1	5.25-1	1 51-1	1.5-1	1.72-1	2 00-1	8.18-2	7 96-2	5 10-2	5.03-2	6 17-2
40	1.91-1	1 7-1	2.88-1	2.57-1	6.42-2	6.2-2	7.06-2	7 74-2	3.19-2	3 13-2	1.89-2	1.88-2	2 06-2
60	5.72-2	5.3-2	7.22-2	7.40-2	1.63-2	1.6-2	1.87-2	2.37-2	7 60-3	7 57-3	4.37-3	4.39-3	4 38-3
80	2 25-2	2.3-2	2.95-2	3.19-2	6.11-3	6.4-3	8.59-3	1.00-2	2.78-3	2 81-3	1 61-3	1 62-3	1 57-3
100	1.21-2	1.2-2	1.55-2	1.62-2	3.01-3	3.2-3	4.12-3	4.11-3	1.38-3	1 39-3	7 95-4	8 04-4	9 16-4
120	6.80-3	8.0-3	9.20-3	1.07-2	1.82-3	2 0-3	2.72-3	–	8.44-3	8 49-4	4 80-4	4 90-4	6 03-4
140	4.84-3	5.9-3	6.50-3	–	1.30-3	1.4-3	1.78-3	–	6.06-4	6 10-4	3 47-4	3.52-4	5 06-4
160	3.97-3	5 0-3	–	–	1.06-3	1.2-3	–	–	5.00-4	5.04-4	2 86-4	2.91-4	–
180	3.73-3	4.7-3	–	–	1 00-3	1.1-3	–	–	4 68-4	4.73-4	2.69-4	2 74-4	–
Q_{el}	1.46	1 46	–	1.83	6 14-1	6 17-1	–	7 89-1	3 75-1	3 82-1	2 69-1	2 76-1	–

[a]SV are the results of Khare and Kusum Lata (Ref. 4) who employed the Schwinger variational method, (23), with $m = 2$ and $p = 1$

[b]UEBS are the results of Byron *et al.* (Refs. 2 and 19) who employed the unitarized eikonal Born series method

[c]W are the experimental data of Williams (Ref. 22).

[d]V are the experimental data of van Wingerden *et al.* (Ref 23)

[e]The notation A-B represents $A \cdot 10^{-B}$.

TABLE III

Differential and integrated cross sections (in a_0^2) for the elastic scattering of positrons by a hydrogen atom

θ(deg)\E(eV)	100		200		300		400	
	SV	UEBS	SV	UEBS	SV	UEBS	SV	UEBS
0	2.58	2.3	1.75	1.6	1.45	1.39	1 29	1 25
10	1.08	9.8-1	7.35-1	7 1-1	6.03-1	5.98-1	5.19-1	5 18-1
20	4.36-1	4.2-1	2.74-1	2.8-1	1.92-1	1.94-1	1.41-1	1 42-1
30	1.98-1	2.0-1	1.06-1	1.1-1	6.44-2	6.42-2	4 27-2	4.25-2
40	9.74-2	9 8-2	4.57-2	4.5-2	2.56-2	2.50-2	1.61-2	1.58-2
60	3.11-2	2.8-2	1.23-2	1 2-2	6.36-3	6.06-3	3 84-3	3 73-3
80	1.34-2	1.1-2	4.84-3	4.5-3	2.40-3	2.27-3	1 43-3	1.39-3
100	7.23-3	5.8-3	2.45-3	2 3-3	1.21-3	1.13-3	7.18-4	6 92-4
120	4 60-3	3.6-3	1.51-3	1.4-3	7 45-4	6.97-4	4 36-4	4.23-4
140	3.38-3	2.6-3	1 09-3	1.0-3	5 38-4	5 03-4	3.16-4	3 05-4
160	2.82-3	2.2-3	8.99-4	8 6-4	4.45-4	4.16-4	2.61-4	2 53-4
180	2.66-3	2.1-3	8.46-4	8 1-4	4 17-4	3.91-4	2.46-4	2 38-4
Q_{el}	7.29-1	6.90-1	4.15-1	4 12-1	2 90-1	2.92-1	2.23-1	2.26-1

SV and UEBS represent the same methods as in Table II.

latest method Byron *et al.* have put emphasis on the unitarization whereas Khare and Prakash based their method on the Schwinger variational principle. Both of these methods seem to be attractive and their application to different processes for heavier elements and the comparison of the resulting cross sections will be of future interest.

Acknowledgments

SPK gratefully acknowledges the award of a Visiting Professorship by Wayne State University. JMW gratefully acknowledges the support of the Air Force Office of Scientific Research through Grant number AFOSR-87-0342.

S. P. KHARE* and J. M. WADEHRA
Department of Physics and Astronomy,
Wayne State University,
Detroit, Michigan 48202

References

1. C. J. Joachain, *Quantum Collision Theory* (North Holland, Amsterdam, 1975).
2. F. W. Byron, Jr., C. J. Joachain and R. M. Potvliege, J. Phys. B **18**, 1637 (1985).
3. S. P. Khare and S. Prakash, Phys. Rev. A **32**, 2689 (1985).
4. S. P. Khare and Kusum Lata, J. Phys. B **18**, 2941 (1985); Kusum Lata, Ph.D. thesis, Meerut University, Meerut, India (1984).
5. R. Aaron, R. D. Amado and B. W. Lee, Phys. Rev. **121**, 319 (1961).
6. L. Rosenberg, Phys. Rev. **134**, B937 (1964).
7. A. M. Ermolaev and H. R. J. Walters, J. Phys. B **12**, L779 (1979).
8. H. R. J. Walters, Phys. Rep. **116**, 1 (1985).
9. H. S. W. Massey and C. B. O. Mohr, Proc. Roy. Soc. A **146**, 880 (1934).
10. A. R. Holt and B. L. Moiseiwitsch, J. Phys. B **1**, 36 (1968).
11. S. P. Khare and P. Shobha, Phys. Lett. **31A**, 571 (1970) and J. Phys. B **4**, 208 (1971).
12. B. L. Jhanwar, S. P. Khare and P. Shobha, J. Phys. B **8**, 1228 (1975).
13. C. J. Kleinman, Y. Hahn and L. Spruch, Phys. Rev. **165**, 53 (1968).
14. B. L Jhanwar and S. P. Khare, J. Phys. B **9**, L527 (1976).
15. P. Gupta and S. P. Khare, J. Chem. Phys. **68**, 2193 (1978).
16. R. J. Glauber, *Lectures in Theoretical Physics*, Vol. 1, ed. W F Brittin (Interscience, New York, 1959), p. 315.
17. G. Moliere, Z. Naturf. **2A**, 133 (1947).

*Also affiliated with the Department of Physics, Banaras Hindu University, Varanasi 221 005, India.

18 S. J. Wallace, Ann. Phys. NY **78**, 190 (1973).
19 F W. Byron Jr., C. J. Joachain and R. M. Potvliege, J. Phys. B **15**, 3915 (1982).
20. D P. Dewangan, J Phys. B **13**, L595 (1980).
21. F J. de Heer, M. R. C. McDowell and R. W. Wagenaar, J. Phys. B **10**, 1945 (1977).
22. J F. Williams, J Phys. B **8**, 2191 (1975).
23. B. van Wingerden, E. Weigold, F J. de Heer and K. J. Nygaard, J. Phys. B **10**, 1345 (1977).
24 A E. Kingston and H. R J Walters, J. Phys. B **13**, 4633 (1980).

Exact time-dependent evolution of electron-velocity distribution functions in a gas using the Boltzmann equation

P. J. Drallos and J. M. Wadehra
Department of Physics and Astronomy, Wayne State University, Detroit, Michigan 48202
(Received 22 March 1989)

A numerical technique, starting from the Boltzmann equation, for obtaining the time-dependent behavior of the electron-velocity distribution function in a gas is presented. A unique feature of this technique is that, unlike previously used procedures, it does not make use of *any* expansion of the distribution function. This allows the full anisotropy of the distribution function to be included in the solution. Furthermore, the problem associated with multiterm-expansion techniques of choosing a sufficient number of terms for convergence is completely avoided. The distribution function obtained by the present method is exact and, in principle, contains all of the expansion terms of the previous procedures. Details of the algorithm, including stability conditions, treatment of the boundaries, and evaluation of the collision integrals, are presented. This technique has been applied for obtaining the time-dependent behavior of electron swarms in gaseous argon and neon for various values of E/N (the ratio of the applied uniform dc field to the gas density), and the corresponding results are presented.

I. INTRODUCTION

The electron-velocity distribution function (EVDF) is fundamentally important in virtually all aspects of gaseous electronics. The EVDF provides a statistical description of the motion of all of the electrons in an electron swarm. The motion of the electrons in the swarm is affected by externally applied electric and magnetic fields, and by collisions of the electrons with the particles of the ambient gas. These external forces and collisions cause time-dependent changes in the EVDF. Stating this process mathematically, let $f(\mathbf{v},t)$ represent the electron-velocity distribution function at a velocity $\mathbf{v}$, and at a particular time t. Then, at some later time $t+\Delta t$, the EVDF can be described very simply by

$$f(\mathbf{v}+\Delta\mathbf{v},t+\Delta t)=f(\mathbf{v},t)+R(\mathbf{v},t)\Delta t \ . \tag{1}$$

Here, $\Delta\mathbf{v}=\mathbf{a}\Delta t$, with $\mathbf{a}$ as the acceleration of the electrons due to the externally applied forces. $R(\mathbf{v},t)\Delta t$ is the collision term which represents the net change in $f(\mathbf{v},t)$ during the time increment Δt due to all possible collision processes between the electrons and the gas particles. Now, if we expand Eq. (1) to first order in Δt, and then take the limit as Δt goes to zero, the spatially independent Boltzmann equation is immediately obtained:

$$\frac{\partial f(\mathbf{v},t)}{\partial t}+\mathbf{a}\cdot\nabla_v f(\mathbf{v},t)=R(\mathbf{v},t) \ . \tag{2}$$

It is thus clear that the physical content of the Boltzmann equation (2) is entirely equivalent to that of the difference equation (1). Knowledge of the EVDF is usually gained by solution of the Boltzmann equation and, to this end, many techniques for its solution have been developed.

Traditionally, the techniques used for solving the Boltzmann equation for an equilibrium electron-velocity distribution function have involved expansion, usually in the Legendre polynomials, of the distribution function as follows:

$$f(\mathbf{v},t)=\sum_{n=0}^{\infty} f_n(v,t)P_n(\theta) \ . \tag{3}$$

Often, only the first two terms in the expansion, containing f_0 and f_1, are retained, and the time derivative of the distribution function in the Boltzmann equation is set to zero to correspond to the equilibrium situation. The resulting coupled time-independent equations can then be solved for f_0 and f_1 using standard numerical methods. The two-term expansion method, however, breaks down[1] under situations of large E/N (the ratio of the applied uniform dc electric field to the gas density) or for cases in which the inelastic scattering cross sections are comparable in magnitude to the elastic cross sections. The shortcomings of the two-term expansion can, in principle, be overcome by retaining more terms in the Legendre expansion of the distribution function. These multiterm methods, however, have their own drawbacks. As more terms in the expansion are kept, the computational complexity increases rapidly. Furthermore, cross sections which have been adjusted to reproduce experimental swarm parameters in a two-term expansion calculation do not yield the same EVDF or the corresponding swarm parameters when used in a multiterm expansion calculation and vice versa. Clearly, it would be desirable to have a procedure, as described below, which can provide the equilibrium EVDF without involving any expansion of the distribution function. Such a procedure, which incorporates a finite-difference technique, was developed by Tagashira and co-workers.[2] In their procedure, the distribution function was expanded to second order in time using a standard Taylor series. The various time derivatives of $f(\mathbf{v},t)$ were evaluated by direct substitution from

the Boltzmann equation, namely,

$$f(\mathbf{v},t+\Delta t)=f(\mathbf{v},t)+\frac{\partial f(\mathbf{v},t)}{\partial t}\Delta t+O((\Delta t)^2)$$
$$=f(\mathbf{v},t)+[-\mathbf{a}\cdot\nabla_v f(\mathbf{v},t)+R(\mathbf{v},t)]\Delta t$$
$$+O((\Delta t)^2)\,. \tag{4}$$

Tagashira and co-workers chose to evaluate the distribution function of Eq. (4) in spherical coordinates in the velocity space, that is, f was stored as a v-θ array, simply because the evaluation of the collision term $R(\mathbf{v},t)$ is most convenient in spherical coordinates. Evaluation of the $\mathbf{a}\cdot\nabla_v$ term then involved derivatives of f with respect to v and θ. These derivatives, which had to be taken numerically by a finite-difference procedure, are prone to instability. It was in order to alleviate this instability that Tagashira and co-workers had to retain some of the terms proportional to $(\Delta t)^2$ in the Taylor-series expansion of Eq. (4). In a previous paper,[3] we briefly described a finite-difference algorithm for determining the exact time-dependent behavior of electron-velocity distribution functions. A unique feature of our algorithm is that it does not require numerical evaluation of *any* derivatives, nor does it make use of any term expansions of the distribution function in terms of Legendre functions. The present paper will provide details of the procedure, such as the explicit form and evaluation of the collision integrals, conditions of numerical stability, treatment of the numerical boundaries, and techniques for implementing the conditions of numerical stability. We will also present results of the application of this procedure to electron swarms in argon and in neon for various values of E/N.

In the present solution, the following finite-difference equation in Cartesian coordinates for the electron-velocity distribution function is evaluated

$$f(v_x,v_y,v_z+\Delta v_z,t+\Delta t)$$
$$=f(v_x,v_y,v_z,t)+R(v_x,v_y,v_z,t)\Delta t\,. \tag{5}$$

Equation (5) can be obtained directly from Eq. (1), which is equivalent, in its physical content, to the Boltzmann equation (2). Until the collision terms $R(\mathbf{v},t)$ are known, however, Eq. (5) is of little practical use. So, before proceeding any further, we will explicitly define the collision terms $R(\mathbf{v},t)$ and outline procedures for their evaluation.

II. COLLISION TERMS

In order to derive a very general expression for the collision term we will assume an ambient gas of constant density interacting with a spatially homogeneous swarm of projectiles of arbitrary mass (for example, either electrons, positrons, protons, or ions). A general expression for the collision term in Eq. (5) can be written[4]

$$R(\mathbf{v},t)=\sum_p (N/v^2)\int_0^\infty v_p^2 dv_p \int_0^\pi \sin\psi\, d\psi \int_0^{2\pi} d\alpha\, v_p f(\mathbf{v}_p,t)\sigma_p(v_p,\psi)\delta(v-g_p(v_p,\psi))-Nvf(\mathbf{v},t)\sigma_T(v) \tag{6}$$

where $\sigma_p(v_p,\psi)$ is the differential scattering cross section for the pth (p = elastic, excitation, ionization, etc.) collision process, and $\sigma_T(v)$ is the integrated total cross section for all collision processes. The function $g_p(v_p,\psi)$ is defined by the equation

$$v=g_p(v_p,\psi)\,, \tag{7}$$

which relates, via the energy-conserving δ function, the initial speed v_p to the final speed v for the pth collision process. The integral terms in Eq. (6) represent the rate at which the projectile particles are scattered into a velocity-space-volume element d^3v located about $\mathbf{v}$ due to the pth scattering process and will be denoted by $R_p^+(\mathbf{v},t)$. The last term in Eq. (6) represents the rate at which the projectile particles are scattered out of d^3v about $\mathbf{v}$ due to all possible collision processes, and will be denoted by $R_T^-(\mathbf{v},t)$. Thus

$$R(\mathbf{v},t)=\sum_p R_p^+(\mathbf{v},t)-R_T^-(\mathbf{v},t)\,.$$

The differential velocity-space volume elements in Eq. (6) are defined in Fig. 1 and by the following relations:

$$d^3v=v^2dv\sin\theta\, d\theta\, d\phi\,, \tag{8a}$$

$$d^3v_p=v_p^2dv_p\sin(\theta_p)d\theta_p d\phi_p=v_p^2dv_p\sin(\psi)d\psi\, d\alpha\,, \tag{8b}$$

so that the direction of $\mathbf{v}_p$ can be specified, depending on the convenience, with respect to either z or v. These two possible specifications of $\mathbf{v}_p$ lead to the following relationships among various angles:

$$\mathbf{v}=\mathbf{v}(v,\theta)\,, \tag{9a}$$

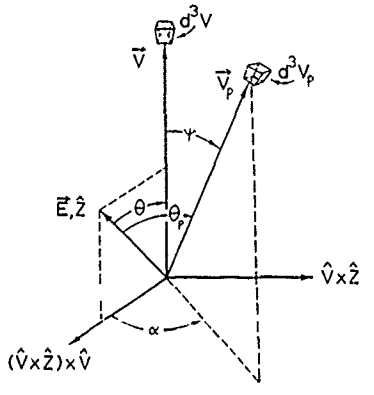

FIG. 1 Geometry used in the derivation of the collision terms. $\mathbf{v}$ the $\mathbf{v}_p$ denote the final and initial velocities, respectively, and ψ is the scattering angle.

$$\cos(\theta_p)=\sin(\theta)\sin(\psi)\cos(\alpha)+\cos(\theta)\cos(\psi)\ , \tag{9b}$$

$$\mathbf{v}_p=\mathbf{v}_p(v_p,\theta_p)=\mathbf{v}_p(v_p,\theta,\psi,\alpha)\ , \tag{9c}$$

and finally,

$$f(\mathbf{v}_p,t)=f(v_p,\theta_p,t)=f(v_p,\theta,\psi,\alpha,t)\ . \tag{9d}$$

In order to evaluate Eq. (6) the function $g_p(v_p,\psi)$ must be specified for various collision processes. For *elastic* collisions ($p=e$), straightforward kinematics yields

$$v=v_e q(\psi)=g_e(v_e,\psi)\ , \tag{10a}$$

where $q(\psi)$ is the following function:

$$q(\psi)=[(1-\mu^2)^{1/2}+\mu\cos\psi]/(1+\mu)\ . \tag{10b}$$

Here, μ is the ratio of the mass m of the projectile and the mass M of the gas particle, that is, $\mu=m/M$. For the case in which the projectile is either an electron or a positron ($\mu\ll 1$), $q(\psi)$ can be simplified to

$$q(\psi)=[1-\mu(1-\cos\psi)]\ . \tag{10c}$$

For *inelastic* collisions ($p=i$) the energy-conserving expression for g_p is

$$v=(v_i^2-2\xi/m)^{1/2}=g_i(v_i)\ , \tag{11}$$

which does not depend on the angle ψ. ξ is the energy loss associated with the inelastic process. Performing the radial v_p integrations to eliminate the Dirac δ functions in Eq. (6), one is left with a two-dimensional angular integral over ψ and α. Because of the δ function, v_p in the integrand, which includes the distribution function f and the collision cross section σ_p, is replaced by $v/q(\psi)$ (for the elastic part) or by $(v^2+2\xi/m)^{1/2}$ (for the inelastic part). For brevity in writing and in accordance with Eqs. (10) and (11), we replace, in the resulting angular integrals, $v/q(\psi)$ and $(v^2+2\xi/m)^{1/2}$ with v_e and v_i, respectively, so that the final expression for the collision term looks like

$$R(\mathbf{v},t)=N\int_0^{\pi}\frac{v_e^4}{v^3}\sigma_e(v_e,\psi)\sin\psi\,d\psi\int_0^{2\pi}f(\mathbf{v}_e,t)d\alpha + \sum_i N\int_0^{\pi}\frac{v_i^2}{v}\sigma_i(v_i,\psi)\sin\psi\,d\psi \times\int_0^{2\pi}f(\mathbf{v}_i,t)d\alpha-Nvf(\mathbf{v},t)\sigma_T(v)\ . \tag{12a}$$

So far, the collision integral is valid for any type of projectile except that the term corresponding to the ionization process has to be treated slightly differently when the projectile is an electron. When ionization is considered, the final energy of both the incident electron and the free electron that is produced via the ionization process must be properly accounted for. To this end, an electron-energy partition ratio $\Delta/(1-\Delta)$ is used, which denotes the ratio of the available energy that goes to each of the two electrons (labeled 1 and 2 below). The integral that represents the rate at which electrons scatter due to the ionization process, into the velocity space element d^3v about (v,θ), then has two parts:

$$R^{+}_{\text{ion},1}(v,\theta)+R^{+}_{\text{ion},2}(v,\theta) =\frac{N}{\Delta}\int_0^{\pi}\frac{v_1^2}{v}\sigma_{\text{ion}}(v_1,\psi)\sin\psi\,d\psi\int_0^{2\pi}f(\mathbf{v}_1,t)d\alpha + \frac{N}{1-\Delta}\int_0^{\pi}\frac{v_2^2}{v}\sigma_{\text{ion}}(v_2,\psi)\sin\psi\,d\psi\int_0^{2\pi}f(\mathbf{v}_2,t)d\alpha\ , \tag{12b}$$

where $v_1=(2\xi/m+v^2/\Delta)^{1/2}$ and $v_2=[2\xi/m+v^2/(1-\Delta)]^{1/2}$. These two terms correspond to two different ionization events in which electrons of initial speeds v_1 and v_2 ionize gas particles. One of the two electrons [having energy ratio $\Delta/(1-\Delta)$] resulting from each of these two ionization events has speed v.

In evaluating Eqs. (6) or (12), proper account must be taken of the vector nature of $\mathbf{v}$ and $\mathbf{v}_p$. Although the distribution function is symmetric about the axis parallel to the electric field (the z axis), the polar axis of the integrals over a solid angle (ψ,α) is tilted with respect to z and cannot take advantage of the symmetry.

The surface over which the distribution function in the *elastic* part of Eq. (12a) is evaluated for angular integration is represented graphically in Fig. 2. Note that, because v_e depends on ψ, the surface is not a perfect sphere but an "egg-shaped" surface with azimuthal symmetry about $\mathbf{v}$. More specifically, such a surface is realized by the tracing of the tip of a vector whose length increases continuously as the polar angle is varied from one pole ($\psi=0$) to the other pole ($\psi=\pi$), but the length of the vector remains fixed as the azimuthal angle α is varied, for a given ψ, from 0 to 2π. The deviation of this surface from a perfect sphere is related, from Eq. (10), to the mass ratio μ. If the projectile particles are electrons or positrons the surface is very nearly a sphere, and very little difference was found on simply replacing v_e by v in Eq. (12a). However, in order to keep the analysis more general and not limit the distribution functions to only those

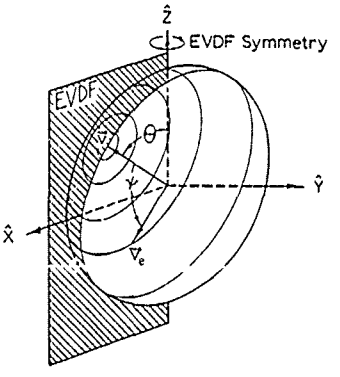

FIG. 2. Surface over which the elastic component of the collision term is evaluated. θ is the polar angle about z, and ψ is the polar angle about $\mathbf{v}$.

of electrons or positrons, we will not make any assumptions about the relative masses of the gas molecules and the projectiles. Nevertheless, Eq. (12a) remains valid in all possible cases including the ones in which the projectile particles are more massive, such as protons or ions, for which the distortion and tilt of the surface would become very important.

Often, the differential scattering cross sections are not sufficiently available to cover all angles and energies for each scattering process in the system of interest. Integrated cross sections, however, can usually be found and may be the only alternative. In this case, or in the cases in which the scattering is not strongly dependent on angle, we may make the approximation of isotropic scattering (σ does not depend on ψ). For isotropic elastic scattering we replace the differential elastic scattering cross section $\sigma_e(v_e,\psi)$ with $\sigma_e(v_e)/4\pi$, where $\sigma_e(v_e)$ is the integrated elastic scattering cross section. Doing this, the elastic part of Eq. (12) can be rewritten as

$$R_e^+(\mathbf{v},t)=\frac{N}{4\pi v^3}\int_0^{\pi} v_e^4\sigma_e(v_e)\sin\psi\, d\psi\int_0^{2\pi} f(\mathbf{v}_e,t)d\alpha\ . \tag{13}$$

If we assume isotropic *inelastic* scattering, then the differential scattering cross section for the ith scattering process $\sigma_i(v_i,\psi)$ can be replaced by $\sigma_i(v_i)/4\pi$, where $\sigma_i(v_i)$ is the integrated cross section for the ith inelastic process. Also, since v_i does not depend on the scattering angle, the surface of integration is spherical with a constant radius v_i, and the terms containing v_i can be taken outside of the angular integral. We can then write

$$R_i^+(\mathbf{v},t)=\frac{Nv_i^2}{4\pi v}\sigma_i(v_i)\int_0^{\pi}\sin\psi\, d\psi\int_0^{2\pi} f(\mathbf{v}_i,t)d\alpha \tag{14a}$$

$$=\frac{Nv_i^2}{4\pi v}\sigma_i(v_i)\int_0^{\pi}\sin\theta_i d\theta_i\int_0^{2\pi} f(\mathbf{v}_i,t)d\phi_i \tag{14b}$$

$$=\frac{Nv_i^2}{2v}\sigma_i(v_i)\int_0^{\pi} f(v_i,\theta_i,t)\sin\theta_i d\theta_i\ . \tag{14c}$$

In going from Eq. (14a) to (14b) we have made use of the fact that the integral is independent of the choice of polar axis and we have chosen the z axis (which is the axis of symmetry for the EVDF) as the polar axis, so that the ϕ_i integration becomes trivial [see Eq. (8b)].

Another problem that must be considered in the evaluation of Eq. (12a) is that f is stored in a rectangular array (in the x-z plane) and has rectangular boundaries, but the surfaces of integration in the R^+ terms are nonrectangular and sometimes lie outside of the region in which f is known. To handle this problem, an extrapolation procedure has to be devised. Regrettably, extrapolations are a risky business, and one can only hope that the relevant numerical errors will be small. What we did was to set up the initial ($t=0$) Maxwellian distribution of projectiles (electrons in our actual calculations) so that the values of the distribution function near the boundaries were less than 10^{-5} of the peak value so that the boundary contributions would be small. Then we assumed that the behavior in the high-velocity regions (near the boundaries and beyond) remained essentially Maxwellian at all later times. Based on the shape of the distribution function near but inside the boundary, we extrapolated the distribution function using the simple recursion relation $f(v+2\Delta v)=[f^2(v+\Delta v)/f(v)]C$, where C is a constant that depends on Δv. This recursion relation follows from the assumed Maxwellian form of the distribution function near the boundary. The case $C=1$ corresponds to the logarithmic approximation for extrapolation used by previous investigators.[2] Several tests were made, by changing the boundaries, showing that the high-velocity tail of the numerically obtained distribution function conformed to this Maxwellian behavior, and that deviation was less than 1%.

III. METHOD OF SOLUTION

For the situation in which the external force on the projectiles (of charge q) is provided by a uniform dc electric field aligned in the z direction, the constant $\Delta v_z=(qE/m)\Delta t$, and Eq. (5) can be rewritten as

$$f(v_x,v_y,v_z+(qE/m)\Delta t,t+\Delta t)$$
$$=f(v_x,v_y,v_z,t)+R(v_x,v_y,v_z,t)\Delta t\ . \tag{15}$$

Equation (15) is well suited for evaluation on a computer. Since there is axial symmetry around the z axis, f need only be stored as a function of v_z and v_x (or v_y) in such a way that the velocity increments Δv satisfy the relation $\Delta v=(qE/m)\Delta t$. Evaluation of f in Eq. (15) then merely involves a shifting of the two-dimensional array $f(v_x,v_z)$ along v_z at each time interval Δt, and then adding to each array element the corresponding collision term $R(v_x,v_z,t)\Delta t$. This shifting procedure accomplishes all the acceleration effects of the projectiles due to the electric field and is inherently immune to round-off error. Carrying out this procedure will require knowledge of the collision integrals for each v_x and v_z at time t. Evaluation of these integrals was described in Sec. II, and involves an integral over the polar angle θ (in velocity space) and thus requires a knowledge of the distribution function at various values of v and θ. This integration can be carried out, even though f is known only as a function of v_x and v_z, by simply interpolating $f(v_x,v_z)$ to get $f(v,\theta)$.

The algorithm for obtaining the time evolution of the velocity distribution function is as follows.

(i) Store an initial distribution function (for instance, a Maxwellian at $t=0$) in a two-dimensional array $f(v_x,v_z)$ such that $\Delta v=(qE/m)\Delta t$.

(ii) From the existing distribution function, evaluate the collision terms $R(v_x,v_z)$ for each v_x and v_z.

(iii) Multiply each of the collision terms by Δt and add to the corresponding distribution function array element $[f(v_x,v_z)\rightarrow f(v_x,v_z)+R(v_x,v_z)\Delta t]$.

(iv) Shift the resulting array along the v_z index $[f(v_x,v_z)\rightarrow f(v_x,v_z+\Delta v_z)]$ to obtain a new distribution function which corresponds to time $t+\Delta t$.

(v) Go to step (ii).

The procedure outlined in steps (ii)–(v) are repeated while various swarm parameters are calculated from the

distribution function obtained in step (iv) for each time cycle. Equilibrium is obtained when the swarm parameters cease to change in time.

IV. STABILITY CONDITIONS

In any numerical solution to a differential equation, stability is always a major consideration. The procedure of shifting the array elements along the v_z index accomplishes all of the acceleration effects due to the electric field and avoids the need to evaluate any derivatives numerically. This procedure in itself greatly enhances the numerical stability of the calculation; however, it is not in itself sufficient. One of the conditions of stability is a restatement of the so-called Courant-Friedrichs-Lewy[5] (CFL) condition and is simply

$$(a\Delta t)/\Delta v \leq 1 , \tag{16}$$

where $a = qE/m$ is, in this case, the acceleration of the projectiles due to the electric field E. Since f is stored so that its velocity increments satisfy $\Delta v = (qE/m)\Delta t$, Eq. (16) is always minimally satisfied as an *equality*. The calculation can satisfy Eq. (16) more strongly by choosing a smaller time increment $\Delta t'$, which is a proper fraction of Δt such that

$$\Delta t' = \Delta t/n, \quad \Delta v' = \Delta v/n , \tag{17}$$

while leaving a and Δv unchanged. Then Eq (5) can be rewritten

$$\begin{aligned} f(v+\Delta v, t+\Delta t') &= f(v+\Delta v-\Delta v', t) \\ &\quad + R(v+\Delta v-\Delta v', t)\Delta t' \\ &= f(v+\Delta v(1-1/n), t) \\ &\quad + R(v+\Delta v(1-1/n), t)\Delta t' . \end{aligned} \tag{18}$$

A consequence of using a time step $\Delta t'$ smaller than $\Delta t = \Delta v m/(qE)$ is that the right-hand side of Eq. (18) calls for values of f and R from velocity-space locations which are not explicitly stored in the array. We can approximate Eq. (18) into a usable form with some simple linear interpolation of the f and R arrays from their stored values to obtain

$$\begin{aligned} f(v+\Delta v, t+\Delta t') &= [(n-1)/n][f(v+\Delta v, t)+R(v+\Delta v, t)\Delta t'] \\ &\quad + (1/n)[f(v, t)+R(v, t)\Delta t'] . \end{aligned} \tag{19}$$

The above procedure for rigorously implementing the CFL stability condition is represented graphically in Fig. 3.

Another condition for the numerical stability requires that each of the array elements of the distribution function f be larger than the corresponding array elements of the collision term. Restating algebraically,

$$f(v, t)/[R(v, t)\Delta t] > 1 . \tag{20}$$

This condition can be met by selecting Δt such that Eq. (20) is satisfied for all v Experience has shown that the ratio in Eq. (20) must be of an order of 10^2 or 10^3 for low

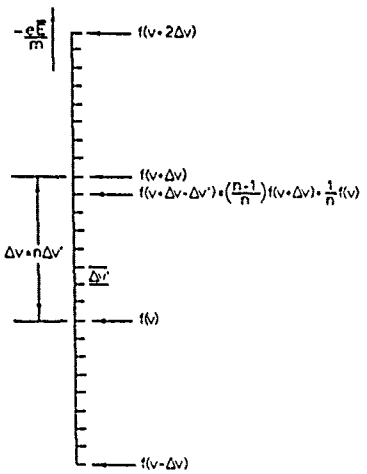

FIG. 3 Schematic representation of the acceleration procedure described in Eq (19), showing the implementation of the Courant-Friedrichs-Lewy stability condition

velocities in order to still be satisfied for high velocities. If the adiabatic condition, Eq. (20), is not met, an obvious consequence is that, if an array element of the collision term is negative, the corresponding array element of the resulting distribution function will become negative, yielding an unphysical result.

V. RESULTS AND DISCUSSION

The algorithm described in Sec. III was used to obtain the transient behavior of the EVDF and of various electron-swarm parameters for electrons in gaseous neon and gaseous argon. The swarm parameters under investigation were V_d, $\langle \varepsilon \rangle$, and R_i, which are the drift velocity, average energy of the electrons, and the ionization rate of the gas atoms, respectively. The time dependence of these quantities was calculated from the *normalized* velocity distribution function, which was obtained at each time step. The normalized distribution function $F(v, \psi, t)$ is defined as follows:

$$F(v, \psi, t) = \frac{f(v, \psi, t)}{A(t)} , \tag{21}$$

where

$$A(t) = 2\pi \int_0^\infty v^2 dv \int_0^\pi f(v, \psi, t) \sin\psi \, d\psi \tag{22}$$

and

$$A(0) \equiv 1 . \tag{23}$$

The various electron-swarm parameters are defined as follows:

$$R_i = 2\pi N \int_0^\pi v^2 dv \int_0^\pi v \sigma_{ion}(v) F(v, \psi, t) \sin\psi \, d\psi , \tag{24}$$

where $\sigma_{ion}(v)$ is the ionization cross section of the atoms by electron impact:

$$V_d = 2\pi \int_0^\infty v^2 dv \int_0^\pi v \cos\psi F(v,\psi,t) \sin\psi \, d\psi \,, \quad (25)$$

and

$$\langle \varepsilon \rangle = 2\pi \int_0^\infty v^2 dv \int_0^\pi \tfrac{1}{2} m v^2 F(v,\psi,t) \sin\psi \, d\psi \,. \quad (26)$$

By using a normalized distribution function, the total number of electrons in the distribution function is kept constant; this situation is analogous to a steady-state Townsend (SST) experiment. A pulsed Townsend (PT) experiment can be simulated by using an *unnormalized* time-evolved distribution function, since in such an experiment the number of electrons does not stay constant. In a PT calculation, the final equilibrium values of the swarm parameters, obtained from the unnormalized final equilibrium distribution function, will depend on the initial conditions. On the other hand, the equilibrium values of the swarm parameters in an SST calculation are independent of the initial conditions. For this reason, we have chosen to present only the normalized SST results for various swarm parameters. In each case a Maxwellian velocity distribution of electrons was assumed at time $t=0$ and a gas density N of 3.54×10^{16} cm^{-3} (1.32×10^{-3} amagat or, equivalently, 1 Torr at 273 K) was used. Isotropic scattering was assumed in all cases.

The convergence of the swarm parameters to their final equilibrium values occurs more quickly as the value of E/N becomes larger. For cases in which the E/N values are small, the time required to reach equilibrium can become large, forcing the calculation to consume more computing time. In cases of small E/N and when only the final equilibrium values of various swarm parameters are of interest, the time-*independent* two-term expansion methods may be computationally more efficient (although the time dependence will be lost). In cases of large E/N, however, convergence is fast enough so that the time-dependent calculations described in this paper become practical with very modest computing resources

A. Electrons in neon

For neon, the velocity steps Δv ranged from 2.05×10^7 to 3.40×10^7 cm/sec, and the time steps Δt ranged from 0.1 to 0.02 nsec as the E/N ratio was varied from 35 to 566 Td. The relevant scattering cross sections used in the calculations were taken from Ref. 2. Figure 4 displays the calculated time-dependent behavior of the electron-swarm parameters for $E/N=566$ Td and with initial average energies of 44 and 20 eV. From this figure, it is evident that, although the final equilibrium values of the swarm parameters are unaffected by the average energy value of the initial velocity distribution function, the transient behavior may be considerably different. For example, an overshoot in the drift velocity is observed if the initial average energy of the EVDF is less than the final equilibrium value, but the overshoot does not appear if the initial average energy is somewhat higher than the final value.

Figure 5 displays the time-dependent behavior of the electron-swarm parameters in gaseous neon with E/N ratios of 35 and 72 Td. The initial value of $\langle \varepsilon \rangle$ for the cases of 35 and 72 Td are 12 and 16 eV, respectively. For

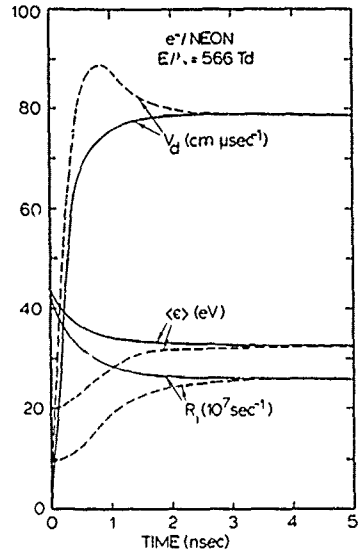

FIG. 4. Time dependence of various electron-swarm parameters in gaseous neon for $E/N=566$ Td. The data corresponding to the solid curves and the dashed curves have initial average electron energy of 44 and 20 eV, respectively

the case in which $E/N=35$ Td, an overshoot of the drift velocity is present and slight undershoots of both the average energy and ionization rate can also be seen. The undershoots are not seen in the 72-Td data; however, a

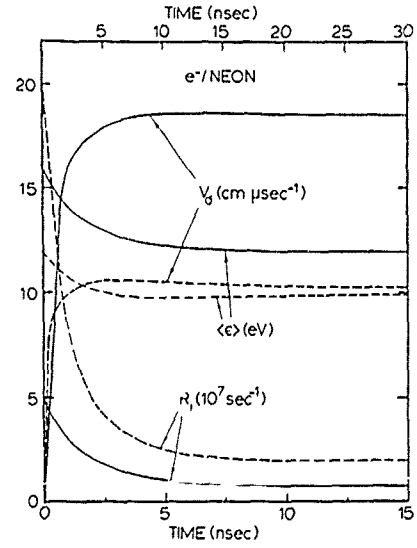

FIG. 5 Time dependence of various electron-swarm parameters in gaseous neon for $E/N=72$ Td (solid curves) and 35 Td (dashed curves). The upper and lower time scales correspond to the 35- and 72-Td data, respectively.

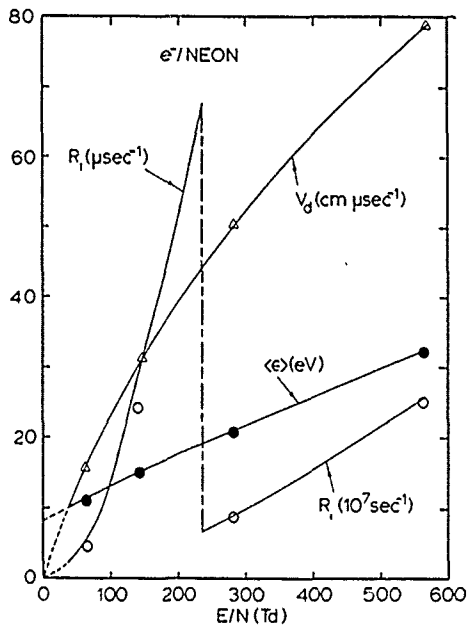

FIG 6. Equilibrium values of various electron-swarm parameters in gaseous neon. The solid circles, open circles, and triangles are, respectively, the equilibrium values of $\langle\varepsilon\rangle$, R_i, and V_d from the calculations of Kitamori *et al.* (Ref. 2). The dashed lines for the values of E/N below 35 Td correspond to extrapolated values of various parameters.

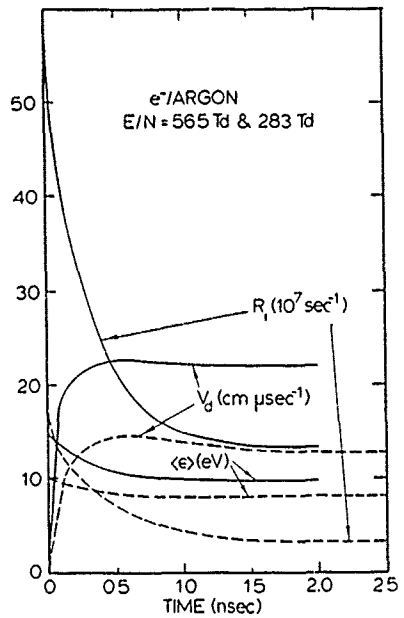

FIG. 7 Time dependence of various electron-swarm parameters in gaseous argon for $E/N = 565$ Td (solid curves) and 283 Td (dashed curves)

slight overshoot of the drift velocity is present. Whether or not these undershoots or overshoots occur depends on the initial value of the average energy of the swarm compared to that of the final equilibrium value. Recently observed[6,7] current overshoots in Ar-Hg and Ne-Hg discharges, and ionization rate overshoots in N_2 discharges, are presumably related to the initial conditions of the electron-energy distribution function.

The final equilibrium values of the electron-swarm parameters as a function of E/N are depicted in Fig. 6, and are in very g[illegible] agreement with the values calculated by Kitamori, Tagashira, and Sakai.[2] The zero-field ($E/N = 0$) values of various parameters can be extrapolated from the curve of Fig. 6. These values are

$$V_d \rightarrow 0.0\text{cm/sec}, \quad R_i \rightarrow 0.0\ \text{sec}^{-1}, \quad \langle\varepsilon\rangle \rightarrow 8.7\ \text{eV}\ .$$

The variation in slope of the drift velocity, particularly near the lower E/N values, suggests that the electron mobility in neon, which is related to $\partial V_d/\partial(E/N)$, is slightly dependent upon E/N.

B. Electrons in argon

The cross sections for the elastic scattering of electrons with argon were taken from Massey and Burhop,[8] and the ionization cross sections were from Rapp and Englander-Golden.[9] The total excitation cross sections were adapted from Sakai *et al.*[10] by assuming a constant energy loss of 11 5 eV for all excitation processes.

Figures 7 and 8 display the time-dependent behavior of the electron-swarm parameters for E/N ratios ranging from 72 to 565 Td. For a given value of E/N, the velocity step Δv and time step Δt in the present case are comparable to those of the neon case. In each of these figures, overshoots in the drift velocities are observed and they are most dramatic when the initial average energy is

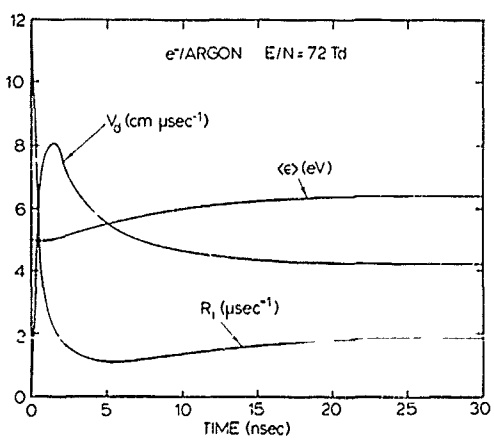

FIG. 8. Time dependence of various electron-swarm parameters in gaseous argon for $E/N = 72$ Td.

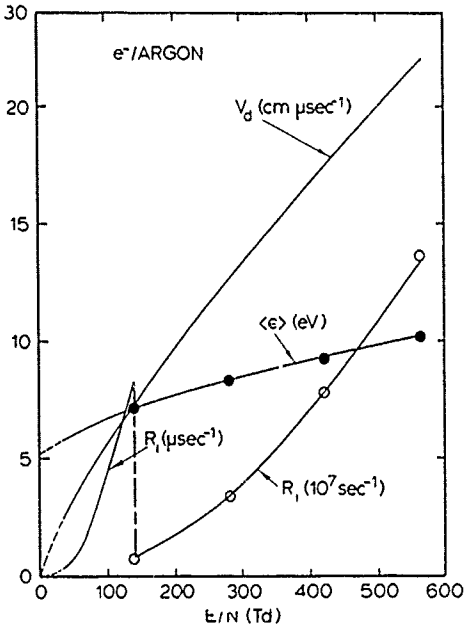

FIG. 9. Equilibrium values of various electron-swarm parameters in gaseous argon. The solid circles and the open circles are, respectively, the equilibrium values of $\langle \varepsilon \rangle$ and R_t from the SST calculations of Sakai *et al.* (Ref. 10).

closest to the final equilibrium average energy. That the size of the overshoot seems to vary inversely with the E/N ratio is merely an artifact resulting from the fact that the initial average energy values just happened to be chosen closer to the equilibrium values as the E/N ratios were reduced. In fact, the overshoot can be enhanced or completely eliminated at any E/N ratio by merely adjusting the value of the initial average energy.

Some preliminary analysis of the transient behavior of the presently calculated electron-swarm parameters (for both neon and argon) suggests that their time-dependent behavior can be accurately fitted by a sum of two exponentials. In fact, exponential behavior of the time dependence of various swarm parameters can be analytically justified,[11,12] especially for low values of E/N, by assuming a constant collision frequency which leads to a very simplified collision term.

The equilibrium values of the electron-swarm parameters in argon, plotted as a function of E/N, are shown in Fig. 9. As was done in the case of neon, the zero-field values of various swarm parameters can be obtained by extrapolation from this figure; this extrapolation procedure yields the following values:

$$V_d \rightarrow 0.0 \text{ cm/sec}, \quad R_t \rightarrow 0.0 \text{ sec}^{-1}, \quad \langle \varepsilon \rangle \rightarrow 5.2 \text{ eV} .$$

The equilibrium values in Fig. 9 can be compared with the values calculated by Sakai *et al.*[10] In their paper, various expressions used to define the drift velocity V_d were different from the expression used in the present calculations [Eq (25)]. Thus meaningful comparisons could not be made for that parameter. The expressions for R_t and $\langle \varepsilon \rangle$ used in the SST condition calculations of Ref. 10 were equivalent to the expressions used in the present paper so that comparisons among these parameters are feasible. Figure 9 shows that the agreement between the two calculations is excellent.

The unnormalized equilibrium EVDF in argon is shown for two different values of E/N in Fig. 10. In both cases the initial distribution function (at $t=0$) is a spheri-

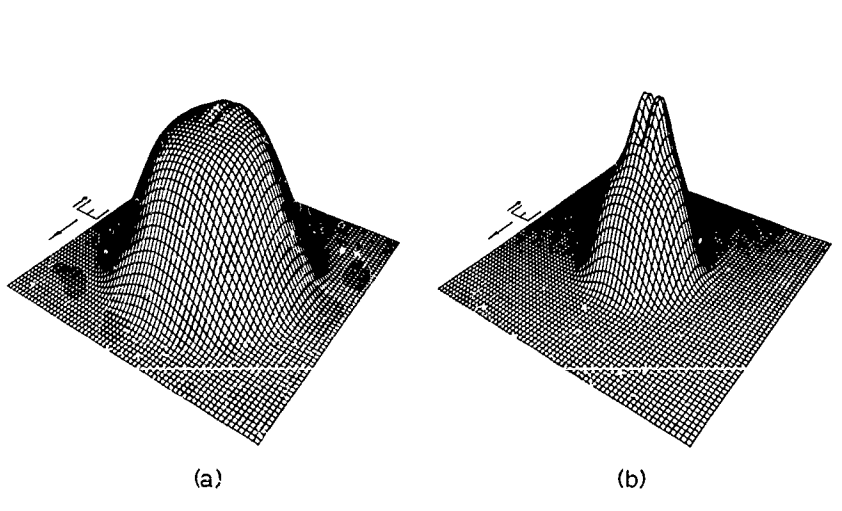

FIG. 10. Equilibrium velocity distribution function of electrons in argon for (a) $E/N = 35$ Td and (b) $E/N = 424$ Td.

cally symmetric Maxwellian with $\langle\varepsilon\rangle=5$ eV for $E/N=35$ Td and $\langle\varepsilon\rangle=30$ eV for $E/N=424$ Td. At equilibrium, the distribution function retains much of its spherical symmetry for low E/N. For large values of E/N, however, the equilibrium EVDF becomes highly asymmetric, suggesting that the effect of the electric field on the distribution function dominates over the effects of collisions. This clearly indicates that the two-term expansion procedure, which retains only first-order deviations from spherical symmetry, for obtaining the equilibrium EVDF, would be valid only for small values of E/N The present procedure for obtaining the EVDF is valid for any value of E/N, small or large.

The "valley" near the origin ($v=0$) of the distribution function, which becomes very pronounced for large values of E/N, is probably due to the fact that very-low-energy electrons have a very small collision probability and are quickly accelerated by the electric field to a higher velocity where they become more likely to have collisions. On the other hand, the "upstream" electrons are not as efficiently accelerated into the origin (where they would replace those that have been accelerated out), because their velocities are already large enough so that they are inhibited by collisions.

VI. CONCLUSIONS

A very simple numerical algorithm has been described which obtains the time-dependent behavior of an electron-velocity distribution function in a gas. Aside from its simplicity, the algorithm has many unique and valuable features. Unlike many other methods of solution of the Boltzmann equation, the present method does not make use of any term expansions of the distribution function, and in this respect the solution is exact. The need for numerical evaluation of derivatives has been completely eliminated, which allows for a much more stable solution. The computational algorithm itself only involves summing and shifting of various array elements, which can be done without incurring any round-off error; this fact enhances the stability of the numerical procedure. Because of the simplicity of the procedure, the calculation can be performed with very modest computing resources. This is especially true in cases of high-E/N values for which convergence to equilibrium is much faster than for low E/N.

Although the calculations that are presented in this paper are for electron swarms in a pure gas, like neon or argon, subjected to a constant electric field, other more complicated situations can be very easily adapted to the present procedure. For instance, the present algorithm could be easily adapted to the case in which the electron swarm interacts with a gas mixture. Other situations of interest include the cases in which the projectile particles are more massive than electrons such as muons, protons, and heavy ions. Furthermore, the present procedure can easily accommodate the case in which the external electric field varies with time, such as an rf field. These other applications of the present procedure are under current investigation.

ACKNOWLEDGMENTS

It is a pleasure to thank Professor A. Garscadden for introducing us to this research problem and Professor H. H. Denman for valuable conversations. The support of the U S. Air Force Office of Scientific Research through Grant No. AFOSR-87-0342 is gratefully acknowledged.

[1]A V Phelps and L C Pitchford, Phys Rev A **31**, 2932 (1985)
[2]K. Kitamori, H. Tagashira, and Y Sakai, J. Phys D **11**, 283 (1977).
[3]P. J. Drallos and J. M. Wadehra, J Appl. Phys. **63**, 5601 (1988)
[4]T. Holstein, Phys Rev. **70**, 367 (1946).
[5]R Courant, K Friedrichs, and H. Lewy, Math. Ann **100**, 32 (1928)
[6]M. E. Duffy and J. H. Ingold, Bull. Am. Phys Soc **34**, 307 (1989).
[7]J T Verdeyen, L. C Pitchford, Y M Li, J B. Gerardo, and G N. Hays, Bull. Am. Phys Soc. **34**, 322 (1989).
[8]H. S. W Massey and E H. S Burhop, *Electronic and Ionic Impact Phenomena*, 2nd ed. (Clarendon, Oxford, England, 1969), Vol 1
[9]D Rapp and P. Englander-Golden, J. Chem Phys **43**, 1464 (1965).
[10]Y Sakai, H. Tagashira, and S. Sakamoto, J. Phys D **10**, 1035 (1977).
[11]B. Shizgal and D. R. A McMahon, Phys. Rev. A **32**, 3669 (1985); D. R. A McMahon, K. Ness, and B Shizgal, J. Phys. B **19**, 2759 (1986).
[12]L C. Pitchford, Air Force Wright Aeronautical Laoratory Technical Report No. AFWAL-TR-85-2106, 1985, G. N Hays, L. C Pitchford, J B. Gerardo, J. T Verdeyen, and Y. M. Li, Phys Rev. A **36**, 2031 (1987)

INTERNATIONAL JOURNAL OF QUANTUM CHEMISTRY, VOL. XXXVII, 797–809 (1990)

Analytical Expressions and Recursion Relations of Two-center Harmonic Oscillator Matrix Elements of Arbitrary Functions

P. J. DRALLOS AND J. M. WADEHRA
Department of Physics and Astronomy, Wayne State University, Detroit, Michigan 48202

Abstract

The matrix elements of various analytical functions $f(X)$, X being the internuclear separation, are required for the description of transition probabilities and other molecular properties. These matrix elements can be conveniently estimated by assuming vibrational wave functions of two relatively displaced linear harmonic oscillators of arbitrary frequencies to represent the vibrational levels of two electronic states of a molecule. Using this assumption, analytical expressions for the matrix elements of an *arbitrary* analytical function $f(X)$ are obtained. Useful recursion relations among these matrix elements are derived and an elegant graphical representation of the recursion relations is obtained. These graphical representations are utilized to obtain new more general recursion relations among matrix elements of the arbitrary function $f(X)$.

I. Introduction

In describing various physical properties, like the oscillator strengths, the transition rates etc., of a molecule, the matrix elements of various functions of the internuclear separation X appear naturally in the formulation. A part of these matrix elements is normally to be evaluated between vibrational wave functions belonging to two different electronic states of the molecule. For small vibrational quantum numbers it is reasonably accurate to replace the actual potential curves of the relevant electronic states by those of linear harmonic oscillators. For the cases of large vibrational quantum numbers, where the effects of anharmonicity are relatively significant, one could use a Morse-type potential to represent the potential curves. If one were then to use the standard perturbative techniques, with the linear harmonic potential as the zeroth order approximation, the harmonic oscillator matrix elements of various functions of X would appear in the correction terms. In a recent paper [1] we obtained closed form expressions and recursion relations among two-center harmonic oscillator matrix elements of some *definite* functions of X. The two linear harmonic oscillators (LHO) were assumed to have arbitrary frequencies and equilibrium positions. The functions of X considered earlier [1] were the exponential, Gaussian, and powers of X. In the present paper we will generalize the earlier results to include any *arbitrary* analytical function $f(X)$ which could be expanded as a power series in X.

The use of linear harmonic oscillator wave functions in obtaining the Franck-Condon overlap integral dates back [2] to 1930; however, there has been some recent interest [3–5] in obtaining analytical expressions as well as recursion relations among the

 CCC 0020-7608/90/060797-13$04.00

two-center harmonic oscillator integrals of arbitrary functions of X because of their possible applications in molecular physics and vibrational spectroscopy. Two important conclusions reached previously [1] will be of interest in the present discussion. First, the two-center LHO matrix elements of X-dependent functions like the exponential [$\exp(-\alpha X)$] and the Gaussian [$\exp(-\beta X^2)$] could be obtained from the corresponding Franck-Condon overlap integrals by a simple scaling procedure Second, the two-center LHO matrix elements of powers of X (the Franck-Condon overlap integral is a special case of these corresponding to X^0) satisfy four- or five-term recursion relations which can be utilized for rapid evaluation of various matrix elements. We will show below that the two-center LHO matrix elements of an arbitrary analytical function $f(X)$ also satisfy some simple recursion relations and, furthermore, these recursion relations can be represented in an elegant graphical manner The graphical representation of these generalized recursion relations will be used as an aid in obtaining new general recursion relations which are also valid for any analytical function of X.

II. Arbitrary Function $f(X)$

In the present notation $\langle X|m\rangle$ is the wave function of the mth level of the harmonic oscillator associated with the potential $V_1 = \mu \quad \nu^2/2$, and $\langle\langle X|n\rangle\rangle$ is the wave function of the nth level of the harmonic oscillator associated with the potential $V_2 = \mu\omega_2(X - X_0)^2/2$. X_0 is the separation between the two oscillators and, for convenience, define $\omega_0 = \hbar/(\mu X_0^2)$. The wave functions $\langle X|m\rangle$ and $\langle\langle X|n\rangle\rangle$ of the two harmonic oscillators are written in terms of standard Hermite polynomials H_m and H_n Note the analogy of the present single and double ket notation (for example, $|m\rangle$ and $|n\rangle\rangle$) with the standard single and double prime notation which is used to distinguish between the vibrational eigenfunctions belonging to the two different electronic states of a molecule. For convenience, define $a = [2\omega_1/(\omega_1 + \omega_2)]^{1/2}$, $b = [2\omega_2/(\omega_1 + \omega_2)]^{1/2}$ and $c = [(\omega_1 + \omega_2)/2\omega_0]^{1/2}$ Using the LHO wave functions, the matrix element of the arbitrary function $f(X)$ can be written as

$$\begin{aligned}\langle m|f(X)|n\rangle\rangle &= \int_{-\infty}^{\infty} dX\left\{(2^m m!)^{-1/2}\left(\frac{\omega_1}{\pi\omega_0 X_0^2}\right)^{1/4}\exp\left[-\frac{\omega_1 X^2}{2\omega_0 X_0^2}\right]H_m\left[\left(\frac{\omega_1}{\omega_0}\right)^{1/2}\frac{X}{X_0}\right]\right\}f(X)\\ &\quad\times\left\{(2^n n!)^{-1/2}\left(\frac{\omega_2}{\pi\omega_0 X_0^2}\right)^{1/4}\exp\left[-\frac{\omega_2(X - X_0)^2}{2\omega_0 X_0^2}\right]H_n\left[\left(\frac{\omega_2}{\omega_0}\right)^{1/2}\frac{X - X_0}{X_0}\right]\right\}\\ &= N_{mn}\pi^{-1/2}\int_{-\infty}^{\infty} du\\ &\quad\times f[X(u)]\exp\left[-\left(u - \frac{b^2 c}{2}\right)^2\right]H_m(au)H_n[b(u - c)], \qquad (1)\end{aligned}$$

where, in the last step, the integration variable has been changed from X to dimensionless u as

$$u = [(\omega_1 + \omega_2)/(2\omega_0)]^{1/2}\cdot X/X_0 = c\cdot X/X_0$$

and

$$N_{mn} = (\omega_1\omega_2)^{1/4}[(\omega_1 + \omega_2)2^{m+n-1}m!\,n!]^{-1/2}\exp\{-\omega_1\omega_2/[2\omega_0(\omega_1 + \omega_2)]\}$$
$$= [ab/(2^{m+n}m!\,n!)]^{1/2}\exp\{-(abc/2)^2\}$$

Applying the recursion relation for Hermite polynomials, Eq. (A 1), to either $H_m(au)$ or $H_n[b(u - c)]$ in Eq. (1) yields, respectively,

$$2ac\langle m|Xf(X)|n\rangle = [2(m + 1)]^{1/2}X_0\langle m + 1|f(X)|n\rangle + (2m)^{1/2}X_0\langle m - 1|f(X)|n\rangle \quad (2a)$$

and

$$2bc\langle m|(X - X_0)f(X)|n\rangle = [2(n + 1)]^{1/2}X_0\langle m|f(X)|n + 1\rangle + (2n)^{1/2}X_0\langle m|f(X)|n - 1\rangle \quad (2b)$$

Using, in the integrands of Eqs. (2),

$$u\exp[-(u - y)^2] = -1/2(d/du)\exp[-(u - y)^2] + y\exp[-(u - y)^2]$$

with $y = b^2c/2$, then performing integration by parts and the necessary derivatives [using Eq. (A.2)], we obtain two independent recursion relations for the matrix elements of $f(X)$:

$$X_0\langle m|df(X)/dX|n\rangle = [2(m + 1)]^{1/2}(c/a)\langle m + 1|f(X)|n\rangle + (2m)^{1/2}(c/a)(1 - a^2)\langle m - 1|f(X)|n\rangle - (2n)^{1/2}bc\langle m|f(X)|n - 1\rangle - b^2c^2\langle m|f(X)|n\rangle \quad (3)$$

and

$$X_0\langle m|df(X)/dX|n\rangle = [2(n + 1)]^{1/2}(c/b)\langle m|f(X)|n + 1\rangle + (2n)^{1/2}(c/b)(1 - b^2)\langle m|f(X)|n - 1\rangle - (2m)^{1/2}ac\langle m - 1|f(X)|n\rangle + a^2c^2\langle m|f(X)|n\rangle. \quad (4)$$

Equations (3) and (4) are independent and can be combined to obtain two additional recursion relations [which are not independent from (3) and (4)]. These four relations are generalizations of the recursion relations for two-center LHO Franck-Condon overlap integrals obtained previously by Ansbacher [6] and Manneback [7]. The relations of Ansbacher and Manneback are obtained by setting $f(X)$ = constant in (3) and (4) above.

An arbitrary analytical function $f(X)$ can always be expanded in a Taylor series, so that

$$f(X) = \sum_{l=0}^{\infty}\frac{f^{(l)}(0)}{l!}X^l \quad (5)$$

where $f^{(l)}(0)$ denotes the lth derivative of $f(X)$ evaluated at $X = 0$. Operating on Eq. (5) with $\langle m|$ from the left and $|n\rangle$ from the right, a simple expression for the matrix element of $f(X)$ in terms of the matrix elements of X^l is obtained:

$$\langle m|f(X)|n\rangle = \sum_{l=0}^{\infty} \frac{f^{(l)}(0)}{l!} \langle m|X^l|n\rangle . \tag{6}$$

On using the closed form expression for the matrix elements of X^l, given by Eq. (A.3), the matrix elements of $f(X)$ can finally be written as

$$\langle m|f(X)|n\rangle = \sum_{l=0}^{\infty} f^{(l)}(0) \frac{X_0^l}{(2c)^l} \sum_{p=0}^{\lceil m,l\rceil} \sum_{q=0}^{\lceil n,l-p\rceil} \left[\frac{2^{p+q} m!\, n!}{(m-p)!(n-q)!}\right]^{1/2} \times \frac{a^p b^q (-1)^{l-p-q} H_{l-p-q}\left(\frac{ib^2c}{2}\right)}{p!\, q!\, (l-p-q)!} \langle m-p|n-q\rangle . \tag{7}$$

The notation $\lceil a, b\rceil$ refers to the smaller of a and b. The overlap integral $\langle m-p|n-q\rangle$ can be easily obtained from Eq. (A.4).

III. Graphical Representation

Two different kinds of recursion relations are obtained above for the matrix elements of $f(X)$. One type of recursion relation relates a single matrix element $\langle m|Xf(X)|n\rangle$ (m and n refer to the vibrational quantum numbers of the two oscillators) to a linear combination of matrix elements of $f(X)$. Equations (2a) and (2b) embody such recursion relations. In the other kind of recursion relation, which are of interest to us here, a single matrix element of $df(X)/dX$ is expressed as a linear combination of matrix elements of $f(X)$. Equations (3) and (4), which are examples of this kind of recursion relation, can be further generalized by writing the arbitrary function $f(X)$ as the lth derivative of another arbitrary analytical function $g(X)$, that is, $f(X) = g^{(l)}(X)$:

$$\begin{aligned} X_0\langle m|g^{(l+1)}(X)|n\rangle = {} & [2(m+1)]^{1/2}(c/a)\langle m+1|g^{(l)}(X)|n\rangle \\ & + (2m)^{1/2}(c/a)(1-a^2)\langle m-1|g^{(l)}(X)|n\rangle \\ & - (2n)^{1/2}bc\langle m|g^{(l)}(X)|n-1\rangle - b^2c^2\langle m|g^{(l)}(X)|n\rangle \end{aligned} \tag{8}$$

and

$$\begin{aligned} X_0\langle m|g^{(l+1)}(X)|n\rangle = {} & [2(n+1)]^{1/2}(c/b)\langle m|g^{(l)}(X)|n+1\rangle \\ & + (2n)^{1/2}(c/b)(1-b^2)\langle m|g^{(l)}(X)|n-1\rangle \\ & - (2m)^{1/2}ac\langle m-1|g^{(l)}(X)|n\rangle + a^2c^2\langle m|g^{(l)}(X)|n\rangle . \end{aligned} \tag{9}$$

Generalized recursion relations (8) and (9) are shown graphically in Fig. 1a and b, respectively. Each solid circle in this figure represents a matrix element (depending upon m, n, and l) in the recursion relation. Here, l is the order of derivative of $g(X)$ with respect to X. A similar graphical representation of the recursion relations for the Franck-Condon overlap integrals [which are obtained by setting $g^{(l)}(X)$ = constant] was presented by Manneback [7]. Note that in Eqs. (8) and (9) matrix elements of different orders of derivative of $g(X)$ are mixed and, therefore, in reality the various terms in these relations represent matrix elements of different functions of X. A recursion relation that does not mix matrix elements of different derivatives of a func-

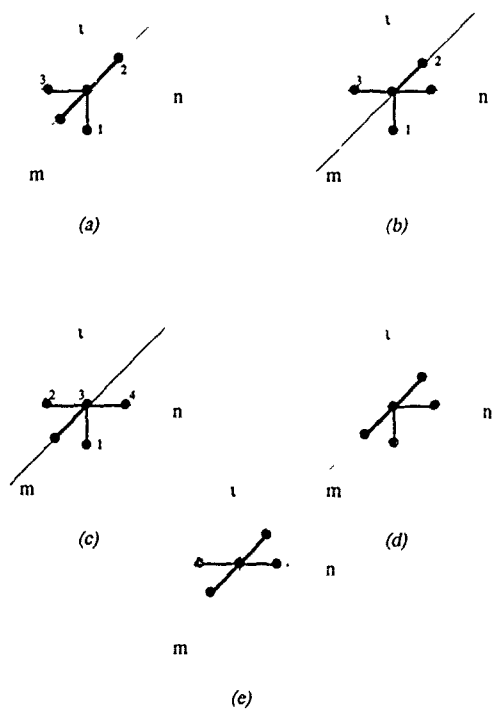

Figure 1 The recursion relations of Eqs (8), (9), (11), (12), and (10) are represented graphically in a, b, c, d, and e, respectively. m and n are the vibrational quantum numbers of the two linear harmonic oscillators, and l is the order of derivative of the arbitrary function $g(X)$ with respect to X. Each solid circle represents a single matrix element appearing in the recursion relation.

tion of X, making it truly valid for matrix elements of *any* analytical function of X, is easily obtained by combining Fig. 1a and b and eliminating points labelled 1 in the figures. The resulting five-term recursion relation is represented graphically in Fig. 1e, and it corresponds to the following equation:

$$\begin{aligned}(2)^{1/2}abc\langle m|g^{(l)}(X)|n\rangle = b \cdot \{&[(m+1)]^{1/2}\langle m+1|g^{(l)}(X)|n\rangle \\ &+ (m)^{1/2}\langle m-1|g^{(l)}(X)|n\rangle\} \\ - a \cdot \{&[(n+1)]^{1/2}\langle m|g^{(l)}(X)|n+1\rangle \\ &+ (n)^{1/2}\langle m|g^{(l)}(X)|n-1\rangle\}. \end{aligned} \tag{10}$$

In this relation, both of the indices (m and n) of the matrix elements vary. The relation (10) is also a generalization of the so-called "diamond" relation [8] for one-center LHO matrix elements of arbitrary functions. We note, in passing, that relation (10) is also obtained by combining Eqs. (2a) and (2b).

Sometimes one needs [9] to have a recursion relation, such as relation (2), in which only one of the indices (either m or n) varies and the other index remains constant. To derive alternate recursion relations of this kind, we first obtain Fig. 1c and d by combining Fig. 1a and b and eliminating the points labelled 2 and 3, respectively. The two relations obtained in this manner are merely alternative forms of the recursion relations (8) and (9) and do not contain any information that is not already in (8) and (9). The algebraic expressions for these alternative recursion relations corresponding to Fig. 1c and d are, respectively,

$$\begin{aligned} X_0\langle m|g^{(l+1)}(X)|n\rangle\rangle = {} & [2(m+1)]^{1/2}ac\langle m+1|g^{(l)}(X)|n\rangle\rangle - a^2c^2\langle m|g^{(l)}(X)|n\rangle\rangle \\ & + [2(n+1)]^{1/2}(c/b)(1-a^2)\langle m|g^{(l)}(X)|n+1\rangle\rangle \\ & - (2n)^{1/2}(c/b)\langle m|g^{(l)}(X)|n-1\rangle\rangle \end{aligned} \tag{11}$$

and

$$\begin{aligned} X_0\langle m|g^{(l+1)}(X)|n\rangle\rangle = {} & [2(n+1)]^{1/2}bc\langle m|g^{(l)}(X)|n+1\rangle\rangle + b^2c^2\langle m|g^{(l)}(X)|n\rangle\rangle \\ & + [2(m+1)]^{1/2}(c/a)(1-b^2)\langle m+1|g^{(l)}(X)|n\rangle\rangle \\ & - (2m)^{1/2}(c/a)\langle m-1|g^{(l)}(X)|n\rangle\rangle . \end{aligned} \tag{12}$$

Next the points labelled 1, 2, 3, and 4 of Fig. 1c are eliminated using point 2 of Fig. 1b successively. Figure 2 depicts this elimination procedure. The resulting fig-

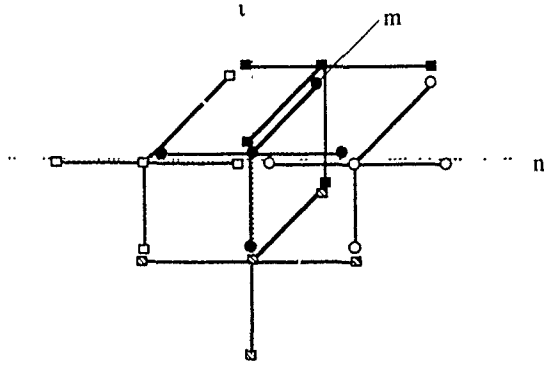

Figure 2 The graphical aid used for deriving the recursion relation (13) for matrix elements of the arbitrary function $g(X)$. The shaded portion encompasses the matrix elements that appear in the derived recursion relation

ure, which is in the form of a triangle lying completely in the n-l plane with m fixed, represents a nine-term recursion relation in which the matrix elements of different orders of derivative are still mixed. The resulting algebraic expression for this relation is

$$\begin{aligned}
&+b^2(X_0/c)^2\langle m|g^{(l+2)}|n\rangle + b^3(X_0/c)(2n)^{1/2}\langle m|g^{(l+1)}|n-1\rangle - \\
&\quad b^3(X_0/c)[2(n-1)]^{1/2}\langle m|g^{(l+1)}|n+1\rangle + \\
&2(1-a^2)[n(n-1)]^{1/2}\langle m|g^{(l)}|n-2\rangle - a^4bc(2n)^{1/2}\langle m|g^{(l)}|n-1\rangle + \\
&\quad \{-a^4b^2c^2 - 2(2n+1) + 2a^2b^2(m+n+1)\}\langle m|g^{(l)}|n\rangle - \\
&\quad a^4bc[2(n+1)]^{1/2}\langle m|g^{(l)}|n+1\rangle + \\
&\quad 2(1-a^2)[(n+2)(n+1)]^{1/2}\langle m|g^{(l)}|n+2\rangle = 0. \qquad (13)
\end{aligned}$$

The same procedure of eliminating four terms of Fig. 1d using a single point of Fig. 1a repeatedly can be used again to obtain the following nine-term recursion relation with n fixed and m and l varying:

$$\begin{aligned}
&+a^2(X_0/c)^2\langle m|g^{(l+2)}|n\rangle + a^3(X_0/c)(2m)^{1/2}\langle m-1|g^{(l+1)}|n\rangle - \\
&\quad a^3(X_0/c)[2(m+1)]^{1/2}\langle m+1|g^{(l+1)}|n\rangle + \\
&2(1-b^2)[m(m-1)]^{1/2}\langle m-2|g^{(l)}|n\rangle + ab^4c(2m)^{1/2}\langle m-1|g^{(l)}|n\rangle + \\
&\quad \{-a^2b^4c^2 - 2(2m+1) + 2a^2b^2(m+n+1)\}\langle m|g^{(l)}|n\rangle + \\
&\quad ab^4c[2(m+1)]^{1/2}\langle m+1|g^{(l)}|n\rangle + \\
&\quad 2(1-b^2)[(m+2)(m+1)]^{1/2}\langle m+2|g^{(l)}|n\rangle = 0. \qquad (14)
\end{aligned}$$

IV. Special Cases

The above general results can be presented in simplified forms for some important special cases.

Case 1

For $\omega_1 = \omega_2 = \omega$ but $X_0 \neq 0$ [$a = b = 1$ and $c^2 = \omega/\omega_0$] the most general matrix element can be written as

$$\begin{aligned}
\langle m|f(X)|n\rangle = \sum_{l=0}^{\infty} f^{(l)}(0)\left(\frac{X_0}{2c}\right)^l \sum_{p=0}^{\lceil m,l\rceil} \sum_{q=0}^{\lceil n,l-p\rceil} \left[\frac{2^{p+q}m!\,n!}{(m-p)!\,(n-q)!}\right]^{1/2} \\
\times \frac{(-1)^{(l-p-q)}H_{l-p-q}(ic/2)}{p!\,q!\,(l-p-q)!}\langle m-p|n-q\rangle
\end{aligned}$$

with

$$\langle m|n\rangle = N_{mn}\sum_{k=0}^{\lceil m,n\rceil} \frac{m!\,n!}{(m-k)!\,(n-k)!\,k!}2^k(-c)^{(n-k)}(c)^{(m-k)} \qquad (15)$$

The recursion relations of Eqs. (8) and (9) become

$$\begin{aligned}
X_0\langle m|g^{(l+1)}(X)|n\rangle = [2(m+1)]^{1/2}c\langle m+1|g^{(l)}(X)|n\rangle \\
- (2n)^{1/2}c\langle m|g^{(l)}(X)|n-1\rangle - c^2\langle m|g^{(l)}(X)|n\rangle \qquad (16a)
\end{aligned}$$

and

$$X_0\langle m|g^{(l+1)}(X)|n\rangle\rangle = [2(n+1)]^{1/2}c\langle m|g^{(l)}(X)|n+1\rangle\rangle - (2m)^{1/2}c\langle m-1|g^{(l)}(X)|n\rangle\rangle + c^2\langle m|g^{(l)}(X)|n\rangle\rangle . \quad (16b)$$

The recursion relations of Eqs. (13) and (14) become

$$+(X_0/c)^2\langle m|g^{(l+2)}|n\rangle\rangle + (X_0/c)(2n)^{1/2}\langle m|g^{(l+1)}|n-1\rangle\rangle - (X_0/c)[2(n+1)]^{1/2}\langle m|g^{(l+1)}|n+1\rangle\rangle - c(2n)^{1/2}\langle m|g^{(l)}|n-1\rangle\rangle + \{2(m-n)-c^2\}\langle m|g^{(l)}|n\rangle\rangle - c[2(n+1)]^{1/2}\langle m|g^{(l)}|n+1\rangle\rangle = 0 \quad (17a)$$

and

$$+(X_0/c)^2\langle m|g^{(l+2)}|n\rangle\rangle + (X_0/c)(2m)^{1/2}\langle m-1|g^{(l+1)}|n\rangle\rangle - (X_0/c)[2(m+1)]^{1/2}\langle m+1|g^{(l+1)}|n\rangle\rangle + c(2m)^{1/2}\langle m-1|g^{(l)}|n\rangle\rangle + \{2(n-m)-c^2\}\langle m|g^{(l)}|n\rangle\rangle + c[2(m+1)]^{1/2}\langle m+1|g^{(l)}|n\rangle\rangle = 0 . \quad (17b)$$

Case 2

When ω_1 is not equal to ω_2 but $X_0 = 0$ [that is, $(X_0/c)^2 = 2\hbar/\{\mu(\omega_1+\omega_2)\}$ and $c = 0$], the two-center harmonic oscillator matrix element of the arbitrary function $f(X)$ becomes,

$$\langle m|f(X)|n\rangle\rangle = \sum_{l=0}^{\infty} f^{(l)}(0)\left(\frac{\hbar}{2\mu(\omega_1+\omega_2)}\right)^{l/2} \sum_{p=0}^{\lceil m,l\rceil} \sum_{q=0}^{\lceil n,l-p\rceil} \times \left[\frac{2^{p+q}m!\,n!}{(m-p)!\,(n-q)!}\right]^{1/2} \frac{a^p b^q}{p!\,q!\left(\frac{l-p-q}{2}\right)!}\langle m-p\,|\,n-q\rangle\rangle$$

with

$$\langle m\,|\,n\rangle\rangle = N_{mn} \sum_{k=0}^{\lceil m,n\rceil} \frac{m!\,n!}{\left(\frac{m-k}{2}\right)!\left(\frac{n-k}{2}\right)!\,k!}(2ab)^k(b^2-1)^{\left(\frac{n-k}{2}\right)}(a^2-1)^{\left(\frac{m-k}{2}\right)}. \quad (18)$$

Only those terms in the triple sum [over l, p, and q] for which $(l-p-q)$ is an even integer contribute to the sum. Also only those terms in the k sum for which $(n-k)$ and $(m-k)$ are even integers contribute to the overlap integral $\langle m\,|\,n\rangle\rangle$. The recursion relations of Eqs. (8) and (9) reduce to

$$a(X_0/c)\langle m|g^{(l+1)}(X)|n\rangle\rangle = [2(m+1)]^{1/2}\langle m+1|g^{(l)}(X)|n\rangle\rangle + (2m)^{1/2}(1-a^2)\langle m-1|g^{(l)}(X)|n\rangle\rangle - (2n)^{1/2}ab\langle m|g^{(l)}(X)|n-1\rangle\rangle \quad (19a)$$

and

$$b(X_0/c)\langle m|g^{(l+1)}(X)|n\rangle\rangle = [2(n+1)]^{1/2}\langle m|g^{(l)}(X)|n+1\rangle\rangle + (2n)^{1/2}(1-b^2)\langle m|g^{(l)}(X)|n-1\rangle\rangle - (2m)^{1/2}ab\langle m-1|g^{(l)}(X)|n\rangle\rangle . \quad (19b)$$

The recursion relations of Eqs (13) and (14) reduce to

$$+b^2(X_0/c)^2\langle m|g^{(l+2)}|n\rangle\rangle + b^3(X_0/c)(2n)^{1/2}\langle m|g^{(l+1)}|n-1\rangle\rangle - b^3(X_0/c)[2(n+1)]^{1/2}\langle m|g^{(l+1)}|n+1\rangle\rangle + 2(1-a^2)[n(n-1)]^{1/2}\langle m|g^{(l)}|n-2\rangle\rangle + \{-2(2n+1)+2a^2b^2(m+n+1)\}\langle m|g^{(l)}|n\rangle\rangle + 2(1-a^2)[(n+2)(n+1)]^{1/2}\langle m|g^{(l)}|n+2\rangle\rangle = 0 \quad (20a)$$

and

$$+a^2(X_0/c)^2\langle m|g^{(l+2)}|n\rangle\rangle + a^3(X_0/c)(2m)^{1/2}\langle m-1|g^{(l+1)}|n\rangle\rangle - a^3(X_0/c)[2(m+1)]^{1/2}\langle m+1|g^{(l+1)}|n\rangle\rangle + 2(1-b^2)[m(m-1)]^{1/2}\langle m-2|g^{(l)}|n\rangle\rangle + \{-2(2m+1)+2a^2b^2(m+n+1)\}\langle m|g^{(l)}|n\rangle\rangle + 2(1-b^2)[(m+2)(m+1)]^{1/2}\langle m+2|g^{(l)}|n\rangle\rangle = 0 \quad (20b)$$

Case 3

In the case in which $\omega_1 = \omega_2 = \omega$ as well as $X_0 = 0$ the two wave functions $\langle X|m\rangle$ and $\langle\langle X|n\rangle\rangle$ belong to the *same* LHO, and the single-center matrix element of the arbitrary function $f(X)$ simplifies to

$$\langle m|f(X)|n\rangle\rangle = \sum_{l=0}^{\infty} f^{(l)}(0)\left(\frac{\hbar}{4\mu\omega}\right)^{l/2}\sum_{p=0}^{\lceil m\ l\rceil}\sum_{c}^{\lceil n\ l-p\rceil} \times\left[\frac{2^{p+q}m!\,n!}{(m-p)!\,(n-q)!}\right]^{1/2}\frac{\delta_{m-p,\,n-q}}{p!\,q!\left(\frac{l-p-q}{2}\right)!}, \quad (21)$$

where the Kronecker delta represents the overlap integral $\langle m-p|n-q\rangle\rangle$ Analytical expressions for single-center harmonic oscillator matrix elements for a few definite functions of X have been obtained previously [10]. The reduction of Eq. (21) to those expressions has provided a useful check on the present work The recursion relations (8) and (9) also simplify to the following three-term relations:

$$(X_0/c)\langle m|g^{(l+1)}(X)|n\rangle\rangle = [2(m+1)]^{1/2}\langle m+1|g^{(l)}(X)|n\rangle\rangle - (2n)^{1/2}\langle m|g^{(l)}(X)|n-1\rangle\rangle \quad (22a)$$

and

$$(X_0/c)\langle m|g^{(l+1)}(X)|n\rangle\rangle = [2(n+1)]^{1/2}\langle m|g^{(l)}(X)|n+1\rangle\rangle - (2m)^{1/2}\langle m-1|g^{(l)}(X)|n\rangle\rangle \quad (22b)$$

The recursion relations (13) and (14) simplify to the following four-term relations

$$+(X_0/c)^2\langle m|g^{(l+2)}|n\rangle\rangle + (X_0/c)(2n)^{1/2}\langle m|g^{(l+1)}|n-1\rangle\rangle - (X_0/c)[2(n+1)]^{1/2}\langle m|g^{(l+1)}|n+1\rangle\rangle + 2(m-n)\langle m|g^{(l)}|n\rangle\rangle = 0 \quad (23a)$$

and

$$+(X_0/c)^2\langle m|g^{(l+2)}|n\rangle + (X_0/c)(2m)^{1/2}\langle m-1|g^{(l+1)}|n\rangle - (X_0/c)[2(m+1)]^{1/2}\langle m+1|g^{(l+1)}|n\rangle + 2(-m+n)\langle m|g^{(l)}|n\rangle = 0. \quad (23b)$$

Case 4

Consider the case in which all three ω_1, ω_2, and X_0 are nonzero such that $\omega_1, \omega_2 \gg \omega_0$ and $b^2 \gg (\omega_0/\omega_2)$. It follows from Eq. (7), on taking the limit $b^2 \gg (\omega_0/\omega_2)$, that

$$\langle m|f(X)|n\rangle \longrightarrow \langle m|n\rangle \cdot f(b^2X_0/2). \quad (24)$$

Note that this scaling property is valid for any arbitrary analytical function f

V. Discussion and Conclusions

In this paper we have derived a closed form expression, Eq. (7), for the matrix element of an *arbitrary* analytical function $f(X)$ between the vibrational states belonging to two distinctly separated linear harmonic oscillators of different frequencies. We have explicitly verified that for the cases where $f(X)$ is a definite specified function like an exponential, a Gaussian or powers of X, the expression (7) reduces to the previously derived analytical expressions [1, 11] It essentially provides a useful check on the correctness of the present work. For the case of diatomic molecules, various matrix elements obtained above by using one-dimensional harmonic oscillators could be used in a straightforward manner. For the cases of polyatomic molecules, on the other hand, one will have more degrees of freedom and it would be necessary to use two or more dimensional oscillators. Even in such cases, as long as the relevant functions f are *separable* in Cartesian coordinates, the matrix elements of f can be evaluated using the techniques presented above. In particular, for a function f which is separable in Cartesian coordinates x, y, and z, a general matrix element of f will become a product of three one-dimensional matrix elements, one each for x, y, and z. The recursion relations outlined above will, then, be valid for any one of these one-dimensional matrix elements.

A number of recursion relations [Eqs (2), (8)–(14)] among the matrix elements of the arbitrary function $f(X)$ and its derivatives are presented. It should be noted that relation (10) can be used for obtaining the matrix element $\langle m|f(X)|n\rangle$ for *any* m and n from a knowledge of merely two numbers $\langle 0|f(X)|0\rangle$ and $\langle 0|f(X)|1\rangle$ (or $\langle 0|f(X)|0\rangle$ and $\langle 1|f(X)|0\rangle$). Indeed the numerical merit of this procedure is that one needs to evaluate only the two lowest-order (and, therefore, the simplest) matrix elements using the time-consuming summation form (7) One can then utilize the recursion relations for rapid evaluation of *any* higher-order matrix element $\langle m|f(X)|n\rangle$. Furthermore, the relations (2), (8), (9), (11), and (12) can be used judiciously for quickly obtaining the matrix elements of other functions of X once the complete matrix $\langle m|f(X)|n\rangle$ has been determined for a certain definite function f The recursion relations (2), (13), and (14) are useful in situations where one needs a recursion relation in which one of the vibrational quantum numbers, either m or n, stays fixed. Such situations arise, for example, in investigations of vibrational spectroscopy [9].

As an application of the recursion relations derived in this paper, we have calculated [9] the resonant vibrational excitation ($v_i \rightarrow v_f$) of molecules Li_2 and N_2 by impact of low energy electrons. In the resonance model, the projectile electron forms an intermediate autodetaching molecular anion state which decays into a vibrationally excited molecule after the detachment of the electron. In the simple model that we used [9], the potential curves of the neutral molecule and of the intermediate resonant anion state were replaced by those of two one-dimensional harmonic oscillators of arbitrary frequencies and equilibrium separations. The vibrational excitation amplitude, then, involved matrix elements of the resonance width function between vibrational wave functions of the two oscillators. Using the results obtained in the present paper, we obtained recursion relations among vibrational excitation amplitudes such that when the amplitudes for the transitions ($0 \rightarrow 0$) and ($0 \rightarrow 1$) were known, then excitation amplitude for any other transition, inelastic or superelastic, were easily obtained by simple use of recursion relations. This simple model, involving the recursion relations among the linear harmonic oscillator matrix elements, was able to account successfully the experimentally observed [13] spectacular peaks in the cross sections for vibrational excitation of N_2 by low-energy electron impact.

Finally, we comment briefly on the possible usefulness of the present results. As mentioned in the Introduction, the matrix elements of various functions of internuclear separation X are relevant in the discussions of molecular spectroscopy. For the cases of those diatomic molecules whose potential curves are accurately known, these matrix elements could be computed numerically using the actual potential curves. However, for those molecules for which the potential curves are not accurately known — this includes many diatomic molecules and the majority of polyatomic molecules — the replacement of actual potential curves by those of linear harmonic oscillators or Morse oscillators is a reasonable approximation [14]. Two-center linear harmonic oscillator matrix elements can then reasonably approximate the required matrix elements for low-lying vibrational levels and can provide important correction terms for high-lying vibrational levels. It is appropriate to remark that if one were to obtain the anharmonic correction terms for the linear harmonic oscillator by simply expanding the rotationless Morse potential, the integration coordinate in the matrix elements of the correction terms would be *radial* rather than Cartesian, and the limits of integration would be from zero to infinity. In that case, the matrix elements $\langle m|X^l|n\rangle\rangle$ would not be explicitly given by Eqs. (A.3) and (A.4), even though the recursion relations of Eqs. (2)–(4) and (8)–(14) will still be valid. Use of analytical harmonic oscillator matrix elements along with the recursion relations, as outlined in this paper, has the computational advantage, especially for polyatomic molecules, over the direct numerical evaluation of these matrix elements in terms of little memory and time requirements. Furthermore, analytical results can be applied in ways that are simply inaccessible to numerical solutions since analytical results, unlike the numerical solutions, explicitly show the dependence of matrix elements on various parameters like the mass, frequency, etc., of the oscillator. As a specific example, the numerical observation of Fraser [15] and of Nicholls and Jarmain [16] that the matrix elements $\langle m|X^l|n\rangle\rangle$ for the first positive system of N_2 satisfy, under certain conditions,

$$\frac{\langle m|X^2|n\rangle}{\langle m|X^1|n\rangle} \approx \frac{\langle m|X^1|n\rangle}{\langle m|X^0|n\rangle}$$

could be easily explained as a special case of the scaling law depicted analytically in Eq. (24) above.

Acknowledgments

The support of the Air Force Office of Scientific Research through grant number AFOSR-87-0342 is gratefully acknowledged.

Appendix

Some of the useful relations that we have used in this paper are appended here for convenience. Two standard relations among Hermite polynomials are

$$2xH_n(x) = H_{n+1}(x) + 2nH_{n-1}(x) \tag{A 1}$$

and

$$dH_n(x)/dx = 2nH_{n-1}(x)\,. \tag{A.2}$$

The two-center matrix elements of powers of X using harmonic oscillator wave functions are [1]

$$\langle m|X^l|n\rangle = \frac{X_0^l l!}{(2c)^l} \sum_{p=0}^{\lceil m,l\rceil} \sum_{q=0}^{\lceil n,l-p\rceil} \left[\frac{2^{p+q} m!\, n!}{(m-p)!\,(n-q)!}\right]^{1/2} \times \frac{a^p b^q (-i)^{l-p-q} H_{l-p-q}\left(\dfrac{ib^2c}{2}\right)}{p!\,q!\,(l-p-q)!} \langle m-p|n-q\rangle \tag{A 3}$$

with the overlap integral given by [1, 12]

$$\langle m|n\rangle = N_{mn} \sum_{k=0}^{\lceil m,n\rceil} \frac{m!\,n!}{(m-k)!\,(n-k)!\,k!} (2ab)^k (1-b^2)^{(n-k)/2} \times (1-a^2)^{(m-k)/2} H_{n-k}\left[-\frac{a^2bc}{2(1-b^2)^{1/2}}\right] H_{m-k}\left[\frac{ab^2c}{2(1-a^2)^{1/2}}\right] \tag{A.4}$$

As before, the notation $\lceil x, y\rceil$ means the smaller of x and y. The constants a, b, and c have been defined earlier in terms of ω_1, ω_2, and ω_0.

Bibliography

[1] P J Drallos and J M. Wadehra, J Chem Phys 85, 6524 (1986)
[2] E Hutchisson, Phys Rev 36, 410 (1930).
[3] J Morales, L Sandoval, and A. Palma, J Math. Phys. 27, 2966 (1986)
[4] J Morales, L Sandoval, A Palma, and J Lopez-Bonilla, Chem Phys Lett 135, 149 (1987)
[5] J. Morales, Phys. Rev. A36, 4101 (1987)
[6] F Ansbacher, Z Naturforsch Teil A 14, 889 (1959)
[7] C Manneback Physica 17 1001 (1951)

[8] S I Chan and D Stelman, J. Chem Phys 39, 545 (1963)
[9] J M. Wadehra and P J. Drallos, Phys Rev. A36, 1148 (1987)
[10] R M. Wilcox, J Chem. Phys 45, 3312 (1966)
[11] K Nishikawa, Int. J Quantum Chem 12, 859 (1977)
[12] S. Waldenstrom and K Razi Naqvi, Chem. Phys Lett 85, 581 (1982)
[13] G J Schulz, Phys Rev 135, A988 (1964).
[14] G D Carney, L L Sprandel, and C. W Kern, Adv. Chem Phys 37, 305 (1978)
[15] P A. Fraser, Can. J. Phys 32, 515 (1954)
[16] R. W Nicholls and W R Jarmain, Proc Phys Soc A 69, 253 (1955)

Received May 22, 1989
Accepted for publication August 31, 1989

Rovibrationally enhanced dissociative electron attachment to molecular lithium

J. M. Wadehra
Department of Physics and Astronomy, Wayne State University, Detroit, Michigan 48202 and Wright Research and Development Center, Wright-Patterson Air Force Base, Ohio 45433*
(Received 23 August 1989)

We have investigated the role played by initial rovibrational excitation of Li_2 on the cross sections and rates for dissociative electron attachment to the molecule. For a given internal energy, the vibrational excitation enhances the attachment cross section more than the rotational excitation. The attachment cross sections and the attachment rates reach their maximum values when the process of dissociative attachment to rovibrationally excited molecules is still endoergic and, furthermore, these quantities stay close to their maximum values even when the process changes from being endoergic to exoergic. The upper bounds on the cross sections and the rates for dissociative electron attachment to Li_2 are 12.8 $Å^2$ and 1.25×10^{-8} $cm^3 s^{-1}$. At a fixed electron temperature, the kinetic energy of the negative ion formed by this process increases as the vibrational quantum number of the initial neutral molecule increases; the maximum kinetic energy of the Li^- ion formed by attachment to the $v=12$ level of Li_2 is 0.153 eV

I. INTRODUCTION

It has been amply demonstrated, both theoretically[1] as well as experimentally,[2] that the cross sections for H^- formation via the process of dissociative electron attachment to molecular hydrogen are significantly enhanced if the molecule H_2 is initially rovibrationally excited. In order to assess the analogous degree of enhancement for other molecular systems, we have presently investigated in detail the effect of initial rovibrational excitation on the rate of production of Li^- via the process of dissociative electron attachment to diatomic lithium molecules. Investigations of electron attachment to lithium molecules are especially appropriate at this time due to several reasons. First, recent experimental observations[3] reveal that the rate of Li^- formation by the impact of thermal electrons on highly vibrationally excited Li_2 is $(2\pm1)\times10^{-8}$ $cm^3 s^{-1}$. One of the principal aims of the present work is to confirm this experimental observation of attachment rate by explicit calculations as well as to provide detailed cross sections for electron attachment to Li_2. Second, the Li^- ions could possibly play, in the future, the same roles as have been played by H^- ions for neutral beam formation. Third, since lithium dimers are isovalent with H_2, an investigation of the dependence of the electron attachment to Li_2 on the initial rovibrational excitation of the molecule would be similar to the previous detailed study[4] on H_2.

Similarities between Li_2 and H_2 suggest that theoretical methods used successfully in the past for obtaining the cross sections and rates of electron attachment to H_2 can be employed for analogous investigations for Li_2. In particular, the process of dissociative electron attachment to Li_2 is understood to proceed through the formation of an intermediate resonant anion state Li_2^- which, on dissociation, leads to Li^-. The fact that both the lithium dimer molecules and the hydrogen molecules are isovalent provides similarities between the electronic configurations of the two molecules. For example, the lowest electronic states of the negative molecular ions with configurations $(1\sigma_g)^2(1\sigma_u)^2(2\sigma_g)^2(2\sigma_u)$ for Li_2^- and $(1\sigma_g)^2(1\sigma_u)$ for H_2^- have similar symmetry, namely, $^2\Sigma_u^+$. However, compared to the hydrogen molecule, the lithium molecule possesses a large polarizability and a weak bond strength which makes the ground state of Li_2^- a true bound state. In the case of H_2^-, on the other hand, the $^2\Sigma_u^+$ state is a true bound state only for internuclear separations R larger than 2.9 a.u. and is an autodetaching state for smaller values of R. The first excited state of the negative molecular ions with symmetry $^2\Sigma_g^+$ and configurations $(1\sigma_g)^2(1\sigma_u)^2(2\sigma_g)(2\sigma_u)^2$ for Li_2^- and $(1\sigma_g)(1\sigma_u)^2$ for H_2^- is partly Feshbach and partly shape resonance in nature for both. This state is the essential channel for dissociative attachment of low-energy electrons to lithium molecules. The process of dissociative electron attachment to molecular lithium, then, is:

$$e^- + Li_2(X\,^1\Sigma_g^+) \rightarrow Li_2^- \ (A\,^2\Sigma_g^+) \rightarrow Li + Li^- \ .$$

II. CALCULATIONS

Fortunately, a number of accurate calculations[5-9] of the potential curves of the $X\,^1\Sigma_g^+$ state of Li_2 and the $A\,^2\Sigma_g^+$ state of Li_2^- are available. The potential curves that we utilize in the present work were obtained[9] by an *ab initio* calculation using optimized configuration-interaction (CI) wave functions built from orthonormal Slater-type orbitals (STO's). Because of its nature (namely Feshbach) the $^2\Sigma_g^+$ resonance of Li_2^- is expected to have a small width and a long lifetime. Potential curves of the electronic states of Li_2 and Li_2^- relevant to the attachment process are shown in Fig. 1. The $A\,^2\Sigma_g^+$ electronic state of Li_2^- exhibits, due to its autodetaching nature, a complex potential-energy curve whose real part

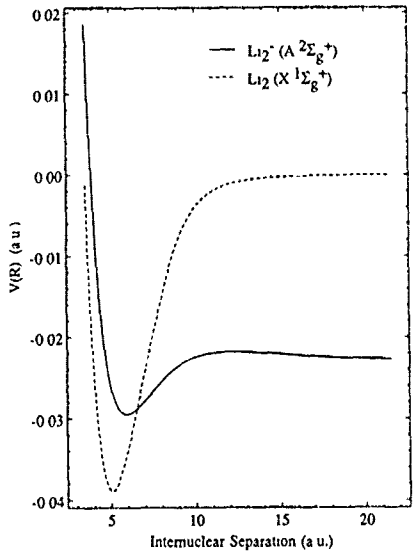

FIG. 1. The potential curves of $Li_2(X\ ^1\Sigma_g^+)$ and $Li_2^-(A\ ^2\Sigma_g^+)$.

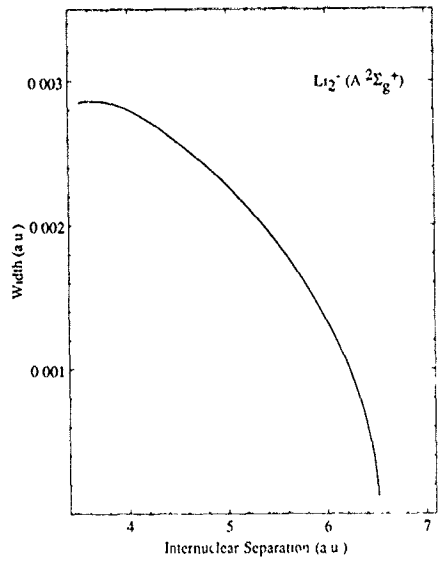

FIG. 2. The width of the $A\ ^2\Sigma_g^+$ state of Li_2^-

$V^-(R)$, along with the potential curve of the $X\ ^1\Sigma_g^+$ state of Li_2, is shown. The potential minima of the X and the A curves are at 5.05 and 5.91 a.u., respectively. The two curves cross at $R=R_s=6.51$ a.u. and, therefore, the possibility of autodetachment of the resonant molecular anion exists only for internuclear separations smaller than R_s, the so-called stabilization radius. The width (or, equivalently, the lifetime) $\Gamma(R)$ of this resonance is related to the imaginary part of the complex potential-energy curve of the $A\ ^2\Sigma_g^+$ state of Li_2^-. In the present autodetachment process $^2\Sigma_g^+ \rightarrow {}^1\Sigma_g^+ + e^-$, the lowest contributing partial wave is an s wave and, thus, by Wigner's threshold law[10] the width of this state is given by $\Gamma(R)=ck(R)$, where $k(R)$ is the wave number of the electron emitted at internuclear separation R and c is a constant. This constant c is obtained as follows. The autodetachment width Γ is related, by Fermi's golden rule, to the matrix element $V(R)$ coupling the discrete resonant state with the continuum state of the electron-molecule system.[11] The wave function of the discrete $A\ ^2\Sigma_g^+$ state was estimated by smoothly extrapolating the fully optimized exponents of the CI wave functions from the variationally stable region ($R \geq R_s$) into the autodetaching region ($R < R_s$). The continuum state was approximated by extrapolation of a series of wave functions constructed by adding an electron, in a series of diffuse STO's, to the unperturbed ground-state wave function for $Li_2(X\ ^1\Sigma_g^+)$. The coupling matrix element $V(R)$ was then calculated by using these two wave functions. A comparison of the width calculated by using the golden rule with the threshold law expression, given above, yielded $c=0.0143$ a.u. The width of the $A\ ^2\Sigma_g^+$ state of Li_2^- as a function of the internuclear separation R is shown in Fig. 2 and is given, in atomic units, by $\Gamma(R) = 0.0143k(R)$.

In the traditional resonance theory, within the local approximation, the radial nuclear wave function $\xi(R)$ of the resonant anion state satisfies[12]

$$\left\{-\frac{\hbar^2}{2M}\frac{d^2}{dR^2}+\frac{\hbar^2 J_i(J_i+1)}{2MR^2}+V^-(R) - \tfrac{1}{2}i\Gamma(R)-E\right\}\xi(R)=-V(R)\xi_{v_iJ_i}(R)\,, \quad (1)$$

where $\xi_{v_iJ_i}(R)$ is the nuclear wave function of the initial rovibrational state of the neutral molecule and M is the reduced mass of the nuclei. E is the total energy of the system and its conservation in the initial channel (electron plus molecule) and the final channel (atom plus negative ion) provides an expression for the threshold for dissociative electron attachment (DA) to the molecule that is rovibrationally excited to a particular level,

$$E_{\rm th}^{\rm DA}=\begin{cases} D-N_{\rm EA}-E_{vJ} & \text{if } E_{vJ}<D-N_{\rm EA}, \\ 0, & \text{otherwise.}\end{cases} \quad (2)$$

Here D is the dissociation energy of the lithium molecule (1.0372 eV), $N_{\rm EA}$ is the electron affinity of the lithium atom (0.6182 eV) and E_{vJ} is the excitation energy of the initial rovibrational level of the molecule.

The nuclear wave function $\xi(R)$ is obtained by numerically solving Eq. (1) subject to the boundary conditions

$$\xi(R=0)=0\,,$$

$$\xi(R\rightarrow\infty)\rightarrow KRh_{J_i}^{(1)}(KR)\,.$$

Here $\hbar^2K^2/2M$ is the relative kinetic energy of the ion-atom pair after dissociative electron attachment and $h_{J_i}^{(1)}$

is the spherical Hankel function of the first kind.

If, after the formation of the temporary resonant state, the nuclei separate to $R > R_s$ without autodetachment having occurred, the detachment of the electron becomes energetically impossible and dissociative attachment can result. Thus for $R < R_s$, the envelope of $|\xi(R)|^2$ decreases with R because of the possibility of autodetachment and it is the asymptotic ($R \to \infty$) value of $|\xi(R)|^2$ which determines the probability of dissociative electron attachment to the molecule. In fact, the integrated cross section for dissociative attachment of an electron with energy $\hbar^2 k_i^2/2m$ to the molecule is given by[12] (assuming momentum-normalized functions)

$$\sigma_{DA} = 4\pi^2 \frac{m}{M} \frac{K}{k_i} \lim_{R \to \infty} |\xi(R)|^2 . \tag{3}$$

In order to convert the attachment cross sections into attachment rates one needs the energy distribution of electrons. In the present work we take this distribution to be Maxwellian, namely,

$$f(E) = \left[\frac{27E}{2\pi \bar{E}^3} \right]^{1/2} \exp\left[-\frac{3E}{2\bar{E}} \right] , \tag{4}$$

where the average energy $\bar{E}$ is related to the electron temperature T via $\bar{E} = 3k_B T/2$. The attachment rate $k(\bar{E})$ is merely a convolution of $(2E/m)^{1/2}\sigma_{DA}(E)$, that is,

$$k(\bar{E}) = \left[\frac{2}{m} \right]^{1/2} \int_0^\infty E^{1/2} \sigma_{DA}(E) f(E)\, dE . \tag{5}$$

III. RESULTS AND DISCUSSION

In the present work we have calculated the cross sections and the rates for dissociative electron attachment to molecular lithium when the molecule is either in one of the vibrational levels $v = 0$ to 12, all rotationless, or in one of the rotational levels $J = 0$ to 25, all with $v = 0$. Figure 3 shows the cross sections, as a function of the incident electron energy, for electron attachment to Li_2 in various (v,J) levels. Besides the lowest level (0,0), the other two levels shown in Fig. 3 (1,0) and (0,22) have approximately the same internal energy. The attachment cross sections exhibit a rapid increase at the threshold, attaining a peak value σ_{peak}, followed by a uniform decrease as the energy of the incident electron increases. This almost vertical onset of the cross section is attributed to the attractive nature of the potential curve of the resonant anion state.[13] The attachment rate is essentially determined by the peak attachment cross section. The results in Fig. 3 clearly show that the attachment cross section is enhanced if the molecular lithium is initially rovibrationally excited. A part of the enhancement of the cross section occurs due to the lowering of the threshold for attachment as the molecule is rovibrationally excited. Furthermore, for a fixed internal energy, vibrational excitation of the molecule is more effective in enhancing the cross section than rotational excitation. For example, when the molecule is initially provided with an internal energy of 0.04 eV, then the peak attachment cross section

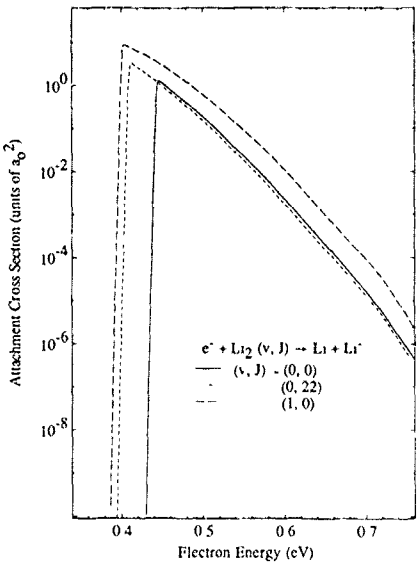

FIG. 3 The cross sections for dissociative attachment of low-energy electrons to molecular lithium in various rovibrational (v,J) levels

is increased by a factor of 6 8 if this internal energy is purely vibrational (from $v = 0$ to 1) and by a factor of 2.5 if the internal energy is purely rotational (from $J = 0$ to 22). Table I provides the energetics as well as the peak cross sections for dissociative electron attachment to the ground electronic state of molecular lithium in various

TABLE I Internal rovibrational energy ($E_{v,J}$), threshold for dissociative attachment (E_{th}^{DA}) and peak attachment cross section (σ_{peak}) for various rovibrational levels of the ground electronic state of Li_2. Asterisk denotes exoergic.

v	J	$E_{v,J}$ (eV)	E_{th}^{DA} (eV)	σ_{peak} (Å^2)
0	0	0 0	0 4190	0.368
1	0	0 04292	0.3761	2 50
2	0	0 08514	0 3339	3 96
3	0	0.1267	0.2923	3.69
4	0	0.1676	0.2514	4 52
5	0	0 2078	0.2112	4.02
6	0	0.2472	0.1718	9.26
7	0	0.2860	0.1330	12.8
8	0	0 3240	0 0950	12 8
9	0	0.3612	0.0578	8.94
10	0	0 3976	0.0214	10 3
11	0	0.4333	*	9.43
0	1	0 00017	0 4188	0.369
0	2	0.00050	0.4185	0.372
0	5	0.00249	0 4165	0.389
0	10	0.00910	0.4099	0.450
0	20	0.03461	0.3844	0 809
0	22	0.04164	0 3774	0.930
0	25	0 05338	0.3656	1.16

rovibrational levels. It is interesting that, unlike molecular hydrogen, the peak attachment cross section here does not increase uniformly as the internal vibrational energy is increased. Whether this is due to the local nature of our present calculations or to the nature of the potential curves of the lithium molecule remains to be ascertained in the future. However, to maintain numerical consistency of our calculations the following equality was satisfied, as a check, to within a few parts in 10^4 for all values of the incident electron energy and for all rovibrational levels of the molecule,

$$\frac{\hbar^2 K}{M}\lim_{R\to\infty}|\xi(R)|^2+\int_0^\infty \Gamma(R)|\xi(R)|^2 dR = 2\int_0^\infty \mathrm{Im}[\xi^* V(R)\zeta_{v_i J_i}(R)]dR \ . \quad (6)$$

This relationship is obtained by multiplying Eq. (1) by $\xi^*(R)$, subtracting the resulting equation from its complex conjugate and then integrating over R from 0 to ∞.

Unlike the case of molecular hydrogen, the width of the resonance responsible for attachment to Li_2 is quite small (or, equivalently, the lifetime is large) so that the resonance model is very reasonable. The enhancement of the attachment cross section is directly related to the increment of the range of internuclear separations, due to internal rovibrational excitation, over which the electron can be captured. This range is increased due to an increased vibrational amplitude during vibrational excitation and centrifugal stretching during rotational excitation. The probability of an electron capture, to form the resonant anion state, is maximum at an internuclear separation at which the energy difference between the potential curves of Li_2 and Li_2^- is equal to the energy of the incident electron. This internuclear separation is referred to the capture radius, R_c. As the nuclei separate from R_c to R_s the autodetachment of the electron from the anion state, leaving behind a rovibrationally excited neutral molecule, is a distinct possibility. Dissociative attachment, of course, results when the internuclear separation far exceeds the stabilization radius R_s. For Li_2 molecules in levels $v \geq 7$ with $J=0$ the range of intermolecular separations over which the electron could be captured includes R_s. The energetic threshold for dissociative electron attachment to Li_2 is nonzero for vibrational levels $v \leq 10$. If the molecule is initially in vibrational levels $v \geq 11$, the attachment process is exoergic.

Figure 4 shows the effect of initial vibrational versus rotational excitation of the molecule on the rate of electron attachment as a function of electron temperature. As seen in this figure, the initial vibrational excitation to the $v=1$ ($J=0$) level enhances the attachment rate more dramatically than the initial rotational excitation to the $J=22$ ($v=0$) level which has roughly the same internal energy. The rate of electron attachment to Li_2 in various vibrational levels is shown in Fig. 5. We note the interesting feature that the attachment rate saturates at the value 1.25×10^{-8} $cm^3 s^{-1}$ which is reached when the molecule Li_2 is initially in vibrational levels $v \sim 8$–12. Furthermore, this rate is achieved for electrons with an average energy of ~ 0.2 eV. These results are consistent

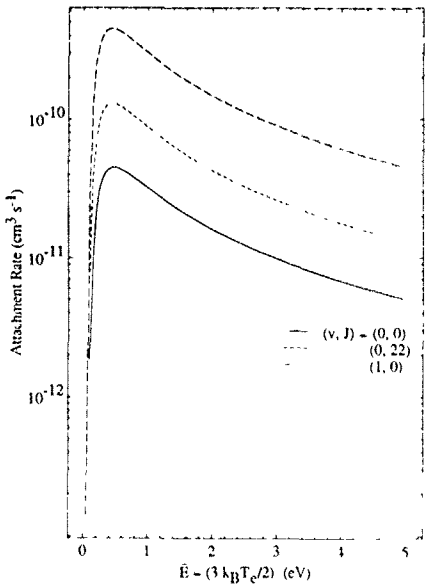

FIG. 4 Rates of dissociative electron attachment to Li_2 in various rovibrational (v,J) levels as a function of the electron temperature. The levels (1,0) and (0,22) have approximately the same excitation energy

with the recent experimental observations[3] of the rate of attachment of thermal electrons to molecular lithium.

A quantity which often is of interest to experimentalists and is useful for plasma diagnostic purposes is the en-

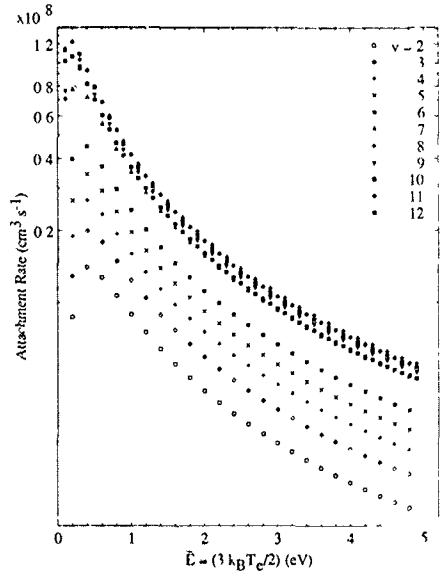

FIG. 5. Rates of dissociative electron attachment to Li_2 in various vibrational levels as a function of the electron temperature.

ergy of the negative ion formed during the process of dissociative electron attachment. The energy of this ion depends on the energy of the incident electron E_e as well as on the excitation energy E_{vJ} of the initial rovibrational level of the molecule. In case of a homonuclear diatomic molecule like Li_2 the atomic anion carries one-half of the relative kinetic energy of the ion-atom pair. The kinetic energy of the anion is

$$E^- = \tfrac{1}{2}(E_e - D + N_{EA} + E_{vJ}) . \quad (7)$$

Assuming a Maxwellian distribution of energies for the electrons, the *average* kinetic energy of the negative ions is given by

$$\langle E^- \rangle = \int_0^\infty E^- \sigma_{DA}(E) f(E)\, dE \Big/ \int_0^\infty \sigma_{DA}(E) f(E)\, dE . \quad (8)$$

Figure 6 shows, as a function of the electron temperature, the average energy of the Li^- ions formed by dissociative electron attachment to Li_2 in various vibrational levels. Since the attachment process becomes exoergic when the molecule is initially in vibrational levels $v \geq 11$, the relative kinetic energy of the ion-atom pair, then, is *more* than the energy of the incident electron and therefore the average energy of Li^- ions formed by dissociative electron attachment to molecular lithium continues to increase as the internal vibrational energy increases. Among the vibrational levels that we have investigated ($v \sim 0$–12) the maximum kinetic energy of the Li^- ions is 0.153 eV.

In an actual plasma, though, the energy distribution of electrons is non-Maxwellian and only a detailed solution of the Boltzmann equation[14] including all possible collision mechanisms of electrons provides the real distribution. If available, this real energy distribution of electrons should be used for calculating the attachment rates and the average energy of the negative ion.

We conclude by noting that the limited experimental information[3] on the rates of dissociative electron attachment to molecular lithium that is currently available is consistent with our theoretical results. Detailed experiments investigating the effect of initial rovibrational excitation of Li_2 on the cross sections for formation of Li^- would be worthwhile in the future.

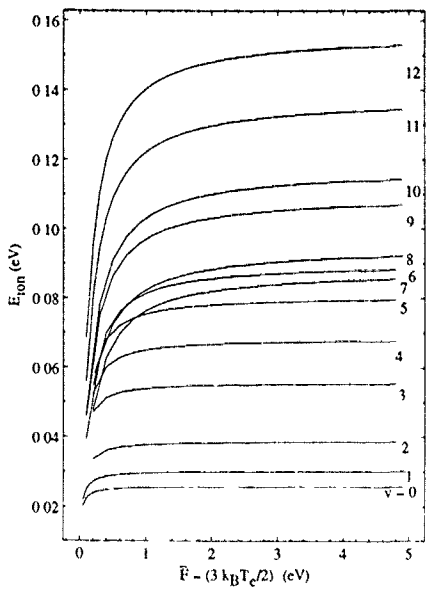

FIG. 6. Average energy of Li^- ions formed by dissociative electron attachment to Li_2 in various vibrational levels as a function of electron temperature.

ACKNOWLEDGMENTS

It is a pleasure to thank Dr. H. H. Michels for providing the potential curves of Li_2 and Li_2^- in numerical form and Dr. A. Garscadden for providing the conducive atmosphere of the Wright Research and Development Center where much of this work was done and written. The support of the U.S. Air Force Office of Scientific Research through Grant No. AFOSR-87-0342 is gratefully acknowledged.

*Permanent address

[1] J. M. Wadehra and J. N. Bardsley, Phys. Rev. Lett. **41**, 1795 (1978).

[2] M. Allan and S. F. Wong, Phys. Rev. Lett. **41**, 1791 (1978).

[3] M. W. McGeoch and R. E. Schlier, Phys. Rev. A **33**, 1708 (1986).

[4] J. M. Wadehra, Phys. Rev. A **29**, 106 (1984).

[5] P. Kusch and M. M. Hessel, J. Chem. Phys. **67**, 586 (1977), M. M. Hessel and C. R. Vidal, *ibid.* **70**, 4439 (1979).

[6] H. Partridge, C. W. Bauschlicher, Jr., and P. E. M. Siegbahn, Chem. Phys. Lett. **97**, 198 (1983).

[7] D. D. Konowalow and J. L. Fish, Chem. Phys. **77**, 435 (1983); Chem. Phys. Lett. **104**, 210 (1984).

[8] K. K. Sunil and K. D. Jordan, Chem. Phys. Lett. **104**, 343 (1984).

[9] H. H. Michels, R. H. Hobbs, and L. A. Wright, Chem. Phys. Lett. **118**, 67 (1985).

[10] E. P. Wigner, Phys. Rev. **73**, 1002 (1948).

[11] U. Fano, Phys. Rev. **124**, 1866 (1961).

[12] J. M. Wadehra, in *Nonequilibrium Vibrational Kinetics*, edited by M. Capitelli (Springer-Verlag, Heidelberg, 1986), p. 191.

[13] T. F. O'Malley, Phys. Rev. **150**, 14 (1966).

[14] P. J. Drallos and J. M. Wadehra, J. Appl. Phys. **63**, 5601 (1988); Phys. Rev. A **40**, 1967 (1989).

PROCEEDINGS

SPIE—The International Society for Optical Engineering

Microwave and Particle Beam Sources and Directed Energy Concepts

Howard E. Brandt
Chair/Editor

16-20 January 1989
Los Angeles, California

Volume 1061

Particle Beam Production via Dissociative Electron Attachment to Molecules

J.M. Wadehra

Department of Physics, Wayne State University, Detroit, Michigan 48202

ABSTRACT

Formation of beams of negative ions by the process of dissociative electron attachment to a molecule AB ($e^- + AB \rightarrow A + B^-$) is investigated. It is demonstrated that the initial rovibrational excitation of the molecule AB plays a significant role in enhancing the rate of production of negative ions. A simple physical picture, involving the formation of a transient resonant state of the molecular anion, is used to explain this enhancement.

1. INTRODUCTION

Production of high intensity neutral particle beams by neutralization of negative ion beams is now well established[1]. The negative ion beams are accelerated to high energies and then neutralized by electron detachment. One efficient way of producing beams of negative ions is by the process of dissociative electron attachment to molecules. Schematically, this process for attachment to a molecule AB is: $e^- + AB \rightarrow A + B^-$. It has been extensively demonstrated, both experimentally[2] as well as theoretically[3], that the cross sections and the rates of production of negative ions by this process are dependent upon the initial rovibrational level of the attaching molecule. In the cases of molecular hydrogen and molecular lithium, the rates of production of negative ions H^- (as well as D^- and T^-) and Li^- by dissociative electron attachment to H_2 (and its five isotopes) and Li_2, respectively, are known to be *strongly* dependent upon the amount of internal rovibrational energy of the neutral molecule. For example, the rates for negative ion beam production via electron attachment to molecular hydrogen (and its isotopes) are enhanced[4] by orders of magnitude if H_2 is initially vibrationally pumped. In the present paper only the results of our investigations on the effect of initial rovibrational excitation on the cross sections and rates of dissociative electron attachment to molecular hydrogen and its five isotopes will be discussed.

2. THE RESONANCE MODEL

A traditional way of describing the physics of the process of dissociative electron attachment to a molecule AB is[5] via the formation of a temporary compound state of the electron-molecule system. In this molecular anion state AB^- (also called the resonance state) the electron can autodetach with a finite lifetime (related to the width, Γ, of the resonance), leaving behind a vibrationally excited neutral molecule. On the other hand, if the lifetime of the resonance is long enough, the anion AB^- can dissociate into $A + B^-$, corresponding to the process of dissociative electron attachment.

A possible scenario of the resonance model is depicted in Figure 1. Shown schematically in this Figure are the potential curves of the neutral molecule AB (labelled V_0) and of the resonant state AB^- (labelled V^-). The two potential curves cross at an internuclear separation $R = R_s$ such that, for $R \geq R_s$, the autodetachment of the electron is energetically not permitted and the resonance turns into a stable bound state. R_s is referred to as the stabilization radius. Before electron capture, the nuclei are rovibrating

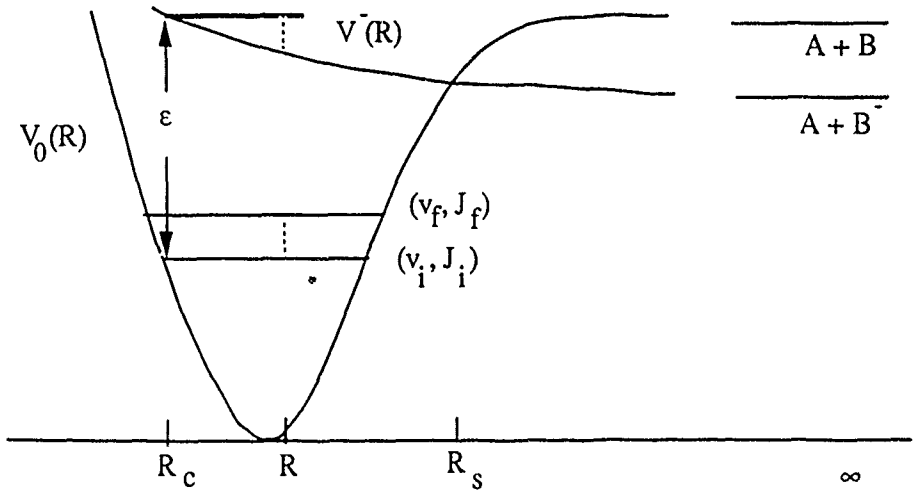

Figure 1. A schematic representation of the processes of dissociative electron attachment and vibrational excitation of a molecule AB via resonance formation.

in the level (v_i,J_i) under the influence of the potential $V_0(R)$. After electron capture, the nuclei of the anion move under the influence of $V^-(R)$. The probability of electron capture to form the resonant molecular anion state depends on the internuclear separation and this probability is maximum at an internuclear separation (labelled R_c in the Figure and referred to as the capture radius) at which the energy separation between the two potential curves is equal to the energy of the incident electron. If the potential curve V^- is repulsive in nature, the nuclei in the anion state begin to separate such that the electronic potential energy is converted into nuclear kinetic energy. Now if the autodetachment of the electron occurs at some specific internuclear separation, labelled R in the Figure, the neutral molecule is left in a rovibrationally excited level due to the gain in the nuclear kinetic energy (indicated by a vertical dotted line in the Figure). The exact rovibrationally excited level (v_f,J_f) achieved by the molecule depends on the gain in the kinetic energy of the nuclei as well as on the relevant selection rules. Depending upon the lifetime of the resonance the nuclei in the anion state may separate to an internuclear separation larger than R_s beyond which the autodetachment of the electron is energetically not possible and dissociative attachment may occur resulting in the formation of a stable negative ion.

3. RESULTS AND DISCUSSION

The relative masses of the six isotopes H_2, HD, HT, D_2, DT and T_2 are 1.00, 1.33, 1.50, 2.00, 2.40 and 3.00, respectively. We have done fully quantum mechanical calculations of cross sections and rates of dissociative electron attachment to these six isotopes. In particular, we have investigated[6] the effect of initial rovibrational excitation in enhancing the rate of negative ion production. The qualitative behavior of the attachment cross sections is the same for all isotopes , namely, a sharp threshold peak followed by a rapid decrease on increasing the impact electron energy. The numerical results are provided in Table 1 which summarizes three enhancement factors:

(a) For a given rovibrational level, the factor R_I by which the peak attachment cross section σ_{peak} is altered on replacing H_2 by one of its isotopes X,

$R_I = \sigma_{peak}(H^-, v = 0, J = 0)/\sigma_{peak}(X^-, v = 0, J = 0)$.

(b) For a given isotope X, the factor R_v by which the peak attachment cross section σ_{peak} is altered on exciting the molecule vibrationally from v = 0 to v = 1,

$R_v = \sigma_{peak}(X^-, v = 1, J = 0)/\sigma_{peak}(X^-, v = 0, J = 0)$.

(c) For a given isotope X, the factor R_J by which the peak attachment cross section σ_{peak} is altered on exciting the molecule rotationally from J = 0 to J = 10,

$R_J = \sigma_{peak}(X^-, v = 0, J = 10)/\sigma_{peak}(X^-, v = 0, J = 0)$.

The cross sections for electron attachment to various isotopes of molecular hydrogen are shown, as a function of electron energy, in Figure 2. For each isotope three cross sections are shown in this Figure. The first set of six curves provides the cross sections for electron attachment to the six isotopes in the lowest rovibrational levels, namely, (v,J) = (0,0). The next set of six curves in Figure 2 shows the cross sections for attachment to the vibrationally excited isotopes in the levels (1,0). The third set of six curves depicts cross sections for attachment to rotationally (0,J) excited molecular isotopes; the value of rotational quantum number J is chosen, for each isotope, in such a manner that the rotational excitation energy is roughly equal to the vibrational excitation energy of the (1,0) level. For each of the isotopes, the rovibrational excitation is seen to enhance the attachment cross section. Furthermore, vibrational excitation is more effective in enhancing the cross section than rotational excitation. The fundamental reason for the enhancement of the electron attachment cross sections is an increase in the range of internuclear separations over which the electron can be captured for anion formation once the molecule is internally excited. This increase in range occurs due to an increased vibrational amplitude during vibrational excitation and due to centrifugal stretching during rotational excitation.

Table 1. Various factors indicating the enhancement of the peak cross section for attachment to rovibrationally excited H_2 and its isotopes.

Isotope	R_I	R_v	R_J
H_2	1.0	33.8	15.9
HD	10.3	39.4	11.8
HT	29.6	42.1	10.5
D_2	527	48.9	8.04
DT	4064	54.2	6.89
T_2	65217	60.9	5.72

Various enhancement factors, R_I, R_v and R_J, depend upon the mass (M) of the isotope and empirically it is determined that the mass dependences of these factors are:

$$R_I \propto \exp(-\text{constant} \cdot M^{1/2}) \qquad (1a)$$

$$R_v \propto M^{17/32} \tag{1b}$$

$$R_J \propto M^{-1/2}. \tag{1c}$$

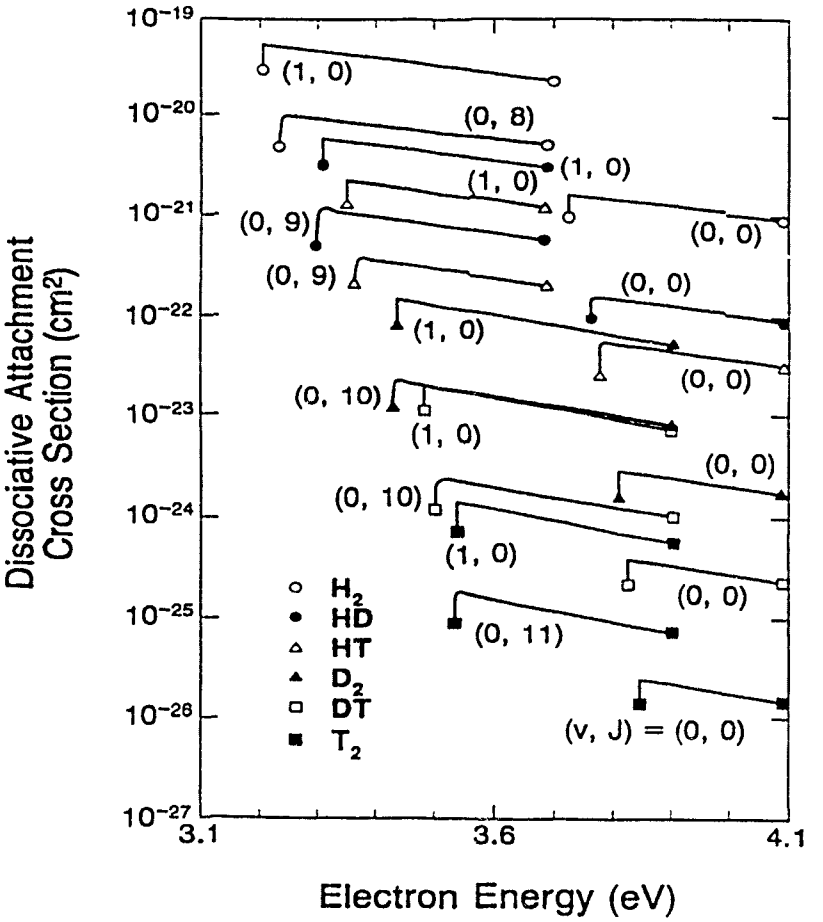

Figure 2. Cross sections for dissociative electron attachment to rovibrationally excited H_2 and its isotopes.

The change in the peak attachment cross section on isotope substitution, namely R_I, is referred to as the isotope effect. The isotope effect is most dramatic for lighter molecules like hydrogen because of the greater relative change in the reduced mass of the nuclei on isotope substitution. The effect could be completely understood in terms of a semiclassical analysis[7,8]. In such an analysis the cross section for dissociative electron attachment, σ_{DA}, can be written as a product of two factors:

$$\sigma_{DA} = \sigma_{cap}\, S.$$

The first factor, σ_{cap}, is interpreted as the cross section for the formation of the resonant anion state by the capture of the incident electron. The second factor, S, is interpreted as the probability that the separation of the nuclei in the anion state increases from the capture radius R_c to the stabilization radius R_s

without electron autodetachment to assure the process of dissociative electron attachment to occur. The factor S is referred to as the survival probability and, in the semiclassical analysis, is given by:

$$S = \exp\left(- \int_{R_c}^{R_s} \frac{\Gamma(R)}{\hbar} \frac{dR}{v(R)} \right), \tag{2}$$

where $\Gamma(R)$ is the width of the resonant state and $v(R)$ is the speed with which the nuclei are moving apart at the internuclear separation R. Now, in the semiclassical expression, Eq. (2), the survival probability S is a strongly mass-dependent quantity. It can roughly be approximated by $\exp(-\bar{\Gamma}\tau/\hbar)$ where τ, the time taken by nuclei to separate from the capture radius R_c to the stabilization radius R_s, is directly proportional, by simple kinematical considerations, to $M^{1/2}$. Thus nuclei of heavier isotopes, taking a longer time than nuclei of H_2 to separate out to R_s, experience stiffer competition from the process of electron autodetachment which reduces the probability of dissociative attachment.

As an example of the isotope effect one should note, using the values of R_I in Table 1, that the value of the ratio

$$\frac{\ln\left[\sigma_{peak}(T_2) / \sigma_{peak}(H_2)\right]}{\ln\left[\sigma_{peak}(D_2) / \sigma_{peak}(H_2)\right]} \tag{3}$$

is ln(65217) / ln(527) = 1.7688. The values of the peak attachment cross sections are obtained by fully quantum mechanical calculations. Now, if the isotope effect of the semiclassical Eq. (1a) is valid, this ratio should be

$$\frac{M_{T_2}^{1/2} - M_{H_2}^{1/2}}{M_{D_2}^{1/2} - M_{H_2}^{1/2}} = \frac{\sqrt{3} - 1}{\sqrt{2} - 1} \tag{4}$$

whose value is 1.7673. The two values are quite close, any difference being due to the mass dependence of the vibrational frequencies of the various isotopes.

For the purpose of having a particle beam with high energy deposition characteristics, one looks for beam particles as massive as possible. To investigate the production of massive negative ions we have obtained the factors by which the cross sections (and, therefore, the rates) for the production of Li^- from Li_2 as well as of Cl^- from HCl are enhanced on vibrationally exciting the neutral molecules. These enhancement factors are approximately 8 for Li^- production[9] and 40 for Cl^- production[10,11] when the molecules Li_2 and HCl are initially excited from the $v = 0$ to the $v = 1$ level. The corresponding enhancement factor for H^- production from H_2 is calculated to be approximately 34. Furthermore, the maximum rate of Li^- production from Li_2 is calculated[9] (as well as observed[12]) to be about 10^{-8} cm^3 s^{-1}, which is same as the rate of production[6] of H^- from H_2. This is not surprising since Li_2 is isovalent with H_2.

4. FUTURE POSSIBILITIES

Calculations of the *rate* of negative ion production require a knowledge of the electron energy distribution in the ion source. In our previous calculations[4,6] a simple Maxwellian distribution for electron

energies was assumed . Using this electron energy distribution the maximum possible rate for dissociative electron attachment to H_2 was calculated to be about 10^{-8} cm^3 s^{-1}. Using the same distribution function the maximum kinetic energy carried by the negative ion H^- formed by dissociative electron attachment to H_2 was estimated to be less than 0.5 eV. We have recently developed[13] a novel procedure for obtaining the time-dependent behavior of the electron swarms in a gas mixture. This numerically stable algorithm generates an exact, time-dependent solution of the Boltzmann equation for charged particle swarms in a dilute gas and uniform electric field and, thereby, provides a temporal evolution of the electron energy distribution in the gas. We have already tested this procedure for generating the time-dependent behavior of various parameters like the average electron energy, average drift velocity, ionization rate etc. for electron swarms in gaseous neon and argon. We are currently utilizing the same numerical procedure for obtaining the time-dependent behavior of parameters used for diagnostics purposes in a source containing a mixture of atomic and molecular hydrogen.

5. ACKNOWLEDGEMENTS

The support of the US Air Force Office of Scientific Research through Grant Number AFOSR-87-0342 is gratefully acknowledged.

6. REFERENCES

1. See, for example, Proceedings of the Fourth International Symposium on the Production and Neutralization of Negative Ions and Beams, J. Alessi, ed., American Institute of Physics, New York (1987).

2. M. Allan and S. F. Wong, "Effect of vibrational and rotational excitation on dissociative attachment in hydrogen", Phys. Rev. Lett. 41, 1791 - 1794 (1978).

3. J. M. Wadehra and J. N. Bardsley, "Vibrational- and rotational-state dependence of dissociative attachment in e-H_2 collisions", Phys. Rev. Lett. 41, 1795 - 1798 (1978).

4. J. M. Wadehra, "Rates of dissociative attachment of electrons to excited H_2 and D_2", Appl. Phys. Lett. 35, 917 - 919 (1979).

5. J. M. Wadehra, "Vibrational excitation and dissociative attachment", in Nonequilibrium Vibrational Kinetics, M. Capitelli, ed., pp. 191 - 232, Springer-Verlag, Heidelberg (1986).

6. J. M. Wadehra,"Dissociative attachment to rovibrationally excited H_2", Phys. Rev. A29, 106 - 110 (1984).

7. J. N. Bardsley and F. Mandl, "Resonant scattering of electrons by molecules", Rep. Prog. Phys. 31, 471 - 531 (1968).

8. I. S. Elets and A. K. Kazanskii, "Quasiclassical approximation in the theory of resonance dissociative attachment of an electron to a molecule", Sov. J. Chem. Phys. 2, 1439 - 1449 (1985).

9. J. M. Wadehra, "Rovibrationally enhanced dissociative electron attachment to molecular lithium", to be published (1989).

10. M. Allan and S. F. Wong, "Dissociative attachment from vibrationally and rotationally excited HCl and HF", J. Chem. Phys. 74, 1687 - 1691 (1981).

11. J. N. Bardsley and J. M. Wadehra, "Dissociative attachment in HCl, DCl and F_2", J. Chem. Phys. 78, 7227 - 7234 (1983).

12. M. W. McGeoch and R. E. Schlier, "Dissociative attachment in optically pumped lithium molecules", Phys. Rev. A33, 1708 - 1717(1986).

13. P. J. Drallos and J. M. Wadehra, "A novel algorithm for calculating the time evolution of the electron energy distribution function in gaseous discharges", J. Appl. Phys. 63, 5601 - 5603 (1988).

CONFERENCE PROCEEDINGS NO. 210

PARTICLES AND FIELDS SERIES 40

PRODUCTION AND NEUTRALIZATION OF NEGATIVE IONS AND BEAMS

FIFTH INTERNATIONAL SYMPOSIUM

BROOKHAVEN, NY 1990

EDITOR:
ADY HERSHCOVITCH
BROOKHAVEN NATIONAL LABORATORY

AIP
American Institute of Physics
New York

DISSOCIATIVE ELECTRON ATTACHMENT TO LIGHT MOLECULES A COMPARATIVE STUDY OF H_2, LiH AND Li_2

H H Michels
United Technologies Research Center
East Hartford, Connecticut 06108

and

J M Wadehra
Department of Physics and Astronomy
Wayne State University, Detroit, Michigan 48202

ABSTRACT

In this paper we have compared the energetics of three light molecules (H_2, LiH and Li_2) to form negative ions by the process of dissociative electron attachment For two light homonuclear molecules (H_2 and Li_2) we have done explicit calculations, using the local formalism of the resonance model, to obtain the electron attachment cross sections and the rates of negative ion formation

INTRODUCTION

Much has been said in the past[1] about the formation of H^- via the process of dissociative attachment of low energy electrons to molecular hydrogen. It has also been well established that the cross sections for dissociative electron attachment to H_2 are quite significantly enhanced if the molecule H_2 is initially rovibrationally excited The purpose of the present paper is to provide a *comparative study* of the energetics of a few light molecules (including H_2) for forming negative ions by the process of dissociative electron attachment. Such a comparative study will explicitly show the similarities among several molecules and will, thus, provide a general insight about the degree of enhancement of negative ion formation when the molecule under investigation is rovibrationally excited Furthermore, these investigations will have practical utility since other light negative ions (such as Li^- ions) could possibly play, in the future, the same roles as have been played by H^- ions for neutral beam formation Finally, the observation that the production rate of H^- is enhanced in discharge type negative ion sources by seeding an alkali (Cs) into the system suggests that now is the appropriate time to investigate dissociative attachment to alkali hydrides

ENERGETICS OF H_2, LiH AND Li_2

The three molecules H_2, LiH and Li_2 are covalent and, therefore, exhibit similarities in their electronic configurations For example, the two homonuclear molecules H_2 and Li_2 in the ground state have configurations $(1\sigma_g)^2$ and $(1\sigma_g)^2 (1\sigma_u)^2 (2\sigma_g)^2$, respectively Each of these two states has symmetry $^1\Sigma_g^+$ and these two states dissociate into $H(^2S) + H(^2S)$ and $Li(^2S) + Li(^2S)$, respectively The heteronuclear molecule LiH, on the other hand, has the lowest energy state that dissociates into $Li(^2S) + H(^2S)$ and has configuration which in the united atom limit can be expressed as $(1s\sigma)^2 (2s\sigma)^2$ with symmetry $^1\Sigma^+$

The lowest electronic states of the negative molecular ions with configuration $(1\sigma_g)^2 (1\sigma_u)^2 (2\sigma_g)^2 (2\sigma_u)$ for Li_2^- and $(1\sigma_g)^2 (1\sigma_u)$ for H_2^- also have the same symmetry, namely, $^2\Sigma_u^+$. However, compared to the hydrogen molecule, the lithium molecule possesses a large polarizability and a weak bond strength which makes[2] the ground state of Li_2^- a true bound state for all values of the internuclear separation R In the case of H_2^-, on the other hand, the $^2\Sigma_u^+$ state is a true bound state only for internuclear separations larger than 2 9 a u and is an autodetaching state for smaller values of R. The first excited state of the negative molecular ions Li_2^- and H_2^-, each with symmetry $^2\Sigma_g^+$ and configurations $(1\sigma_g)^2 (1\sigma_u)^2 (2\sigma_g) (2\sigma_u)^2$ for Li_2 and $(1\sigma_g) (1\sigma_u)^2$ for H_2^-, is a partly Feshbach and a partly shape resonance in nature For both H_2 and Li_2, the potential curve of the $^2\Sigma_g^+$ resonance crosses the potential curve of the ground $X\ ^1\Sigma_g^+$ state of the corresponding neutral molecule such that the $^2\Sigma_g^+$ state becomes a true bound state for internuclear separations larger than 5 81 a u. for H_2^- and 6 50 a u for Li_2^-. This $^2\Sigma_g^+$ state is the essential channel for dissociative attachment of low energy electrons to lithium molecules. Similarly, the ground state of LiH^-, that dissociates into $Li(^2S) + H^-(^1S)$, has configuration $(1s\sigma)^2 (2s\sigma)^2 (2p\sigma)$ and symmetry $^2\Sigma^+$. This state of LiH^-, analogous to the ground state of Li_2^-, is a true bound state[3] for all values of the internuclear separation R The first excited state of LiH^- dissociates into $Li^-(^1S) + H(^2S)$ and is the lowest energetic channel for dissociative electron attachment to LiH. This state of LiH^- is a true bound state only for internuclear separations larger than 5 58 a u and is an autodetaching resonance for smaller values of R Incidentally, the electron affinities (EA) of atomic hydrogen and atomic lithium are 0.75 eV and 0.62 eV, respectively.

Figure 1 shows the potential curves of the ground states of the molecules H_2, LiH and Li_2 as well as the potential curves of the states of corresponding molecular anions that are primarily responsible for dissociative electron attachment to these molecules As one progresses from H_2 to LiH to Li_2 the equilibrium internuclear separation increases from 1.40 a u to 3 08 a u to 5.06 a u. and the dissociation energy (D) of the molecule decreases from 4 73 eV to 2 33 eV to 1 06 eV. Furthermore, the energy spacing between the same two low-lying adjacent vibrational levels *decreases* as one proceeds from H_2 to LiH to Li_2, in such a manner that the total number of bound vibrational levels *increases* on increasing the molecular mass. These energetics have different quantitative effects on the threshold for dissociative electron attachment to these molecules as well as on the factor by which the attachment cross section is enhanced on vibrationally exciting these molecules. The threshold energy for dissociative attachment to a molecule that is rovibrationally excited to a particular level (v, J) is $E_{th}^{DA} = D - EA - E_{v,J}$ if $E_{v,J} < D - EA$, and $E_{th}^{DA} = 0$ otherwise

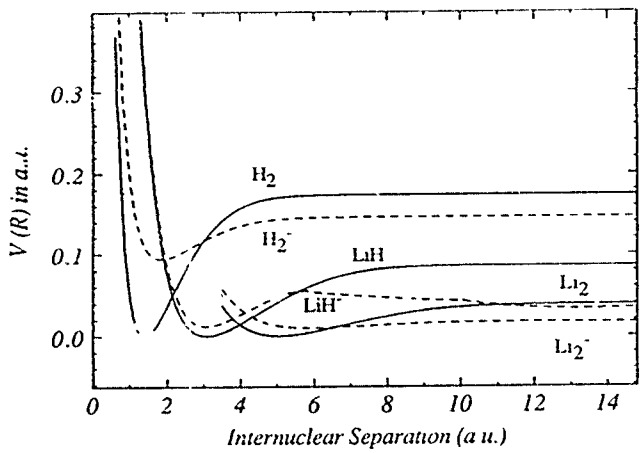

Figure 1. The potential curves (solid lines) of the ground states of the molecules H_2, LiH and Li_2 as well as the potential curves (dashed lines) of the states of corresponding molecular anions that are primarily responsible for dissociative electron attachment to these molecules

DISSOCIATIVE ATTACHMENT TO H_2 AND Li_2

The process of dissociative electron attachment to a molecule is understood[4] to proceed via an intermediate formation of the electron-molecule resonance that is capable of autodetaching the temporarily bound electron with a finite lifetime (related to the width, Γ, of the resonance). The potential curves of the neutral molecule (H_2 or Li_2) and of the resonant state (H_2^- or Li_2^-) cross at an internuclear separation $R = R_s$ such that, for $R \geq R_s$, i.e. autodetachment of the electron is energetically not possible and the resonance turns into a stable bound state. Essentially, then, the cross section for dissociative electron attachment is determined by the asymptotic value of the radial nuclear wave function $\xi(R)$ of the resonant state (assuming energy normalized continuum functions):

$$\sigma_{DA} = \frac{\pi}{k_i^2}\left\{\frac{2\pi\hbar^2 K}{M}\lim_{R\to\infty}\left|\xi(R)\right|^2\right\}$$

Here $\hbar K/M$ is the relative velocity of the ion atom pair after the attachment process Note that the 'geometrical' cross section π / k_i^2 provides an upper bound[5] to the attachment cross section since the quantity within the curly parenthesis can be interpreted as a product of two probabilities, one for the capture of an electron to form the resonant state and the other (called the survival probability) for the nuclei in the resonant state to separate out to the stabilization radius R_s. Using a semiclassical analysis the cross section for dissociative electron attachment, σ_{DA}, can also be written as[6] a product of two factors

$$\sigma_{DA} = \sigma_{cap}\, S$$

The first factor, σ_{cap}, is interpreted as the cross section for the formation of a resonant anion state by the capture of the incident electron and the second factor S (the survival probability) is interpreted as the probability that the separation of the nuclei in the resonant anion state increases up to the stabilization radius R_s without electron autodetachment having occurred This separation ensures the process of dissociative electron attachment to occur The survival probability S, in the semiclassical analysis, is approximated by

$$\exp(-\bar{\Gamma}\tau/\hbar)$$

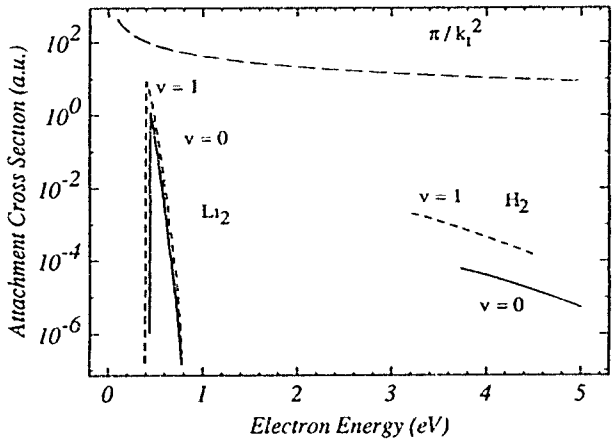

Figure 2 Cross sections for dissociative attachment to H_2 as well as to Li_2 when the molecules are initially in vibrational levels v = 0 and v = 1 π / k_i^2 represents the upper bound to the attachment cross sections.

where τ, the time taken by the nuclei to separate after resonance formation to the stabilization radius R_s, is directly proportional, by simple kinematical considerations, to $M^{1/2}$. $\bar{\Gamma}$ is the 'average' width of the resonance. As a measure of $\bar{\Gamma}$ we note that the values of the actual width of various resonant states, at the equilibrium internuclear separation of the neutral molecule, are[2,7].

$$\Gamma(H_2^-\,;\,^2\Sigma_u^+\,;\,R = 1.40\ a.u.) = 0.306\ a.u.$$
$$\Gamma(H_2^-\,,\,^2\Sigma_g^+\,,\,R = 1.40\ a.u.) = 0.0612\ a.u.$$
$$\Gamma(Li_2^-\,;\,^2\Sigma_g^+\,;\,R = 5.06\ a.u.) = 0.00223\ a.u.$$

Now, since $\bar{\Gamma}$ is smaller for Li_2^- than for H_2^-, the survival probability as well as the cross section for dissociative electron attachment would be expected to be larger for Li_2 than for H_2. Moreover, the lower energy threshold for dissociative electron attachment to Li_2 (essentially because of the lower dissociation energy for Li_2) would further enhance the cross section for attachment to Li_2 over that for H_2.

Figure 2 explicitly compares the cross sections for dissociative attachment to H_2 as well as to Li_2 and the factors by which the attachment cross sections are enhanced when the molecules H_2 and Li_2 are initially vibrationally excited from $v = 0$ to $v = 1$. As expected, the cross sections for attachment to Li_2 are larger than the cross sections for attachment to H_2. The factor by which the peak attachment cross section is enhanced on vibrationally exciting the molecule from $v = 0$ to $v = 1$ is 33.8 for H_2 and 6.8 for Li_2. The upper bound to the attachment cross section (namely, π / k_i^2) is reached when the process of dissociative electron attachment becomes exoergic for either molecule.

FUTURE POSSIBILITIES

The radial nuclear wave function $\xi(R)$ of the resonant state, in the most general theoretical description, satisfies[4] an integrodifferential equation with nonlocal potentials. If either the electron energy is large or the vibrational spacing is small, then the integrodifferential equation can be approximated by an ordinary differential equation with local potentials. The cross sections for dissociative electron attachment to H_2 and Li_2 presented above were obtained using the local formalism. In the immediate future we intend to investigate the effect of nonlocal potentials on the cross sections for electron attachment to molecular hydrogen and lithium. We are also planning to investigate in the future, using the insights gained from the present comparative study, the formation of negative ions from other molecules containing atomic hydrogen such as LiH, NaH, CH, SiH etc.

It is a pleasure to thank Mr. Dale E. Atems and Professor Walter E. Kauppila for providing assistance. Support of the US Air Force Office of Scientific Research through Contract Number F49620-89-0019 and Grant Number AFOSR-87-0342 is gratefully acknowledged.

REFERENCES

1. J.M. Wadehra, Phys. Rev. **A29**, 106 (1984).
2. H.H. Michels, R.H. Hobbs and L.A. Wright, Chem. Phys. Lett. **118**, 67 (1985).
3. B. Liu, K. O-Ohata and K. Kirby-Docken, J. Chem. Phys. **67**, 1850 (1977).

4. J. M. Wadehra, in *Nonequilibrium Vibrational Kinetics*, edited by M. Capitelli (Springer - Verlag, Heidelberg, 1986), p. 191.
5. J. P. Gauyacq, *Dynamics of Negative Ions* (World Scientific, Singapore, 1987).
6. J. N. Bardsley, A. Herzenberg and F. Mandl, in *Proc. 3rd Int. Conf. Atomic Collisions* (North-Holland, Amsterdam, 1964), p. 415.
7. J. N. Bardsley and J. M. Wadehra, Phys. Rev. **A20**, 1398 (1979).

CONFERENCE PROCEEDINGS NO. 210

PARTICLES AND FIELDS SERIES 40

PRODUCTION AND NEUTRALIZATION OF NEGATIVE IONS AND BEAMS

FIFTH INTERNATIONAL SYMPOSIUM

BROOKHAVEN, NY 1990

EDITOR:
ADY HERSHCOVITCH
BROOKHAVEN NATIONAL LABORATORY

AIP
American Institute of Physics
New York

ISOTOPE EFFECT IN VIBRATIONAL EXCITATION OF H_2 BY LOW ENERGY ELECTRON IMPACT

D. E. Atems and J. M. Wadehra
Department of Physics and Astronomy
Wayne State University, Detroit, Michigan 48202

ABSTRACT

Cross sections for the vibrational excitation of molecular hydrogen and its five heavier isotopes by the impact of low energy electrons are calculated using both the local and the nonlocal versions of the resonance model. It is demonstrated that, for a given incident electron energy, the cross sections for the vibrational excitation of heavier isotopes can be obtained from those of molecular hydrogen by a simple scaling procedure. It is seen that the scaling law holds for cross sections with values ranging over eight orders of magnitude.

The vibrational excitation of a molecule (such as H_2) occurs via the formation of an intermediate resonant state (H_2^-) which can either autodetach the temporarily bound electron (and, then, leaves behind a vibrationally excited molecule) or can dissociate into $H + H^-$ (that is, leads to dissociative electron attachment). Schematically, these two complementary processes are:

$$e^- + H_2(v_i, J_i) \rightarrow H_2^-(^2\Sigma_u^+ \text{ or } ^2\Sigma_g^+) \begin{cases} \rightarrow e^- + H_2(v_f, J_f) \\ \rightarrow H + H^-. \end{cases}$$

The nuclear wave function ξ of the resonant state, in the most general theoretical description, satisfies[1] a integrodifferential equation with nonlocal potentials:

$$[T_N(\vec{R}) + V^-(R) - E]\,\xi(\vec{R}) = -V(E - E_{v_i}, R)\,\chi_{v_i}(\vec{R})$$

$$-\int d\vec{R}' \sum_v \chi_v^*(\vec{R}')\,\chi_v(\vec{R}) \left\{ P\int d\varepsilon \frac{V^*(\varepsilon, R')\,V(\varepsilon, R)}{E - E_v - \varepsilon} - i\pi V^*(E - E_v, R')\,V(E - E_v, R) \right\} \xi(\vec{R}'). \tag{1}$$

Here χ_v are the vibrational bound state wave functions of the neutral molecule, T_N is the nuclear kinetic energy operator and $V^-(R)$ is the potential curve of the resonant anion state. The sum on the right hand side includes all energetically open channels The matrix elements $V(\varepsilon,R)$ couple the discrete resonant state with the background continuum; this coupling leads to an energy-shift of the resonance (the principal part integral on the right hand side) and provides a width to the resonance (the imaginary part on the right hand side) which determines the lifetime of the resonance. The total cross section for vibrational excitation, in atomic units, is[1] (assuming momentum normalized continuum functions),

$$\sigma(v \rightarrow v') = \frac{16\pi^4 k'}{k} \int d\hat{k}' |T(v \rightarrow v')|^2.$$

Here k and k' are the wave numbers describing the incident and the outgoing electron motion. The transition matrix element $T(v \rightarrow v')$ is obtained as.

$$T(v \rightarrow v') = \int d\vec{R}\, \chi_{v'}^{*}(\vec{R})\, V^{*}(\varepsilon', R)\, \xi(\vec{R})$$

There are two points to be noted.
(i) One could either numerically solve the integrodifferential equation (Eq (1)) with nonlocal potentials (and the results for cross sections would be referred to as the nonlocal results) or one could approximate the nonlocal potentials by some appropriate local potentials which will reduce the integrodifferential equation into an ordinary differential equation (and the results for cross sections would, then, be referred to as the local results).
(ii) The actual potentials to be used in the integrodifferential equation (for the nonlocal case) or in the ordinary differential equation (for the local case) could be obtained either by some separate *ab initio* calculations or by some judicious choice of parameters in semiempirical potentials.

Our previous calculations[2] of vibrational excitation cross sections of H_2 were done using a local formalism of the theory with an *ab initio* potential curve for H_2 (from the work of Kolos and Wolniewicz[3]) and a semiempirical potential curve for H_2^-; the complex potential energy curve of H_2^- was adjusted to ensure that, first, the calculated cross section for dissociative electron attachment to H_2 in the ($v = 0$, $J = 0$) level, as well as the isotope effect (that is, the ratio $\sigma_{DA}(H_2) / \sigma_{DA}(D_2)$) in attachment cross sections agreed with the experimental values and, second, the real part of the potential curve of H_2^- agreed with the *ab initio* curve calculated by Bardsley and Cohen[4].

The nonlocal equation (1) can be reduced to a local equation by noting that the level shift and the level width functions depend on $E - E_v$, the energy of the scattered electron when the target molecule undergoes the transition $0 \rightarrow v$. Now, if either the electron energy is large or the vibrational spacing is small, then during the vibrational transition the energy of the electron is not significantly changed. In such a situation one can replace $E - E_v$ by either the incident electron energy or the local classical electron energy, $V^{-}(R) - V_0(R)$. Here $V_0(R)$ represents the potential energy curve of the neutral molecule. On using the closure property for vibrational wave functions the sum over the vibrational levels on the right-hand-side of Eq (1) then reduces to a delta function $[\delta (R - R')]$ and the integrodifferential equation (1) reduces to an ordinary differential equation.

As mentioned earlier, the process of vibrational excitation is closely related to the process of dissociative attachment in that it, too, proceeds via an intermediate resonant anion state. Using the nonlocal equation described above (Eq (1)), we have obtained cross sections for vibrational excitation of molecular hydrogen via the $^2\Sigma_u^+$ resonance for electron energies up to 5 eV. Our objective in studying vibrational excitation has been twofold: to compare the cross sections obtained on using the nonlocal theoretical formalism with those obtained using the local approximation and also to examine the dependence of the cross sections on the nuclear mass (that is, the isotope effect).

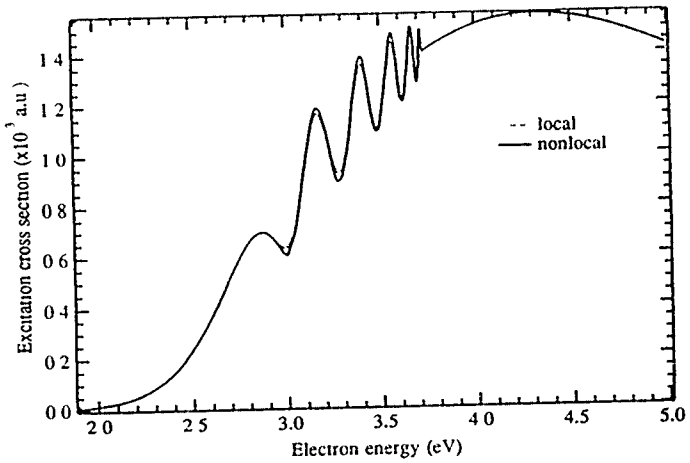

Figure 1. Cross sections for vibrational excitation ($v = 0 \rightarrow 4$) of H_2 using both nonlocal and local formalisms of the theory.

Figure 1 shows, as a typical example, cross sections for excitation from the ground level ($v_i = 0$) to the $v_f = 4$ level of H_2 using both the local and the nonlocal formulations of the theory. The nonlocal effects are seen to be small here, although differences of up to a factor of two are seen for excitation of the highest vibrational levels. The prominent feature here, however, is the well-defined structure in the cross sections which, we emphasize, is by no means a nonlocal effect, being present in the local cross sections as well. This structure is seen only for electron energies below the threshold for dissociative attachment and is entirely absent, for excitation from the ground level, for $v_f < 3$; the structure becomes more pronounced with increasing v_f. This behavior is in qualitative agreement with experimental observations[5], as well as in quantitative agreement (in terms of the location and relative values of peaks) with theoretical results reported by other authors[6]. We have numerically confirmed that as the width is made smaller, the peaks in the cross section become sharper and occur at values of the electron energy which approach those at which an anion bound state could be excited. The same structure is also seen in excitation from higher vibrational levels, and it occurs there for lower values of v_f, appearing in the superelastic cross sections by $v_i = 2$. The exact reason for the behavior of the structure as a function of v_f is, at present, under investigation.

We have also obtained cross sections for excitation from v – 0 to higher vibrational levels for HD, D_2, HT, DT, and T_2 using both the local and the nonlocal formulations of the theory. It has been shown[5] that, in the impulse limit of a resonance, the cross section for vibrational excitation is proportional to $M^{-v/2}$, where M is the reduced nuclear mass of the isotope and v refers to the final vibrational level This scaling law is presumably derived by assuming that the potential curves of the neutral molecule as well as of the resonant anion state can be replaced by those of simple harmonic oscillators. Our calculated excitation cross sections are in quite good agreement with this scaling behavior for values of v_f up to and including $v_f = 5$. This is because the resonant state under present consideration, namely the $^2\Sigma_u^+$ state of H_2^-, has a relatively large width (or small lifetime) and, therefore, can be construed as the impulse limit of the resonance. For convenience, we define for each isotope X (X = H_2, HD, D_2, HT, DT, or T_2) a ratio $\rho = \sigma_X (0 \rightarrow v) / \sigma_X (0 \rightarrow 0)$ Figures 2 and 3, then, display the quantity $\rho \cdot M^{v/2}$ for various isotopes for incident electron energy of 5 eV. The relative masses of the isotopes H_2, HD, D_2, HT, DT, or T_2 are 1.00, 1.33, 1.50, 2.00, 2 40 and 3 00, respectively It is rather remarkable, as seen in Figures 2 and 3, that the above isotope scaling law for vibrational excitation cross sections of molecular hydrogen is applicable for cross section values varying over eight orders of magnitude! Any deviation from this scaling law for large values of v_f is perhaps related to the anharmonic effects. In fact, one can use this scaling law to obtain, within a factor of two, the vibrational excitation cross sections for the heavier isotopes of molecular hydrogen from the corresponding cross sections for H_2 for any v_f.

More recently, Mundel *et al*[6] calculated the potential curves of H_2 and H_2^- using an *ab initio* technique and used those potentials, in a nonlocal theoretical formalism, to obtain the cross sections for dissociative attachment and vibrational excitation. The difference between their local calculations and our previous local calculations is the use of different potential curves of H_2 and H_2^-. In the present course of investigations we have completed our own fully nonlocal calculations for both dissociative attachment and vibrational excitation of H_2 and, indeed, we do not see the kind of difference between local and nonlocal results for cross sections that Mundel *et al* have obtained. More interestingly, since the apparent difference between Mundel *et al*'s calculation and our calculation is the use of different potential curves of H_2^-, we made a few computer runs using their potential curves in our nonlocal computer code and we did not get the same results for attachment cross sections that Mundel *et al* have reported in their paper This has been very intriguing as well as puzzling. Incidentally, our nonlocal as well as local results for the cross sections for vibrational excitation to higher levels of H_2 indeed show the structure, for electron energies below the threshold for dissociative attachment, that was recently seen[5] by Allan in his experiments

In conclusion, we have obtained cross sections for vibrational excitation of molecular hydrogen and its five heavier isotopes by electron impact using both local and nonlocal formulations of the resonance model. Using both formulations one gets a well defined structure, in the excitation cross sections as a function of incident electron energy, for electron energies below the dissociative electron attachment

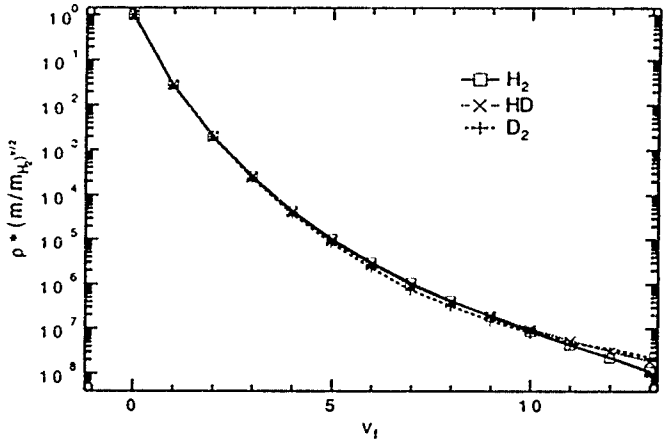

Figure 2. Isotope effect for vibrational excitation of molecular hydrogen.

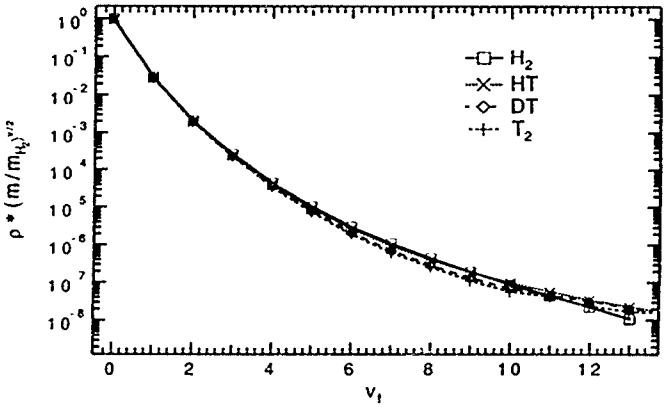

Figure 3. Isotope effect for vibrational excitation of heavier isotopes of molecular hydrogen.

threshold. In any case the nonlocal effects are found to be small. All the excitation cross sections satisfy a useful isotope scaling law such that the vibrational excitation cross sections for the heavier isotopes of molecular hydrogen can be obtained, within a factor of two, from the corresponding cross sections for H_2.

The support of the U.S. Air Force Office of Scientific Research through Grant Number AFOSR - 87 - 0342 is gratefully acknowledged.

REFERENCES

1. J. M. Wadehra, in *Nonequilibrium Vibrational Kinetics*, edited by M Capitelli (Springer - Verlag, Heidelberg, 1986), p. 191.
2. J. N. Bardsley and J. M. Wadehra, Phys. Rev. **A20**, 1398 (1979).
3. W. Kolos and L. Wolniewicz, J. Chem. Phys. **43**, 2429 (1965).
4. J. N. Bardsley and J. S. Cohen, J. Phys. **B11**, 3645 (1978).
5 M. Allan, J. Phys. B. **18**, L451 (1985).
6. C. Mundel, M. Berman, and W. Domcke, Phys Rev **A32**, 181 (1985).
7. E. S. Chang and S. F. Wong, Phys. Rev. Lett. **38**, 1327 (1977).

CONFERENCE PROCEEDINGS NO. 210

PARTICLES AND FIELDS SERIES 40

PRODUCTION AND NEUTRALIZATION OF NEGATIVE IONS AND BEAMS

FIFTH INTERNATIONAL SYMPOSIUM

BROOKHAVEN, NY 1990

EDITOR:
ADY HERSHCOVITCH
BROOKHAVEN NATIONAL LABORATORY

AIP
American Institute of Physics
New York

GAS PHASE ALKALI-HYDROGEN INTERACTIONS IN NEGATIVE ION SOURCES

H H Michels
United Technologies Research Center, East Hartford, CT. 06108

J. M. Wadehra
Wayne State University, Detroit, MI 48202

ABSTRACT

The role of Li_xH_y (Cs_xH_y) molecules, which can be formed from seeding an alkali into a hydrogen plasma, is examined through *ab initio* calculations of the structure and stability of such species. The simplest alkali hydride, LiH, supports a bound anion for all internuclear separations Larger structures, such as Li_2H_2 and Li_3H, do not support stable anions but exhibit thermodynamic stability as gas phase molecules Their possible roles in dissociative attachment to form H^- and/or Li^- is examined

INTRODUCTION

The negative ions of light atoms are currently being studied for their possible application in gaseous discharges, fusion plasmas and gas lasers.[1] One source for the volume production of atomic anions is the process of dissociative electron attachment to molecules.[2] This process has been studied experimentally for low energy electron-hydrogen molecule collisions by Allen and Wong.[3] A parallel theoretical study has been reported by Wadehra and Bardsley.[4] More recently, McGeoch and Schlier[5] have examined dissociative attachment (DA) in electron-lithium molecule collisions and have found large DA rates for attachment to highly vibrationally excited Li_2 molecules. The effect of vibrational excitation on the DA rates has been studied by Hiskes[6] for $e + H_2$ collisions and by Wadehra and Michels[7] for the $e + Li_2$ system. A theoretical study of the absolute cross sections for DA in the $e + Li_2$ system, including enhancement by rotational excitation, has also recently been reported by Wadehra [8,9]

In contrast to the homopolar case, the role of Li_xH_y (Cs_xH_y) molecules, which can be formed from seeding an alkali into a hydrogen plasma, is presently not well understood. The addition of an alkali such as cesium has been shown[10] to enhance the volume production rate of H^-. This observation is interesting in light of the study by Gauyacq, et al,[11] which indicates that charge transfer and collisional detachment processes should reduce H^- production in sodium seeded plasmas Jordan[12] has

suggested that if the dimer of LiH were a linear configuration, the resultant large dipole field would result in enhanced DA of $e + (LiH)_2$ to yield $Li_2H + H^-$ or possibly, $LiH^- + LiH$. In the present study, we assess the stability of several Li_xH_y clusters and examine their possible role in dissociative attachment to form negative ion products

THEORETICAL CONSIDERATIONS

In order to examine the stability of Li_xH_y clusters, *ab initio* calculations were carried out for several species at the MP2 level of theory. The basis set chosen was the Gaussian 6-311G triple split-valence set,[13] augmented by d-polarization functions, [α=0 20] for Li and p-polarization [α=0.75] for H. In addition, a diffuse s-function [α=0.036] and a diffuse *sp*-shell [α=0.0074] were added to hydrogen and lithium respectively, to better describe the negative ion charge distributions. All calculations were performed using CADPAC,[14] an electronic structure code that can perform geometry optimizations and calculate force constant matrices analytically. Optimized geometries were calculated at the MP2 level of theory. Harmonic vibrational frequencies were subsequently calculated at the MP2 stationary points.

In addition, the LiH and LiH^- systems were studied using the DIATOM molecular structures code with a [13σ, 6π, 2δ] STO basis. These STO basis calculations were required to examine the relative behavior of the LiH and LiH^- species at very short internuclear separations

CALCULATED RESULTS AND DISCUSSION

The results of our calculations for the LiH and LiH^- systems, using the DIATOM code, are shown in Fig. 1 for states of $^2\Sigma^+$ symmetry of LiH^-. In Fig. 2, we illustrate the short range behavior of the lowest and first excited $^2\Sigma^+$ states of LiH^-. It is evident that the ground $X^2\Sigma^+$ state of LiH^- is bound, relative to $X^1\Sigma^+$ of LiH, for all internuclear separations. Our calculated adiabatic electron affinity is 0.33 eV, in good agreement with previous theoretical studies [15] The first excited $^2\Sigma^+$ state of LiH^-, which asymmetrically correlates to $Li^- + H$, exhibits repulsive behavior in the region $3.0 \le R \le 6.0$ Å. Thus, DA of $e + LiH$ mainly forms Li^- for $E_{coll} \ge 3.0$ eV. The formation of $Li + H^-$ products may occur by non-adiabatic coupling of the $X^2\Sigma^+$ state of LiH^- to the continuum of $e + LiH$ [$X^1\Sigma^+$] for $E_{coll} \ge 2.1$ eV. However, the cross section for such an indirect electron capture mechanism is predicted to be very small.

The possible role of Li_xH_y clusters was examined through *ab initio* calculations of Li_2H, Li_3H, Li_2H_2 and their respective negative ion states. All cluster calculations were carried out using the CADPAC code. In Fig. 3, we illustrate the stationary geometry of Li_2H and the corresponding negative ion. We find that the C_{2v} structure

for Li_2H has vibrational stability and is thermodynamically stable relative to $Li_2 + H_2$ In addition, the corresponding C_{2v} anion is slightly bound (0 06 eV) relative to the neutral species These results are in qualitative agreement with previous theoretical studies of Li_2H by Cardelino, et al,[16] that were carried out at the SCF level of theory.

The Li_3H species was examined both as a C_{3v} (trigonal pyramid) and as a C_{2v} (kite-like) structure Our previous studies[17] of Li_3H indicated that, although both structures exhibited stable vibrational frequencies, only the C_{2v} structure was thermodynamically stable. In Fig. 4, we illustrate the two stable geometries of neutral Li_3H. *Of these, the C_{2v} structure represents the global minimum* for the system The Li_3H^- anion is not stable as a C_{3v} structure and collapses to $Li_3 + H^-$. The C_{2v} structure of Li_3H^- has the stationary structure shown in Fig 4, but a vibrational analysis indicates that this is probably a saddle region on the potential energy surface In addition, this region is thermodynamically endothermic by 0.24 eV, relative to the *neutral* Li_3H.

Finally, calculations were carried out for the $(LiH)_2$ dimer, as a linear ($C_{\infty v}$), rhomboid (D_{2h}) and y-structure (C_{2v}). The results are shown in Fig. 5 where we show that the linear conformation has one imaginary frequency, and thus represents a saddle point on the surface. The C_{2v} structure is totally unstable and collapses to separate Li_2 + H_2 molecules. The only vibrationally stable geometry in the $^1A_1$ state as a D_{2h} structure. The corresponding negative ion $Li_2H_2^-$ is vibrationally unstable and unbound by over 2 0 eV, relative to Li_2H_2 (D_{2h}).

A summary of the thermodynamics of these Li_xH_y clusters is given in Table 1. A energies are given relative to Li_2 and H_2 as gas phase species. As previously known, the formation of LiH is endothermic by 0.740 eV. However, higher clusters are all thermodynamically stable: Li_2H (–0.280 eV), Li_3H (–1 034 eV) and Li_2H_2 (–1 263 eV)

CONCLUSIONS

The trend of our studies to date indicates that large Li_xH_y (and by analogy, Cs_xH_y) clusters are thermodynamically stable. In particular, the Li_2H_2 species, as a C_{2v} *structure, may be an important component* of alkali-hydrogen mixtures This species can dissociatively attach an electron to form $Li_2H + H^-$ for $E_{coll} \geq 2\,0$ eV The Li_3H (C_{2v}) species should also exhibit DA to form $Li_3 + H^-$, but the concentration of this molecule will be lower than that of the more stable Li_2H_2 cluster. The mechanism for DA to these Li_xH_y clusters can be understood by following their intrinsic reaction coordinate pathways leading to dissociation. In addition, the role of higher order clusters in volume DA processes is uncertain Additional studies of these systems are currently in progress

We thank Drs. J. A. Montgomery, Jr. and J. R. Peterson for helpful discussions and J B Addison for assistance in carrying out the calculations. This work was supported in part by AFOSR under Contract F49620-89-C-0019 and Grant AFOSR-87-0342 Use of the computational facilities at AFSCC-Kirtland is also acknowledged

REFERENCES

1 K. Prelec, ed , Proceedings of the Third International Symposium on the Production and Neutralization of Negative Ions and Beams, AIP Conf. Proc 111, (AIP, New York, 1984).
2. M Bacal, Physica Scripta, T2/2, 467 (1982).
3. M. Allan and S. F Wong, Phys. Rev. Letters 41, 1791 (1978).
4. J. M. Wadehra and J. N Bardsley, Phys. Rev. Letters, 41, 1795 (1978), Phys. Rev. A20, 1398 (1979).
5 M. W. McGeoch and R. E. Schlier, in Proceedings of the Third International Symposium on the *Production and Neutralization of Negative Ions and Beams*, AIP Conf. Proc 111, ed. K. Prelec (AIP, New York, 1984), p.291; Phys. Rev. A33, 1708 (1986).
6 J. R. Hiskes, J. Appl. Phys. 51, 4592 (1980).
7. J. M Wadehra and H. H. Michels, Chem. Phys. Letters, 114, 380 (1985).
8. J. M. Wadehra in Proceedings of the Fourth International Symposium on the Production and Neutralization of Negative Ions and Beams", J. G. Alessi, ed., AIP Conf. Proc. 158 (AIP, New York, 1986)
9. J. M Wadehra, "Rotationally Enhanced Dissociative Electron Attachment to Molecular Lithium", J. Chem Phys., in press.
10. K. N. Leung, S. R. Walther and W. B. Kunkel in "Microwave and Particle Beam Sources and Directed Energy concepts", H. E. Brandt, ed , SPIE Proc. 1061 (SPIE, WA, 1989)
11. J. P. Gauyacq, et al , Phys. Rev. A38, 2284 (1984).
12 K. D. Jordan, Chem. Phys Letters, 40, 441 (1976).
13 R Krishnan, J. S. Binkley, R Seeger and J A. Pople, J. Chem Phys 72, 650 (1980)
14 R D Amos and J E. Rice, CADPAC: The Cambridge Analytic Derivatives Package -Issue 4 0, Cambridge, 1987.
15 K D Jordan, et. al , J. Chem Phys 64, 4730 (1976).
16 B. H Cardelino, W. H Eberhardt and R. F. Borkman, J. Chem. Phys 84, 3230 (1986)
17. J. A. Montgomery, Jr., H. H. Michels, O F. Guner and K Lammertsma, Chem Phys. Letters, 1989, in press.

Table 1 Thermodynamics of Li_xH_y clusters

Reaction					ΔE (eV)	
Li_2 (g)	+	H_2 (g)	→	2LiH (g)	+0.740	(1)
Li_2 (g)	+	1/2 H_2 (g)	→	Li_2H (C_{2v})	−0.280	(2)
3/2 Li_2 (g)	+	1/2 H_2 (g)	→	Li_3H (C_{2v})	−1.034	(3)
Li_2 (g)	+	H_2 (g)	→	Li_2H_2 (D_{2h})	−1.263	(4)

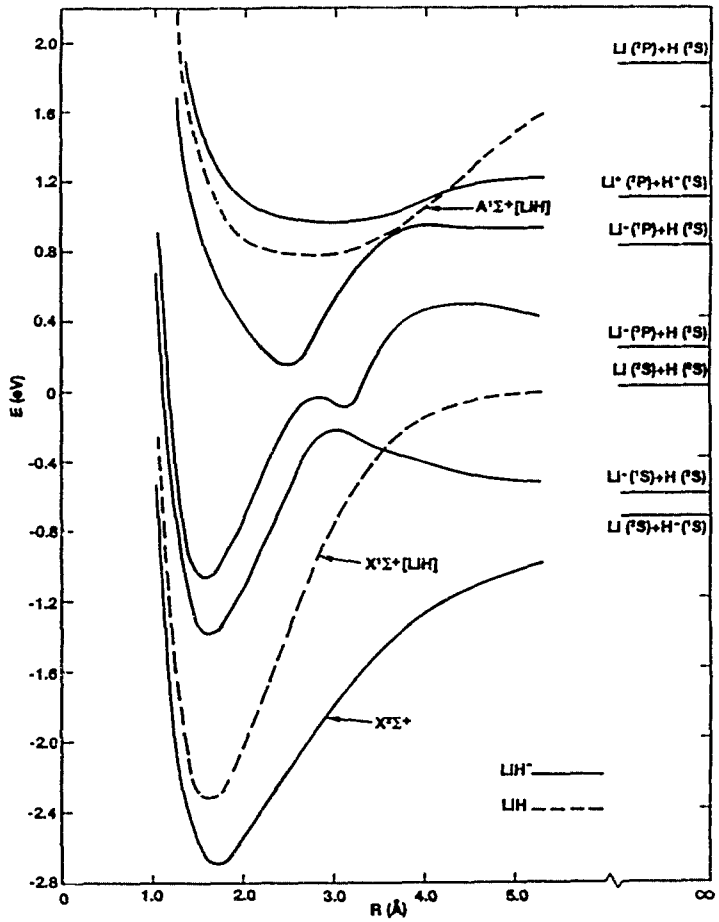

Fig. 1 LiH/LiH⁻ potential energy curves.

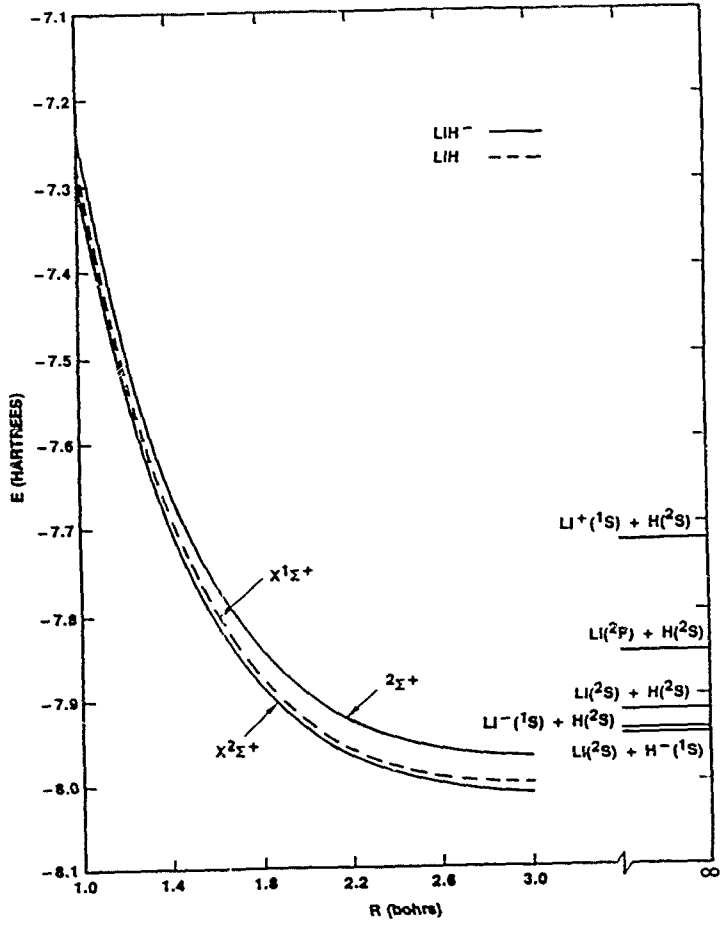

Fig. 2 Short range interaction potentials for LiH/LiH⁻.

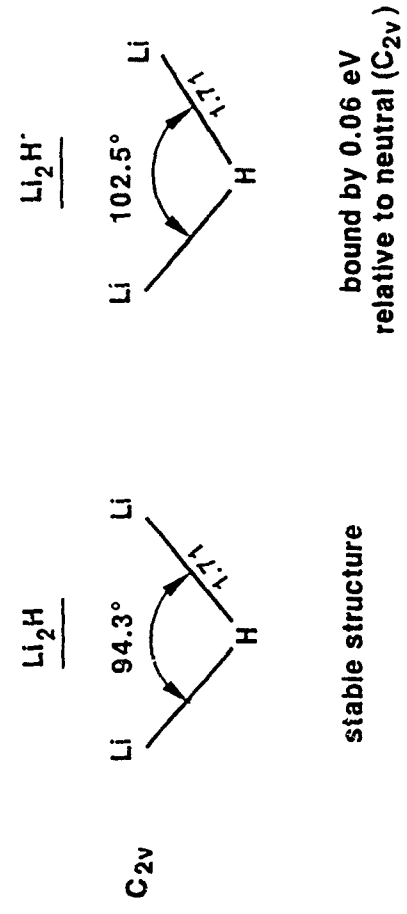

Fig. 3 Li_2H/Li_2H^- structures.

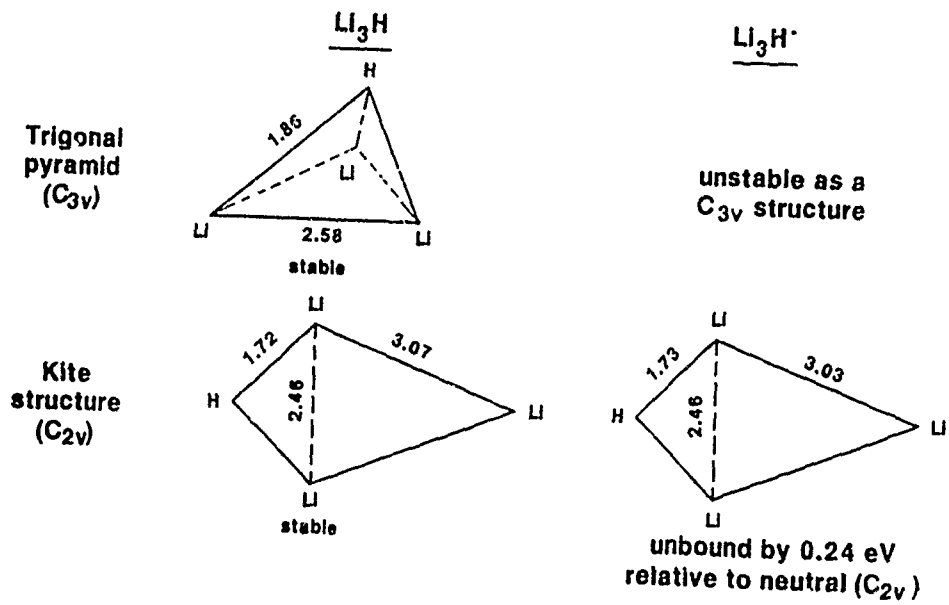

Fig.4 Li_3H/Li_3H^- structures.

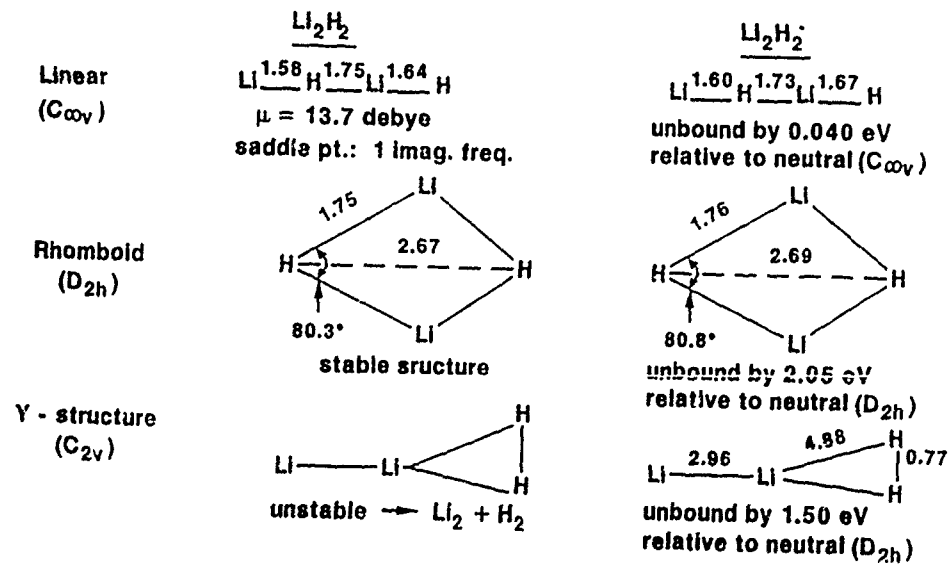

Fig.5 $Li_2H_2/Li_2H_2^-$ structures.

"Relativistic approach for e scattering from argon",
Bull. Am. Phys. Soc. 33, 935 (1988)
presented at the 1988 annual meeting of the Division of Atomic, Molecular and Optical Physics,
Baltimore, Maryland, April 18-20, 1988.

BX33 Relativistic Approach for $e^{\pm}$ Scattering from Argon. SULTANA N. NAHAR, Georgia State State U., and J. H. WADEHRA, Wayne State U.* -- Differential and integrated cross sections and various polarization

parameters, such as polarizarion (P) or the the Sherman function (S) and parameters T and U, for electron and positron scattering from argon are calculated using the relativistic Dirac equation. It contains the spin-orbit interaction. The real part of the projectile-target interaction is represented by a model potential that includes static potential (repulsive) and the Buckingham type model polarization potential (attractive) for the positron scattering and static potential (attractive), the same polarization potential (attractive) and electron exchange potential for electron scattering from argon. The phase shifts with large angular momenta ℓ are calculated by using the Born approximation The polarization parameter P for electron scattering is found to be in good agreement with the available calculated and measured values. A few different models of the absorption potential for the inelastic processes are used to calculate the elastic differential and integrated as well as the total integrated cross sections for positron scattering from argon. It is noticed that even though the calculated total integrated cross sections agree reasonably well with the measured values, the differential cross section curves show features different from those measured for the positron scattering from argon.

* Support of AFOSR is gratefully acknowledged.

[1]S.N. Nahar and J.H. Wadehra, Phys. Rev. A 35, 2051(1987).

"Formation of ground and excited states of antihydrogen",
Bull. Am. Phys. Soc. 33, 991 (1988)
presented at the 1988 annual meeting of the Division of Atomic, Molecular and Optical Physics,
Baltimore, Maryland, April 18-20, 1988.

EX 5 Formation of ground and excited states of antihydrogen. SULTANA N. NAHAR, Georgia State U., and J. H. WADEHRA, Wayne State U.* -- Differential and integrated cross sections for the formation of antihydrogen by the impact of intermediate energy (20 - 500 keV) antiprotons on positronium are calculated using the first Born approximation. The calculations are carried out for the formation of antihydrogen in ground and various excited electronic states (n = 1-3) when positronium, the target atom, is in the ground state, and for the formation of antihydrogen in the ground state when the positronium is in various excited electronic states (n = 1-2). The $1/n^3$ behavior for the capture cross sections is used to calculate the total (that is,

all states added together) integrated cross sections. The cross sections for the formation of antihydrogen presented here are obtained from those for the formation of positronium by the impact of positrons on hydrogen atoms by using the charge invariance and the principle of detailed balance.

*Support of AFOSR is gratefully acknowledge.

"An exact numerical solution of the time dependent Boltzmann equation",
Bull. Am. Phys. Soc. 34, 295 (1989)
presented at the 41st Annual Gaseous Electronics Conference, Minneapolis, Minnesota, October 18-21, 1988.

E-2 An Exact Numerical Solution of the Time Dependent Boltzmann Equation.* P.J. DRALLOS and J.H. WADEHRA, Dept. of Physics, Wayne State Univ.-- An exact, time dependent numerical solution of the Boltzmann equation for charged particle swarms in a dilute gas and uniform electric field is presented in detail. The method incorporates the full anisotropy of both the velocity distribution function and the collision cross sections as it does not involve any term expansions. An exact analysis of the collision terms is described and conditions for numerical stability of the solution are discussed. Results are presented for electron and positron swarms in gaseous Neon and Argon and in some model gases at various values of E/N.

*This work was supported by the Air Force Office of Scientific Research through Grant No. AFOSR-87-0342.

"Energetics of negative ion formation via dissociative attachment of e + LiH",
Bull. Am. Phys. Soc. 34, 1401 (1989)
presented at the 1989 annual meeting of the Division of Atomic, Molecular and Optical Physics,
Windsor, Ontario, May 17-19, 1989.

2:00
FC 6 Energetics of Negative Ion Formation via Dissociative Attachment of e + LiH*. H. H. Michels, UTRC, and J. M.Wadehra, Wayne State U.---- The formation of H^- and Li^- by dissociative attachment (DA) of $e + H_2$ and $e + Li_2$, respectively, is now well characterized both experimentally and theoretically. The role of LiH (or CsH), which could be formed from seeding an alkali into a hydrogen plasma, is presently not well understood, but the addition of

01

Friday Afternoon

an alkali appears to enhance the H^- production rate. This observation is interesting in light of the study by Gauyacq, et al[1], which indicates that charge transfer and collisional detachment processes should reduce H^- production in Na seeded plasmas. We have analyzed the electron attachment to LiH in terms of calculated potential energy curves. In agreement with previous studies, we find that the ground state of LiH^- is thermodynamically bound relative to LiH + e, with a calculated electron affinity of ~ 0.3 eV. The first excited state of LiH^-, which asymptotically correlates to $Li^- + H$, exhibits repulsive behavior in the region $3.0 \leq R \leq 6.0$ Å. Based on these preliminary studies, DA of e + LiH will yield Li^- ions for low-energy collisions H^- ions are not formed by DA of e + LiH but may be formed by energetically allowed electron capture into high vibrational states of LiH which lie above the $Li + H^-$ asymptotic limit.

*Supported in part by AFOSR under Contract F49620-88-C-0019 and Grant AFOSR-87-0342.
[1]J. P. Gauyacq, et al, Phys. Rev. A, 38, 2284 (1988)

"High-field time-dependent positron velocity distribution functions",
Bull. Am. Phys. Soc. 34, 409 (1989)
presented at the 1989 annual meeting of the Division of Atomic, Molecular and Optical Physics,
Windsor, Ontario, May 17-19, 1989.

FX 46 High-Field Time-Dependent Positron Velocity Distribution Functions. P.J. DRALLOS and J.M. WADEHRA, Wayne State U.*--It has been reported[1,2] that for a neon gas density N = 1 amagat, the positron swarm parameter Z_{eff} varies only at very low fields (up to E = 5 V/cm) and then becomes almost independent of E (up to E = 50 V/cm) with a value of about 6.3. In the present calculations, a numerical technique for evaluating the exact time-dependent behavior of electron velocity distribution functions[3] has been adapted to the case of positron swarms in gaseous neon. In these calculations an F/N of 0.9 Td (E = 240 V/cm and N = 1 amagat) was used. With this technique, the time dependence of the average energy, annihilation rate, and Z_{eff} were obtained. The equilibrium value for Z_{eff} under these conditions was about 6.3. This result extends the range of electric field, for which Z_{eff} is a constant to E = 240 V/cm.

*The support of the AFOSR is gratefully acknowledged.
1. P.S. Grover, J. Phys. B 10, 2269 (1977)
2. K.V. Sinha and P.S. Grover, Phys. Rev. A 35, 3309 (1987).
3. P.J. Drallos and J.M. Wadehra, J. Appl. Phys. 63, 5601 (1988)

"Energetics of neutral and negative ions of Li_mH_n clusters",
Bull. Am. Phys. Soc. 35, 1177 (1990)
presented at the 1990 annual meeting of the Division of Atomic, Molecular and Optical Physics,
Monterey, California, May 21-23, 1990.

16 36
DB 9 Energetics of Neutral and Negative Ions of Li_mH_n Clusters*. H H Michels, UTRC, and J M Wadehra, Wayne State U.---- The formation of $H^-(Li^-)$ by dissociative attachment (DA) of $e + H_2(Li_2)$ is thought to be the dominant volume process in discharge type negative ion sources The role of $Li_mH_n(Cs_mH_n)$ molecules, which could be formed from seeding an alkali into a hydrogen plasma, is presently not well understood, but the addition of an alkali such as Cs appears to enhance the H^- production rate This observation is interesting in light of the study by Gauyacq, et al[1], which indicates that charge transfer and collisional detachment processes should reduce H^- production in Na seeded plasmas. In order to examine the structure and stability of Li_mH_n clusters and their anions, *ab initio* calculations were carried out for several species at the MP2 level of theory The basis set chosen was the Gaussian 6-311G triple split-valence set, augmented by d-polarization functions for Li and p-polarization for H and diffuse functions to better describe the negative ion charge distributions Our studies to date indicate that several Li_mH_n (and by analogy, Cs_mH_n) clusters are thermodynamically stable. In particular, the Li_2H_2 species, as a C_{2v} structure, may be an important component of alkali-hydrogen mixtures This species can dissociatively attach an electron to form $Li_2H + H^-$ for $E_{coll} \geq 2.0$ eV The Li_3H (C_{2v}) species should also exhibit DA to form $Li_3 + H^-$, but the concentration of this molecule will be lower than that of the more stable Li_2H_2 cluster

*Supported in part by AFOSR under Contract F49620-89-C-0019 and Grant AFOSR-87-0342
[1] J P Gauyacq, et al Phys Rev A, 38, 2284 (1988)